warwick.ac.uk/lib-publications

INTERACTIONS BETWEEN
GLASS-CERAMIC COATINGS AND
METALS

by

FENG HONG

Department of Physics

University of Warwick

1991.

Submitted for the Degree of Doctor of Philosophy

ACKNOWLEDGEMENTS

MEMORANDUM

The submition of this dissertation to the University of Warwick is to apply for admission to the degree of Doctor of Philosophy. The dissertation is a detailed description of my research project carried out in the Department of Physics of the university during the October 1986 to October 1990 under the supervision of Dr. D. Holland. Apart from what has been specifically acknowledged in the dissertation, the study is an independent effort of my own. So far, no part of the results has been noted in this university or any other universities used for a degree thesis.

Some parts of the thesis work have been published in different journals and conference proceedings, and presentations of some results were also given at various national and international conferences. The list of the publication and presentation is attached to this thesis.

Feng Hong

January 1991

2

ABSTRACT

A study of glass-ceramic coatings on metal substrates was carried out in order to understand how the coatings and substrates interact and how these interactions affect coating microstructures and properties. There are two systems involved. One is a lithium-silicate glass-ceramic coating on Ni/Cr/Co alloy and the other is a lithium-aluminosilicate glass-ceramic coatings (with some other optional compositions) on titanium metal.

Simple techniques such as screen printing or the "droplet" method were used to coat the substrates with a layer of fine glass powder, and then a firing procedure followed to create a vitreous enamel layer on the metals. Heat treatment was usually applied to convert the vitreous coating into a highly crystallized, glass-ceramic coating since this generally results in superior properties.

Because both the Ni/Cr/Co alloy and titanium metal are active metals, complicated interactions were observed at the coating/metal interface. In the Ni/Cr/Co case, Cr from the substrate tends to diffuse into the coating very rapidly at the firing temperature. The rapid diffusion of mainly Cr^{++} ions and subsequent change into Cr^{+++} ions results in saturation of Cr^{+++} ions in the glass coating. The second oxidation step proceeds more rapidly at the coating surface and $LiCr(SiO_3)_2$ crystals start to precipitate on the surface of the coating. Mismatch of TEC, thermal expansion coefficient, between $LiCr(SiO_3)_2$ and the coating causes severe disruption. In addition, some components in the coating, for instance, P_2O_5, react with Cr to form $Cr_{12}P_7$. As a result, in the reaction zone, consumption of the intended nucleating agent P_2O_5 leads to a poorly crystallized structure affecting coating properties.

In the titanium system, though long range diffusion across the interface was not observed, the major problem is the reactivity of titanium with coating com-

3

ponents including SiO_2. Direct reaction between titanium and silica gives Ti_5Si_3 as an interfacial layer and the gaseous O_2 produced may disrupt the molten glass structure during firing. Other interactions such as Ti/P_2O_5 can also proceed to give other damaging effects. In general, the coating on titanium after firing is usually very porous if these interactions are not prevented.

Preoxidation of $Ni/Cr/Co$ alloy created an adherent Cr_2O_3 layer on the alloy surface, and this layer is very stable in the coating glass due to its low diffusivity and solubility. The existence of this layer prevented direct contact of alloy and coating at the firing temperature, minimizing interfacial reactions and leading to the desired coating structure.

From a chemical point of view, preoxidation of titanium metal can create a barrier of TiO_2 between the coating and metal to hinder the formation of Ti_5Si_3. However, the poor bonding strength of this layer meant that it was ineffective in forming a transition layer between the metal and coating. Furthermore, the TiO_2 can be readily dissolved by the coating glass during firing. Addition of an adherence oxide, CoO, was successful in 1) producing TiO_2 in situ at the interfacial area and Co/Ti dendrites, both of which are necessary in maintaining chemical as well as mechanical bonding across the interface 2) diverting and hence minimizing the damaging direct reaction between Ti and SiO_2 because the reaction between Ti and CoO always takes place prior to the reaction between Ti and SiO_2 thermodynamically.

In the systems of glass-ceramic coatings for reactive metal substrates, various complications may occur. In this study, interactions of lithium-silicate/$Ni/Cr/Co$ alloy and a wide range of glass-ceramic coatings/titanium have been studied. Detailed observation has been given together with explanation. Further work has also been suggested so that better understanding and application may generate from what has been observed in this project.

4

LIST OF FIGURES

6

7

9

11

LIST OF TABLES

Contents

1

Chapter 1

INTRODUCTION

1.1 Background

There are many areas of technology where the use of coated metals is important. Metals are used extensively because they are easy to fabricate into a variety of shapes and are tough. They also have many desirable physical properties such as electrical and thermal conduction. However, the usefulness of metals can be further extended if a coating is applied. The coating of metals may be required to a) prevent oxidation or corrosion b) prevent mechanical erosion c) provide a thermal barrier d) provide an electrically resistive barrier. In a word, in many fields of modern technology where the required bulk and surface properties do not occur in one material, the problem can usually be overcome by coating metals with suitable materials. From the wide variety of coatings available, non-metallic inorganic materials, mainly various ceramics and glasses, are the major coating components for metals.

The coating of metal with a thin layer of glass, known as a "vitreous or porcelain enamel", is widely used both in domestic areas and industrial fields. The use of enameled metals can be dated back to the ancient Egyptian times and today enameled metals are so important that the technology and application of these materials are advancing steadily bringing about broader ranging as well as more specialized products from complex electronic devices to parts of aircraft

4

engines[1].

The coating of metal with a thin layer of ceramic as a "refractory coating", is also widely adopted. Its use mainly lies in industry, ranging from furnace components, heat exchangers and turbine engines etc. It can be extended into other fields such as microelectronic, medical and mechanical engineering where refractoriness is perhaps less important than other properties[2].

1.2 Advantages of Glass-ceramic Coatings

As mentioned above, the protection of metallic articles with a coating of glass or vitreous enamel has long been known. Good reviews exist in references[3], [4] and [5]. Since the coating consists of a layer of glass, it exhibits all the desirable properties of glass. However, such coatings have limited resistance to abrasion, to thermal and mechanical shock, and to other mechanical stress. The general uses of such coatings are restricted to applications where such stresses are relatively low and where the superior corrosion resistance or other desirable properties of the glassy structure more than offset its disadvantages. It is not surprising to find that traditional enamel areas are relatively limited, providing the chemical industry with corrosion protection and domestic industry with means of decoration. The mechanical weakness, fragibility and vulnerability to mechanical and thermal shock of these porcelain enamels hinder their further development though there have been plenty of exotic varieties of enamel coatings to suit various purposes.

Glass-ceramics, defined as polycrystalline solids prepared by the controlled crystallization of glass, were discovered and developed mainly by Stookey[6], McMillan[7] and their co-workers. They are distinguished from glass by the presence of major amounts of crystals since glass is amorphous or non-crystalline structurally. It has been found that the properties of glass may be considerably altered and improved by incorporation of crystalline particles. Glass-ceramics retain, in large measure, most of the desirable aspects of the original glass, while some other aspects such as mechanical strength, impact and abrasion resistance,

PROPERTY	UNIT	GLASS	GLASS-CERAMIC
Thermal Expansion	10^{-7} °C^{-1}	+5–+120	-40–+200
Refractoriness	°C	>600	>850
Impact Strength (Charpy)	kgcm	0.5–1.0	3.5–7.5
Cross Breaking Strength	kgcm^{-2}	500–900	1000–4000
Young's Modulus	MNm^{-3}	< 7.5 × 10^4	< 16.7 × 10^4
Dielectric Strength	kvmm^{-1}	<45	<55

Table 1.1: Comparisons between glasses and glass-ceramics

thermal expansion control and high temperature resistance are greatly enhanced. Table.1.1. gives some comparisons between commonly used glasses and glass-ceramics[7].

The adoption of glass-ceramics as preferred coating materials for metallic substrates[8] has extended the traditional porcelain enamel into new fields. As the glass-ceramic coating usually starts from the glassy state which wets metal and forms good adhesion in a similar way to porcelain enameling, it has benefited a great deal from the traditional enameling technology and this makes the glass-ceramic coating one of the easiest and most cost-effective of coating techniques. The additional heat-treatment applied in the later stage to convert the glass structure into glass-ceramic proves equally simple and effective. With the improved properties the glass-ceramic coating shows better mechanical behaviour and higher refractoriness than the traditional enamel. These enable the glass-ceramic coating to work in a hostile environment and have many versatile applications. Especially, as glass-ceramic materials have a much wider range of thermal expansion than glass(Fig.1.1)[9], they can be used to coat most of the commonly used metals without causing excessive thermal expansion mismatch.

The advantages of glass-ceramic over ceramic coatings, which are fully crystallized non-metallic inorganic materials, lie in their ease of control of thermal expansion, easy manufacturing and better control of porosity. Being formed of densely packed crystals, the thermal expansion of a ceramic material is highly de-
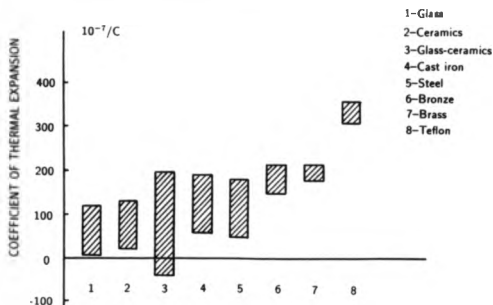
Figure 1.1: Thermal expansion range of different materials

pendent on the crystal type included. This narrows the range of choice between the crystal type desired and thermal expansion required. Hence, the control of the thermal expansion, one of the key factors in achieving a successful coating, sometimes can be difficult, see also in Fig.1.1. Porosity is another concern in dealing with ceramic coatings. Unless complicated pre-treatment and firing procedures are used, such as hot pressing, sintering will not proceed so well as for a glass coating where full sintering is achievable within short firing times. Even a high temperature plasma sprayed coating exhibits high residual porosity[10].

To sum up, glass-ceramics can be regarded as a most valuable addition to the materials available to the design engineer. By careful choice of composition and heat-treatment, the microstructures and properties of glass-ceramics can be tailored to meet different requirements. Being inorganic and non-metallic they combine useful high temperature capabilities with a high degree of chemical stability and corrosion resistance. Their unique combination of properties has made them attractive for many specialized engineering applications. Furthermore, the easy manufacturing technology has made them widely available and acceptable.

Glass-ceramic coating is only one of these applications and this has still to be fully exploited.

1.3 Applications of Glass-ceramic Coating

Most of the well developed glass-ceramic systems have been adapted for coating purposes. For example, oxidation and corrosion protection for mild steel and stainless steel can be produced for domestic cookery using $Li_2O-Al_2O_3-SiO_2$ or $Li_2O-B_2O_3-SiO_2$ systems, see Davis[11], Sturgeon[12]. Copper, molybdenum, tungsten and a chromium alloy have been coated with $Li_2O-Al_2O_3-SiO_2$, $ZnO-Al_2O_3-SiO_2$, $MgO-Al_2O_3-SiO_2$, and $BaO-MgO-B_2O_3-SiO_2$ systems to develop substrate assemblies for electronic devices, see Andrus[13], R.C.A. company[14], Partridge[15] and Logan[16]. In these cases, various glass-ceramics are not only used as an oxidation resistance layer to protect the substrate metals but also act as an insulating layer to suit electronic purposes. A bioactive glass-ceramic based on the $Na_2O-CaO-SiO_2-P_2O_5$ system[17] has been produced to coat some metal substrates for medical implantation to overcome the problems of incompatibility of metals with living tissue. Ni-Cr alloy coated with $K_2O-Al_2O_3-SiO_2$ glass-ceramic[18] has found uses as dental material. Superconductive glass-ceramics based on the $Bi_2O_3-(SrO, CaO)-CuO$ and other systems are also under active research as coating compositions[19].

With further development of glass-ceramics themselves, new systems and technology are to be discovered from time to time. This will no doubt lead to more and more applications of glass-ceramic coatings.

1.4 Aims of This Research Project

To date, most emphasis has been focused on extending the usage of glass-ceramic coating materials. Little information has been gained as to the various kinds of interactions which occur at the interface between the glass-ceramic coatings and substrate metals. Questions of major importance are what factors dominate the

8

interactions and how these interactions affect the glass-ceramic structures, since the properties of coating materials are always structurally controlled.

This research project was mainly intended to investigate those interactions occurring at the interface between metals and glass-ceramic coatings and, in addition, the consequences for the microstructures and properties of coatings. The chosen coating systems are:

1) Nimonic 263 (Ni/Cr/Co alloy) and lithium silicate glass-ceramic

2) Titanium metal and lithium aluminium silicate glass-ceramic (with other optional glass-ceramic systems)

High temperature oxidation and corrosion protection is one of the potential applications of glass-ceramics. Both the chosen metals are base materials used in the aeroindustry as jet engine parts which frequently experience severe oxidation and corrosion problems. Therefore, it is intended in this project to provide protection to these metals against high temperature oxidation and corrosion. However, to obtain some fundamental understanding of these systems, most of the efforts were focused on the academic study rather than practical application. These two metals are very chemically reactive, hence, complicated interactions between the metals and coatings make such understanding very necessary before any real coating application is attempted. It was hoped that the basic knowledge gained in this project will make its own contribution to the practical applications of glass-ceramic coatings at high temperature.

1.5 Thesis Structure

This thesis consists of 7 chapters each of which deals with individual topics.

Chapter 1 is an introduction indicating the relevance of glass-ceramic coatings and the aims of this research project.

Chapter 2 is a survey of current knowledge about glass-ceramic coating. It reviews the overall information covering the basic principles of glass and metal interfacial reactions and bonding.

Chapter 3 is a description of the experimental instrumentation and techniques. It indicates the means by which the necessary information has been gained.

Chapter 4 is a detailed account of the experimental work indicating the controlling parameters.

Chapter 5 presents and discusses the results obtained. Specific interactions involved in the coating systems are identified, their effects on the coating structural changes are observed and suggestions are given to overcome the problems.

Chapter 6 summarizes the conclusions of the whole project and future work is suggested in order to achieve further understanding and explore possible applications.

Chapter 2

THEORIES OF BONDING BETWEEN COATINGS AND METALS

2.1 Introduction

To design glass-ceramic coatings for metals it is necessary to understand the bonding between these two materials. It is generally believed that bonding between metal and glass can be achieved via mechanical keying or chemical bonding.

The mechanical keying theory once was accepted as a major mechanism for two different materials to bond as a highly irregular metal/glass interface tends to interlock the two materials together[20]. But later investigation proved that chemical bonding dominates the interfacial strength. In those interfaces where chemical bonding takes place mechanical keying is of minor importance. Yet mechanical keying can make a significant contribution to the bonding especially when chemical bonding does not exist at the interface.

The chemical bonding, or saturation theory, proposed by King[21] and Pask[22] requires the existence of a chemical equilibrium across the glass/metal interface. This equilibrium produces the structural continuity at the interface which, as a

11

result, leads to a very strong chemical bond. The saturation theory claims that the bonded interface remains saturated with the appropriate metal oxide and a structural transition is achieved since metal oxides are compatible with both metal and glass composition. The chemical bonding is lost, or exists only as a weak Van-der-Waal force, if the saturation at the interface is neither realized nor maintained.

In fact, bonding between two different materials is a very complicated chemical and physical process. To achieve satisfactory bonding strength and bonding structure, many factors are involved. The structural, electronic, mechanical, thermodynamic and thermomechanical aspects are probably the basic areas worth detailed discussion before a full understanding is gained.

2.2   Structural

Most forms of ceramic joints involve creation of interfaces between dissimilar materials. When a glass coating is bonded to a substrate metal, the interface created in fact exists between the metal crystal lattice and a "liquid structure", i.e. the supercooled molten glass. Ceramic coating creates an interface between different crystal phases.

A metal/glass interface can be greatly altered by the interaction occurring during the sealing procedure. The interdiffusion of elements from both glass and substrate metal tend to change the glass composition as well as the metal composition. In the latter case, the microstructure of the metal along the interface can be very different from that of the bulk structure due to either enrichment or depletion of certain elements. Phase changes in the base alloy along a metal/porcelain interface have been observed by Baran[23]. The effect of changing both metal crystal structure and glass composition should be carefully considered in order to satisfy the bonding requirements while avoiding undesirable crystallographic or compositional changes during the sealing process.

A ceramic/metal interface, existing between different crystals, generally gives

rise to a lattice mismatch due to the dissimilar unit cells. Though it is very difficult to make suitable interfacial samples for transmission electron microscopy, which would allow the direct investigation of the crystallographic details, it has become an active subject of recent studies attracting a great deal of attention. Ruhle et. al[24] successfully examined the bonding system of single crystal Nb and Al_2O_3. It was discovered that the crystals were oriented so the close-packed Nb(110) and Al_2O_3(0001) planes were parallel. The perfect lattices of each crystal extended to within 3-4 lattice planes of the interface. Within that region, the lattices were distorted. In some other observations, a thin reaction layer is also seen[25] which creates the discontinuity between the different crystal lattices.

A glass-ceramic/metal interface is believed to have very complex crystallographic features. The different crystals and residual glass phases in bulk glass ceramic material mean that both crystal/crystal and crystal/glass contacts exist in the bond area. Thus, any interaction occurring at the interface will affect the interfacial structures of original metallic, ceramic and glassy structures in a complicated way. Sturgeon[26] found the growth of $LiCrSi_2O_6$ crystals as dendrites between a lithium-silicate glass-ceramic and Cr-steel interface. Pask[22] observed the micro-galvanic growth of various crystals in a glass/Fe system. Titanium silicides were reported to exist at the interface of a glass-ceramic coating and titanium metal[27]. In all cases, the occurrence of the crystal phases attached to the interface not only changes the crystal features of all phases involved but also changes the original bonding condition. The growth of some dendrites or change of some crystal phases can exert positive as well as negative effects on the bonding strength.

2.3 Electronic

There is a change in electronic structure from the metallic bond in the metal to a predominately ionic or mixed ionic-covalent bond in glass or ceramic. A transition between the metallic bond of the substrate and the ionic/covalent bond of the glass or ceramic phase is visualized by King et.al[21] while Pask[22]

13

(a) -M-M-M-M-O-M-O-M-O-Si-O-Si-O-Si-
     metal   metal oxide   glass

(b) -M-M-M-M-O-Si-O-Si-O-Si-
     metal metal oxide glass
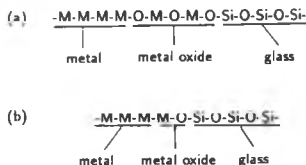
Figure 2.1: Chemical bonding of phases at interfaces a)via multi-oxide layer b) mono-oxide layer

emphasizes the need for a continuous electronic structure achieved through the maintenance of equilibrium compositions.

The different bond characteristics of metals and ceramics result in incompatibility of these two materials. In practice, a metal oxide layer is usually created to produce the transition across the interface, because the oxide layer is compatible with both metal and glass or ceramic phases in the sense that the oxide can bridge both metallic and ionic/covalent characterized bonds. The formation of mono- or multi-molecular oxide layers and subsequent saturation of the glass lead to an equilibrium or chemical bonding at the interface. A typical interfacial structure is shown schematically in Fig.2.1[28]. Theoretically, only a single layer of the oxide is necessary to become a shared layer providing continuity of structure. Though the creation of an oxide layer can be achieved easily by preoxidizing the metal, the layer of oxide may not always be strong enough to adhere to the metal. This can sometimes cause problems as the poorly bonded metal oxide fractures at the interface. Another problem of such preoxidized metal is that the preformed oxide layer tends to dissolve into the coating glass rapidly. This leads to the loss of continuity, i.e. chemical bonding. Further discussion will be found in section 5.2 on how to deal with these non-adherent oxides.

If glass is in direct contact with bare metal, redox reactions take place at the interface in an attempt to establish equilibrium bonding. This results in

14

-M-M-M-M Si-O-Si-O-Si

metal   no oxide layer glass
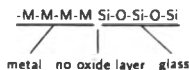
Figure 2.2: Weak Van der Waals bonding at interface

oxidation of the metal and reduction of a cation in the glass or ceramic. These electrochemical reactions proceed readily because of the requirements of local electronic structure, i.e. ionization at the interfacial zone. Consequently, saturation of the coating by metal oxide at the interface can be set up. Pask[22] listed three types of reactions summarized as (1) Gaseous oxidation – oxidation of the base metal by atmospheric oxygen. (2) Redox-Reduction of cation valence – changing of the valence state of cations in the glass (3) Redox-Reduction of cations to metallic state – the substrate metal atoms are oxidized by giving up electrons that are transferred to cations in the glass which are reduced to the metallic or neutral state. The required saturation, or the ideal transitional electronic structure, however, cannot always be maintained at the interface even if these redox reactions proceed. Either the redox reactions are hindered or they are not fast enough to compete with the dissolution of the oxide into the bulk coating. In both cases the saturation or electronic continuity can disappear and only a weak Van der Waals force provides the bonding strength, see Fig.2.2[28]. In brief, those electronic structures involved at the metal/glass interface must satisfy continuity and various electrochemical reactions can take place at the interface if equilibrium is not achieved.

2.4   Mechanical

When a solid surface is subject to microscopic examination it is found to have irregularities, in other words, the surface is neither flat nor smooth. These irregularities are defined as asperities or anchor points. When two solids are

15
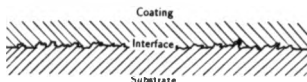
Figure 2.3: Mechnical keying at interface

brought into contact, joining occurs at those points where the asperities of the two surfaces engage across the interface. The application of a load to the solids in contact is sometimes necessary to exceed the materials elastic limit to cause plastic deformation of the asperities. The deformed asperities form irregular mechanical keying leading to certain adhesion between two solids[29].

In the case of a glass/metal joint, mechanically, a similar principle applies, e.g. the formation of a highly irregular interface bonds two materials together via mechanical keying. The mechanically engaged metal/glass interface can be schematically shown in Fig.2.3. However, the irregularity of the metal surface, in most cases, is not due to plastic deformation through load application. It is usually created by sand blasting or chemical etching during the metal pretreatment[30]. The chemical interaction between metal and molten glass, producing some dendrites during the firing process, also roughens the metal surface[31]. In the glass-ceramic coating process, some irregular crystal phases growing at the interface add to the roughness as well[26]. All these factors increase the roughness, or the anchor point density at the metal/glass interface, and therefore, exert a positive effect on mechanical adhesion.

Elastic modulus across the interface is another factor to be considered if satisfactory bonding is to be achieved. Elastic modulus match is important especially for joints subjected to cyclic mechanical stress. A good review on stress concentrations and development of crack propagation at or near the interface of ceramic/metal bonding systems can be found in reference[32].

16
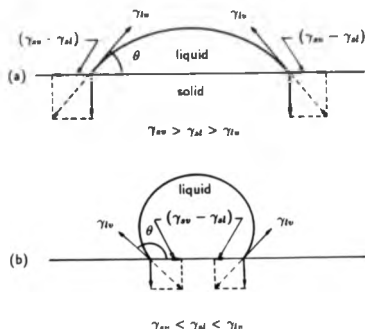
Figure 2.4: Sessile drop configrations: A) wetting B) nonwetting

2.5 Thermodynamic

From the thermodynamic point of view, an equilibrium across the interface should exist if adherence is maintained. The equilibrium consists of two major aspects. They are a) chemical stability b) physical stability.

Physical stability refers to the interfacial wetting and adherence. The basic principles of the wetting process have been described in detail by Passerone in reference[33]. When a solid is brought into contact with a liquid, for example, a metal to a molten glass, a new interface between the solid and liquid, I_{sl}, is created at the cost of the other two interfaces, i.e. interface between air and solid, I_{as}, as well as the one between liquid and air, I_{al}. Schematic cross-sections of both wetting and non-wetting sessile drops can be seen in Fig.2.4[28]. Under non-reactive conditions, the wetting can be represented by a steady-state acute contact angle θ. This configuration shown in A only occurs when $\gamma_{sv} > \gamma_{sl} > \gamma_{lv}$. ($\gamma$ represents interfacial energy: for solid/vapor as sv, solid/liquid as sl, and liquid/vapor as lv) The non-wetting with obtuse contact angle θ can

17

be seen from B and it occurs when $\gamma_{sv} < \gamma_{sl} < \gamma_{lv}$. From Fig.2.4 it seems that wetting actually means the reduction of the interfacial energy γ_{sl}. The spreading of a drop of liquid on a solid surface take place only when the energy of forming a solid/liquid interface is smaller than the total interfacial energy of a solid/vapour and liquid/vapour before the liquid is contacted with solid. The familiar Young-Dupre equation:

$$\gamma_{sv} - \gamma_{sl} = \gamma_{lv} cos\theta \tag{2.1}$$

describes a steady-state contact angle and its relations with the interfacial energies. It is worth pointing out that the case mentioned above only exists in the absence of a reaction between the liquid and solid. The chemical reaction at the interface has sometimes a significant influence on the physical equilibrium discussed above. When a reaction takes place, the Young-Dupre equation can be modified as:

$$\gamma_{sv} - (\gamma_{sl} + \frac{dG_R}{dAdt}) = \gamma_{lv} cos\theta \tag{2.2}$$

because the free energy of reaction per unit interfacial area and unit time enhances the driving force for wetting provided that the solid is an active participant. Here, in a solid-state solution reaction, an active participant is defined as the solvent or unsaturated phase relative to the other phase which does not change its composition. The latter is defined as a passive participant functioning as solute or saturated phase. Sometimes both phases are unsaturated relative to each other, then, both phases are active participants. Sharpe[34] summarized four cases of sessile drop examples from the phase equilibrium diagram of Cu and Ag, see Fig.2.5. Chemical stability refers to the equilibrium across the interface. As briefly discussed in section 2.3, an oxide saturated interface is necessary to achieve adhesion. During the bonding procedure of a glass/preoxidized metal assembly, molten glass wets and dissolves the oxide. The glass at the oxide interface immediately becomes saturated if the solution rate of the oxide is faster than the diffusion rate of the dissolved oxide into the bulk glass. The metal is
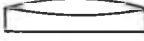
18

Figure 2.5: Sessile drop examples for Cu and Ag under various conditions

19
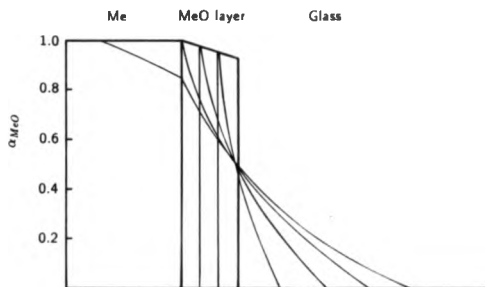
Figure 2.6: Activity gradients of MeO in glass with continuing solution of oxide by glass

saturated with the oxide, as well as the glass, at least at the surface. Therefore, the oxide layer bonds chemically to both metal and glass. The saturated interfaces and oxide layer thus have a chemical activity of one for MeO (metal oxide). As the dissolved oxide diffuses into the glass a concentration gradient is formed as shown schematically in Fig.2.6[28] until the oxide is completely dissolved. At this stage, the oxide saturation at the interface is lost and the chemical activity becomes less than one. Because of the loss of chemical equilibrium, the following redox reactions become thermodynamically favourable, as mentioned in section 2.3. The reduction of cations in the glass is the most important reaction widely reported in glass and metal bonding. Considering an interface between a metal M_I and a molten glass containing a metal oxide $M_{II}O$, a redox type of reaction may occur represented by

$$M_I + M_{II}O(glass) = M_IO(glass) + M_{II} \qquad (2.3)$$

20

and the individual step reactions can be

$$M_I + M_{II}O(glass) = M_IO(interface) + M_{II} \qquad (2.4)$$

$$M_IO(interface) = M_IO(glass) \qquad (2.5)$$

These reactions are actually the formation of the metal oxide at the interface followed by its solution into the glass. The free energy of such a reaction is given as

$$\Delta G = \Delta G^{\circ} + RT \ln \frac{\alpha(M_IO_{glass}) \times \alpha(M_{II})}{\alpha(M_{II}O_{glass}) \times \alpha(M_I)} \qquad (2.6)$$

ΔG – Gibbs free energy

ΔG° – Standard Gibbs free energy

R – Universal gas constant

T – Temperature

α – Chemical activity

When ΔG is negative, thermodynamically reaction (2.3) takes place readily. However, if ΔG° is positive the reaction only proceeds when the activity content is significantly less than unity for ΔG to become negative. The reaction is likely to occur in a low total pressure and low partial oxygen pressure, See Hoge[35].

The free energy of formation of the oxide, M_IO or $M_{II}O$, can be used to judge the direction towards which the reaction(2.3) proceeds. If the formation energy of M_IO is more negative than $M_{II}O$, the reaction(2.3) takes place readily due to the decrease of ΔG for whole reaction. Though the data for free energies of formation of oxides in glass are limited, the standard states at which the standard free energies are derived are always used to estimate the reactions and predict their feasibilities. Table 2.1 [36] lists these values for several metal oxides at 1000°C. The validity of using such values to predict possible reactions in glass has been illustrated by King[21].

Oxide	Energy KJ mole^{-1}
$4Li + O_2 \rightarrow 2Li_2O$	-850.0
$4/3\ Al + O_2 \rightarrow 2/3\ Al_2O_3$	-842.1
$Ti + O_2 \rightarrow TiO_2$	-709.69
$Si + O_2 \rightarrow SiO_2$	-676.6
$4/3\ Cr + O_2 \rightarrow 2/3\ Cr_2O_3$	-533.4
$4Na + O_2 \rightarrow 2Na_2O$	-435.0
$2Zn + O_2 \rightarrow 2ZnO$	-409.5
$2Fe + O_2 \rightarrow 2FeO$	-376.4
$4/5\ P + O_2 \rightarrow 2/5\ P_2O_5$	-361.9
$4N + O_2 \rightarrow 2N_2O$	-351.9
$3/2\ Fe + O_2 \rightarrow 1/2\ Fe_3O_4$	-351.5
$4/3\ Fe + O_2 \rightarrow 2/3\ Fe_2O_3$	-324.5
$Sn + O_2 \rightarrow SnO_2$	-311.9
$2Co + O_2 \rightarrow 2CoO$	-285.6
$4K + O_2 \rightarrow 2K_2O$	-248.3
$2Ni + O_2 \rightarrow 2NiO$	-185.9
$4Cu + O_2 \rightarrow 2Cu_2O$	-148.7
$2Cu + O_2 \rightarrow 2CuO$	-82.9

Table 2.1: Free energies of formation of metal oxides [1000°]C

2.6 Thermomechanical

The desired glass/metal bonding demands not only a chemical equilibrium or structural transition across the interface, but also a favourable stress gradient across the interface and extended into the coating. This stress gradient can be achieved by 1) a proper thermal expansion match between the glass and metal 2) a suitable compositional concentration gradient which is proportional to the thermal expansion coefficient gradient.

The match of the thermal expansion coefficient(TEC) between metal and coating is always a priority to ensure minimum stress at the interface. Typically, for satisfactory bonding of the coating, the thermal expansion coefficients must be within $10 \times 10^{-7}/°C$[2]. Careful choice of composition of glass or glass-ceramic and suitable metals is needed to avoid TEC mismatch problems. Few glasses have the same TEC as their glass-ceramics. When the bonding procedure starts with a glass which then changes to a glass-ceramic, problems can always occur since the TEC's of glass-ceramics are frequently much lower or even higher than those of the parent glasses(Fig.2.7)[7]. An excessive mismatch of TEC between glass or glass-ceramic and substrate metal will lead to cracks at the interface and even total failure of the bonding. A solution to the problem is to carry out the bonding procedure at a reasonable high temperature at which metal and glass bond together while glass is still fluid enough to accommodate the stress caused by the TEC mismatch. Further conversion from the glass to glass-ceramic should be carried out without quenching the glass to a temperature lower than the strain point, see reference[7].

The compositional concentration gradient is also needed even if the two materials have a very close TEC match. The previously discussed reactions and dissolutions occurring at the interface introduce a certain amount of metal oxide, in most cases, into the bulk glass coating. Such an addition of one or more metal oxides to the glass affects its coefficient of expansion because of an increase of the O/Si ratio and introduction of cations with different degree of covalency. Mayer[37] investigated various amounts of Fe_2O_3, NiO and CoO in
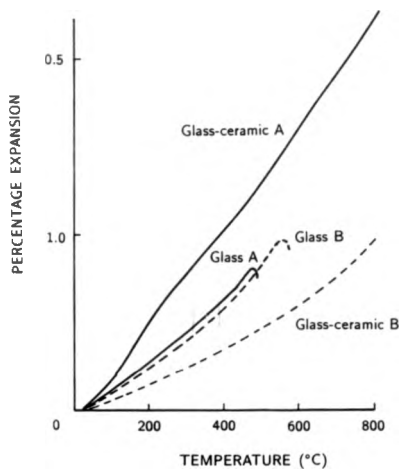
Figure 2.7: Thermal expansion curves of glass-ceramics and parent glasses

24

sodium-disilicate glasses and proposed a correlation between thermal expansion of glass and glass-to-metal adherence. The concentration gradients are proportional to thermal expansion coefficient gradients which generally result in more favourable stress gradients. Additionally, diffused oxides extending to various depths in the bulk glass may also alter the microstructure of the glass-ceramic after heat treatment, resulting in different TEC values at different depths in the coating. Sometimes the change of TEC gradient can be very unfavourable. This damaging effect was confirmed by Sun[38] in a glass-ceramic coating on mild steel. Therefore, to achieve strong bonding, a favourable compositional gradient should be created to assist in setting up a proper thermal expansion gradient across the interface extending into the bulk coating. Under this condition, the bonding can be actually strengthened by realizing a more favourable stress gradient thermomechanicaly, similar to graded seals.

2.7 Diffusion and dissolution

As previously explained, saturation of certain oxides at a glass/metal interface is essential to achieve a satisfactory bonding. However, the oxides can dissolve into the glass and diffuse away from the interface at a glass/preoxidized-metal interface, if the rate of diffusion is higher than that of dissolution. This leads to loss of the saturation resulting in poor adhesion. At a direct glass/metal interface, on the other hand, dissolution and diffusion of oxides can also proceed rapidly after or at the same time as redox reactions which give rise to oxides.

The basic principles of all diffusion and dissolution are the well-known Fick's first and second laws. In the binary one-dimensional case:

$$J_i = -D \frac{dC_i}{dx} \tag{2.7}$$

and

$$\frac{dC_i}{dt} = \frac{d(D\,dC_i/dx)}{dx} \tag{2.8}$$

25

where J_i is the flux of species i, C_i the concentration of i, t the time, x the distance in the diffusion direction, and D the diffusion coefficient. D can be expressed as Di^* (self-diffusion coefficient of species i) if the system does not involve mass transfer. Otherwise, D is expressed as $\bar{D}$ (interdiffusivity) associated with the diffusion of each individual species. Onsager[39] proposed an extension of Fick's laws to a multicomponent diffusion by

$$J_i = -\sum_{j=1}^{n} D_{ij} \frac{dC_i}{dx} \tag{2.9}$$

where n is the number of independently variable components. Oishi et al[40] adopted a simplified approach in describing multi-component diffusion which regards the system as pseudobinary. All other components in the system are combined as one species in respect to the species i and the related diffusion coefficient is renamed as an effective binary diffusion coefficient (EBDC) $\bar{D}_B$. Hofmann[41] gave a detailed review of diffusion in silicate melts, and the ionic transport in glasses can be found in reference[42].

According to Hofmann[41], most glass/metal systems, involving interfaces, in fact exhibit chemical diffusion which means that chemical concentration gradients are present in the systems. The chemical diffusion differs from the self-diffusion by showing higher mobilities of cations under the driving force of the concentration gradient and phase-boundary reactions between metal and glass are fast. So far, the most comprehensive study of the kinetics of interfacial reaction as well as dissolution and diffusion of oxide was in a system of iron and sodium disilicate glass by Borom and Pask[43] [44]. If there is no interfacial reaction involved, the dissolution of the oxide layer can be treated as a moving boundary shown in Fig.2.8[44] assuming that the composition at the interface remains constant with time. The amount of substance, M_+, which has diffused in time t is given by

$$M_+ = \frac{2(C_s - C_0)}{1 + erf(\gamma_2)} \left(\frac{\bar{D}_B}{\pi}\right)^{\frac{1}{2}} t^{\frac{1}{2}} \tag{2.10}$$

where C_s is the phase boundary concentration, C_0 the concentration in glass
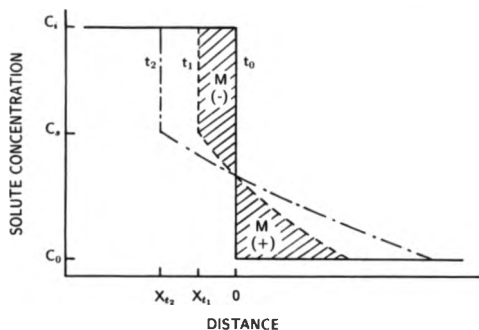
Figure 2.8: Diffusion profile of solute at times t_0, t_1 and t_2 with x indicating position of moving boundary

when $t \leq 0$, $erf(\gamma)$ the error function, and D_B the interdiffusion coefficient of the oxide in the glass.

If, however, the surface concentration of oxide or solute does not remain constant with time, the whole process is considered as a diffusion process controlled by the rate of transfer of material across the interface, i.e. the interfacial reaction. The boundary and initial conditions for this case are

for $0 \leq x \geq \infty$ at $t = 0$, $C = C_0 = 0$;

for $x = 0$ at $t > 0$,

$$J = -D\frac{dC}{dt} = \alpha(C_\infty - C_s) \tag{2.11}$$

where C is the concentration of the solute, C_s the surface concentration at $t > 0$, C_∞ the surface concentration at $t = \infty$, x the distance from the interface, α an exchange coefficient, and D the diffusion coefficient. The diffusion equation under the above condition is given as

27

$$C = C_\infty[erf\frac{x}{2\sqrt{Dt}} - e^{hx+h^2Dt}erfc(\frac{x}{2\sqrt{Dt}} + h\sqrt{Dt})] \qquad (2.12)$$

where $erfc$ is the complement error function and $h = \alpha/D$. The solution to the eq.(2.11) is usually a very complicated process, more important, cases may vary if boundary and initial conditions change, see further discussion in section 5.1.11.

Chapter 3

EXPERIMENTAL

3.1 Scanning Electron Microscopy (SEM)

3.1.1 Introduction

The importance of using scanning microscopy to study metal or ceramic materials has been well established. Extensive literature exists in Bowen & Hall[45], Maurice[46], Greer[47], Newbury[48] and Yokowitz[49].

In a scanning electron microscope, electrons are accelerated by a voltage (5-30kv) from a source, e.g. a filament, through an electron optical column. Lenses form a fine electron beam ($\sim 100 \overset{\circ}{A}$ in diameter) which is focused onto a specimen surface causing electron scattering effects. There are two main types of scattering a) elastic scattering, i.e. electrons change direction with negligible energy loss. b) inelastic scattering, i.e. electrons lose energy with negligible change in direction. These two modes of scattering or interaction between electron beams and specimen, generate a series of electronic signals which are of particular interest. Fig.3.1 and Table 3.1[47] summarize the types of signals and their applications. Among all the information gained in Table 3.1, the secondary electron emission, backscattered electron reflection and characteristic X-rays are the most commonly used analytical mechanisms in scanning electron microscopy.
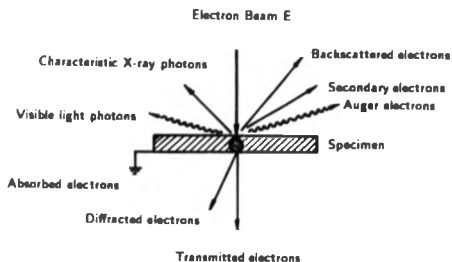
Figure 3.1: Generation of various electron signals under an incident electron beam

MODE	INFORMATION	LIMITS
Secondary electron (emission)	Microtexture Morphology	25 - 100 $\overset{\circ}{A}$
Backscatter electrons (reflective)	Measure of mean atomic number, chemical textural	50 - 2000 $\overset{\circ}{A}$
Cathodoluminescence	Sensitive measure of trace elements	~ 1000 $\overset{\circ}{A}$
Characteristic X-rays	Quantitative chemical analysis Element mapping and distribution displays	> 10^{-17} gramm 1000 $\overset{\circ}{A}$
Specimen absorbed electrons (absorptive)	Surface topograph Atomic number variation	0.1 - 1 μ m
Auger electrons	Light element analysis Element mapping	submicron resolution spatial

Table 3.1: Generation and uses of various eletron signals

3.1.2 Instrumentation

A Cambridge Instruments[50] 250MK III Stereoscan model was used. A lanthanum hexaboride (LaB_6) filament was fitted to act as electron source. In a sample chamber, there are different detectors responsible for picking up various signals such as the secondary electrons, backscattered electrons and characteristic X-rays, all of which are excited from a sample experiencing the direct bombardment of the electron beam. An $8\mu m$ beryllium window is usually placed in front of the X-ray detector for protection. By replacing the window with an ultra thin 1000A Formvar window to decrease the absorption of the X-rays, a windowless detection can be conducted to identify elements with low atomic number $4<Z>7$. This technique is necessary to identify light elements such as oxygen. An energy dispersive X-ray analyzer(EDX), model Link-AN10,000[51], equipped with a microcomputer, was linked to the electron microscope. The X-ray signals were processed in such a way that both quantitative and qualitative analytical data were obtained.

3.1.3 Qualitative and quantitative microanalysis

Qualitative microanalysis provides a rapid identification of the elements in a specimen. When the X-ray spectrum is excited by the electron beam, it may contain several series (K.L.M.) of characteristic peaks which can be used for analysis. For examination of elements below $Z=40$ (Zr), the K series is always chosen while the L series is commonly adopted if $Z>40$. As Z increases, a higher operating voltage is needed to excite K X-ray characteristic lines. This reduces the signal-to-noise ratio and it is claimed that a value of E_oxs (operating voltage) higher than 30kv can increase the possibility of analytical error[49]. In this project, the compositions of specimens (glass-ceramic coatings and metals) have mostly atomic numbers below 40, therefore, the K line is frequently used to identify elements. The operating voltage was chosen between 10-20kV. In general, lower voltage, i.e. 10kV, is suitable for light elements while higher voltage, i.e. 20kV, is ideal for K lines of medium or heavy elements[46]. The specimen, once

cut, was mounted and polished to a $1\mu m$ finish. It was necessary to coat a thin layer of conductive material, usually either carbon or gold, to prevent the localized charging of the specimen under the electron beam. The specimen was tilted at 45° facing the X-ray detector allowing maximum collection of generated characteristic X-rays. A beam current of $6 \times 10^{-8} - 3 \times 10^{-12} A$ was selected with beam diameter of 100-500$\mathring{A}$. A counting rate of typically 1400-2000 cps and collection time of 100s were chosen to collect the X-ray spectrum. A typical qualitative or semi-quantitative X-ray spectrum consists of a horizontal axis displaying the energy in channels of 20ev range and vertical axis representing the total number of counts per channel. With help of the microcomputer, the energy of the characteristic K peaks could be easily located and the elements present identified. Judged from the intensity of the peaks, e.g. the total number of counts within a certain period of time could be compared so that semi-quantitative analysis is achieved.

Quantitative analysis was carried out using similar principles to those described briefly above. The intensities of the peaks were not compared between themselves. Instead, under identical experimental conditions a series of standard materials were analyzed and the characteristic peaks of particular interest were individually stored on the microcomputer. Thus, on analyzing a specimen, the X-ray spectrum was processed such that the identified characteristic peaks were stripped from the spectrum and intensity compared with that of the standard material. The compared relative intensity ratio (commonly called K) can be expressed as following:

$$K = I_{(specimen)}/I_{(standard)} \tag{3.1}$$

A possible source of uncertainty in the K value lies in the statistical nature of the X-ray process. To increase the accuracy of K, count rate, instrumental stability and background radiation effect need to be carefully considered, see Yakowitz[53]. The real concentration of the weight fraction of the element of interest can only be calculated according to the equation:

$$C = K \times K_z \times K_a \times K_f \times K_c \qquad (3.2)$$

K – relative intensity ratio

K_z – atomic number effect

K_a – absorption of X-rays within the specimen

K_f – fluorescence effects

K_c – continuum fluorescence

It is difficult to carry out a quantitative analysis via the above method without lengthy precalibration. Fortunately, a correction programme is usually provided on the microcomputer to overcome the problem. In this project, a ZAF4 correction programme was used and the following comparison is given in Table 3.2(a&b) between the as-mixed composition of multiple component glass used in this project and that determined by quantitative microanalysis described above. It can be seen that the accuracy is within a reasonable range for all detectable elements.

Problems remain particularly with glass and coating/metal interface, though both qualitative and quantitative analysis can be conducted using the SEM linked with the EDX analyzer. Firstly, the glass and glass-ceramic systems used in this research contain lithium and oxygen. They are normally not detectable due to their low atomic number. Even the windowless technique is not adequate to identify lithium. However, lithium is one of the major components in the glass and its role in the system, therefore, remains unclear. Secondly, the determination of light elements, i.e. oxygen, requires a low excitation energy as described previously, also see Barbi et.al[52]. However, according to Rayleigh's law in (3.3), the acceleratin voltage which is inversely related to the wavelength λ must be high enough in order to resolve a very small object. On the other hand,

$$R = 0.61\lambda/a \qquad (3.3)$$

33

Coating Glass	SiO$_2$	Li$_2$O	K$_2$O	ZnO	P$_2$O$_5$	
wt%	78.1	13.0	2.5	4.5	1.9	
Excluding Li and O	Si		K	Zn	P	
Normalized Caculation wt%	84.80		4.81	8.39	1.92	
ZAF4 Analysis wt%	84.77		4.51	8.06	2.65	(a)

Cr$_2$O$_3$ (g) Added per 100g glass	Cr wt% Calculated	Cr wt% EDX Analysed	
0.2	0.316	0.372	
0.5	0.770	0.860	
0.8	1.227	1.488	
1.2	1.829	2.167	
2.0	3.009	3.416	
3.0	4.450	4.937	(b)

Table 3.2: a) Comparison between no-minal glass composition and that obtained by EDX quantitative analysis b) Calibration between EDX analysis and Cr concentration
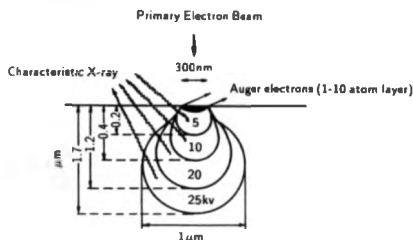
Figure 3.2: Approximate analysis depths given for a chromium sample at varying voltages of the primary electron beam

> R – size of resolved object
>
> a – effective aperture of the objective lens
>
> λ – wavelength of electrons

the resolution is also controlled by the aperture of the objective lens a, which determines the diameters of probe beam. The larger apertures necessary for the smaller beam and higher resolution, however, increases the spherical aberration giving reversed effect on the beam diameter and decreases the depth of field. Therefore, the aperture size has to be compromised. When the investigated area is very small, to image under the limited low accelerating voltage required by the windowless technique whereas using the compromised small aperture will inevitablly lead to poor resolution and low singal to noise ratio. Thirdly, the information depth of EDX analysis varies according to the accelerating voltage. Fig.3.2 shows a schematic diagram of the analysis depths for EDX on a chromium sample at differing accelerating voltages[53]. Using the formula of Read discussed in the following[54], Sturgeon[26] calculated the X-ray emission diameter of similar glass as $1.5\mu m$ for an accelerating voltage of 15kv.

$$r\rho = \kappa(E_o - E_c) \tag{3.4}$$

E_o – accelerating voltage of electrons(kv)

E_c – absorption energy of X-ray edge for element

analyzed(kv)

ρ – density(g/cm3)

r – diameter of X-ray emission volume(μm)

This means that when the size of the investigated area is smaller than 1.5μm, some unwanted information comes from the immediate environment. This phenomenon often occurs when the electron beam hits the thin interfacial layer sitting in a glass-ceramic matrix. As a result, the information sometimes can be very misleading.

3.1.4 Element distribution: line scans

The line scanning technique was used in this project in order to deal with the analysis of element distribution. This is a particularly useful technique to investigate semiquantitatively the interdiffusion across the interface of glass and metal. As the electron beam is scanned continuously, the energy of specific X-ray peaks, intensities representing concentrations of the elements, are picked up and the output used to modulate the CRT screen to display lines showing the element distribution along the scanned route. Because the individual element is processed separately via different "windows" in a linked microcomputer, in a single scan each individual element concentration is presented as intensity along the scanned route without interference to each other. The line scanning time was controlled at 100 seconds and scanning route was in the range of 40-100μm.

3.1.5 X-ray Mapping

The X-ray mapping is a similar technique to the line scan, but the X-ray signals representing elemental distribution from certain areas instead of a scan route

are accumulated within a pre-set period of time. The signals are processed such that the brightness of image is proportional to the concentration of the element. Therefore, X-ray mapping can reveal the local enrichment of different elements in an analytical area of interest.

3.2 Transmission Electron Microscopy(TEM)

3.2.1 Introduction

The use of transmission electron microscopy in materials science has been well developed. The high accelerating voltage and thin specimen allow better resolution and larger magnification of the image than the scanning electron microscope described in section 3.1, also see reference[55] and [56].

Referring back to Fig.3.1, we notice that the electron beam interacting with a specimen causes electron scattering effects. If the specimen is thin enough to transmit the electrons, the transmitted electrons can be used as signals based on which the transmission electron microscope is operated. Basically, the amount of electron scattering which occurs(i.e. the percentage of electrons passing through a certain region of the specimen which are scattered) depends on the number of atoms in that region of the specimen and their mass. Therefore, different structures give different proportions of scattered electrons and contrast can be used to form an image on a screen[57]. Diffraction contrast is another useful mechanism widely adopted in TEM. When the specimen consists of a perfect single crystal of identical atoms, assuming that a homogeneous thickness has been achieved, at all points in the specimen the density and the species of atom are the same and we can expect to see no contrast in the image between one part and another through scattering contrast. But, in terms of Bragg's law: $2d sin\theta = \lambda n$, if the electron beam is exactly at the Bragg angle to a certain set of lattice planes, diffraction will occur and the majority of electrons will leave the specimen at an angle 2θ to the incident beam. Therefore, certain electron diffraction patterns can be generated from which parts of the examined specimen can be

37

distinguished as crystalline, amorphous or regions of both types. Furthermore, the specific crystal structure can be identified according to the regular array whose spacing from the centre of the pattern is inversely proportional to the distance between the lattice planes[58].

The direct study of the interfacial structure of a metal/glass interface by transmission electron microscope is difficult due to specimen preparation problems. The development of a successful procedure for the preparation of a suitable, thin specimen of similar metal/oxide interface for TEM examination and analysis was first accomplished only in 1980 by Manning and Rowlands[59]. Various modifications have been made since then by a number of investigators including Newcomb and Stobbs et. al[60]. While the individual techniques differ in detail, they all involve the shielding of the interface, usually by making a sandwich type specimen with the oxide in the centre, mechanically thinning the "sandwich" until it is less than $100\mu m$ thick and, finally, ion beam milling the sample to the stage required. Actual usage of TEM on some simple metal/ceramic systems can be found in reference [24] and [61]. As for the studies on the interfacial structures of metal/glass or metal/glass-ceramic, there is very limited information. The basic problem remains that the glass coating and metal substrate thin at different rates during the ion beam milling and this results in major difficulties. The problem has been partially alleviated by the recent availability of commercial prethinning or "dimpling" instruments which can be used to reduce the thickness of the specimen (sandwich type), further down to a few tens of micrometers, before ion beam milling. With help of this technique, a few TEM specimens have been successfully prepared in this research project. However, specimen preparation is still far from routine; considerable care and sometimes sheer luck are needed.

3.2.2 Instrumentation

Both JEOL2000FX and JEOL1000 transmission electron microscopes[62] were used in this project. The operating voltages are 200kV and 100kv respectively.
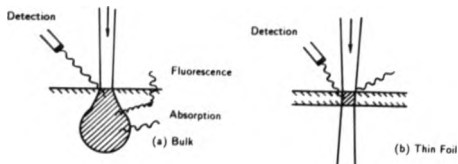
Figure 3.3: Activated volume formed in bulk and in thin specimen

Both TEM have EDX analyzer models 860 series II. When the microanalysis was carried out on the JEOL1000, the counting rate was set at 1500cps while a time of 100s was chosen to ensure a sufficient signal to noise ratio. The JEOL2000FX operates at a higher voltage which gives higher resolution. It is particularly useful for identifying submicron size microstructure and conducting electron diffraction analysis. A camera length of 80cm and operating voltage of 200kv were chosen to standardize the diffraction condition from which the theoretical calculation of the lattice parameters can be derived. When the EDX analysis was conducted on the JEOL2000FX, the operating voltage was 200kv and the counting rates and time were 1000cps and 100s respectively.

3.2.3 Microanalysis via EDX

EDX analysis on the TEM is very similar to the analysis described in section 3.1.3, but has a vast improvement compared with the results gained on the SEM, because the large, bell shaped region produced by the diffusion of the electrons beneath the surface of a bulk specimen, in the case of SEM, is absent in a thin foil specimen used in the TEM, see Fig.3.3[63]. In this thin specimen the activated volume from which X-rays are detected is a cylinder with a diameter
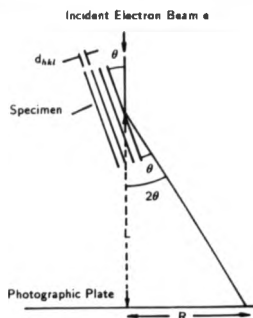
Figure 3.4: Formation of electron diffraction pattern in an electron microscope

equal to that of the incident electron beam. The difference in spatial resolution between a bulk and a thin specimen can be up to $100000\times$. Thus through EDX microanalysis on TEM, smaller microstructures can be resolved with more accuracy.

Problems remain, in spite of improvements on quality of EDX microanalysis by TEM. In the case of glass-ceramic materials, crystals are embedded in the glass matrix. This makes it extremely difficult to strip the background completely from the feature required. Unless both sides of the crystal are ion beam milled free from glass matrix some background information is inevitably excited by the electron probe to give the interference.

3.2.4 Structure Determination via electron diffraction

From Fig.3.4, by combination of simple geometry and the Bragg law, the basic formula for the analysis of diffraction patterns can be derived as:

$$Rd = \lambda L \qquad (3.5)$$

R – distance between the central diffraction spot and

other diffraction spots or rings

d – lattice spacing

λ – electron wavelength, varying with

accelerating voltage, 0.004nm at 80cm

L – diffraction camera length

Therefore, if values of R, L, and λ for a diffraction spot or ring can be measured, then the d-spacing of the set of lattice planes giving rise to that spot or ring can be determined. In this project, a P-Cr compound, a product of interaction between metal substrate and glass-ceramic coating, cannot be adequately identified by EDX analysis on both SEM and TEM since its size is less than $1\mu m$. The electron diffraction was used to determine the structure of this crystal.

3.3 X-ray Diffraction Analysis (XRD)

X-ray diffraction analysis is a well established technique to identify various crystal phases of metal, glass-ceramic and ceramics. The essential Bragg law described in previous sections stating: $n\lambda = 2dsin\theta$ is also the principle for X-ray diffraction. When a beam of X-rays, usually excited from a copper target with a wavelength of $1.5417\overset{*}{A}(K\alpha)$ bombards a crystal phase, a series of diffracted beams is obtained according to the inter-planar d spacings of the crystal. By rotating the crystal sample to change the angles between the incident beam and crystal planes, θ, a series of intensified signals or peaks can be recorded on a diffractometer. The data of different d and θ with a constant λ can lead to an identification of a specific crystal sample simply by comparing the data obtained with the standard J.C.P.D.S. data file.

In this research project, X-ray diffraction analysis was widely used to establish the crystal phases present in the bulk glass-ceramic and the coating. It was also used to identify some interfacial crystal phases produced by interaction at the interface. To determine crystal phases in the glass-ceramic coating, the coating material needs to be ground into fine powder after it is separated from the
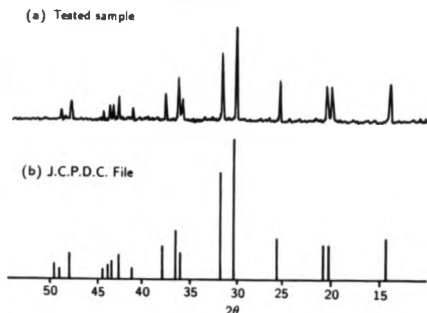
Figure 3.5: Identification of a specific crystal phase $LiCr(SiO_3)_2$ via XRD

substrate metal. In contrast, when the structure of an interfacial layer needs to be identified, the layer is kept on the coating assembly but the unwanted exterior coating is dissolved by HF solution. The XRD in this project was conducted using a Philips powder diffractometer[65] with a sample rotation rate of $1°$ (2θ) per minute and counting rate of 10^3 cps. A typical comparison between crystals in a glass-ceramic and standard J.C.P.D.S. is illustrated in Fig.3.5 showing the best fit of the peak patterns and therefore the confirmation of the crystal phases presented.

3.4 Differential Thermal Analysis (DTA)

Differential thermal analysis (DTA) is a technique involving heating or cooling a test sample and an inert reference sample to record any temperature difference between them under identical conditions. When a transition occurs from glass to crystallized phase, or a crystal phase melts, the energy in the form of heat is released or absorbed. If the change of temperature is plotted against temperature, both exothermic peaks indicating rise of temperature and endothermic dips indicating fall of temperature can be recorded. A full guide to DTA exists

42

A: Annealing point
B and C: Exothermic peaks due to
formation of crystal phases
D: Endothermic effect due to first melting
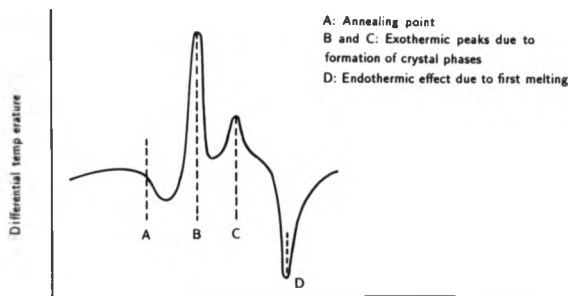
Figure 3.6: Differential thermal analysis curve for a devitrifiable glass

in Pope and Judd[64].

In this project, DTA was carried out on DTA673-4(Stanton Redcroft) [66] and SiO_2 was used as the reference material. The two materials including the test sample were heated at a constant rate of $8°C$ per minute. Fig.3.6[7] shows exothermic and endothermic dips for a typical devitrifiable glass powder. The DTA provides very useful information especially in terms of temperatures at which the desired crystal phase start to grow or disappear. This is particularly important when dealing with glass ceramic material since the essential crystallization process is highly dependent on thermal treatment. Further discussion is given in section 4.1.2.

3.5 Thermogravimetric Analysis (TGA)

Thermogravimetric analysis (TGA) is useful in monitoring the weight change of a sample against temperature in either heating or cooling, or as a function of time for isothermal condition. This technique is particularly effective when the sample

experiences chemical reactions or physi-chemical processes involving weight loss or gain. A Stanton Redcroft TG750 thermobalance[66] was used in this project and both quantitative and qualitative measurement were made to observe mainly metal oxidation as well as other processes. The sample weight could be up to 1g and the maximum temperature was $1000°C$. The results obtained are given in section 4.1.3 and 4.2.2

3.6 Electron Spin Resonance Analysis (ESR)

Electron paramagnetic resonance (or electron spin resonance) is a sensitive method to investigate particular redox states of certain elements[67], and the oxidation-reduction equilibria of multivalent elements in silicate melts or glass have been widely discussed by Schreiber et. al.[68]. The redox reactions between the coating and substrate metal were observed in both Nimonic/glass-ceramic and titanium/glass-ceramic coating systems in this project and therefore the use of ESR was employed to assist the identification of individual redox reactions.

Cr is one of the basic elements in the Nimonic alloy substrate used. Because of its diffusion into the glass-ceramic coatings during the redox reactions, its redox states can exist as Cr^{+2}, Cr^{+3} and Cr^{+6}. Resonance absorptions are obtained in the ESR spectra for Cr^{+3} but not Cr^{+2} or Cr^{+6}[69]. Thus ESR distinguishes redox states of diffused ions and leads to determination of redox reactions. A typical ESR spectrum for Cr doped glass[67] in Fig.3.7 shows two peaks of δ and γ in the Cr spectra. The first peak δ occurs when doped Cr^{+3} has a low concentration so that isolated Cr^{+3} ions are octahedrally coordinated. As the Cr^{+3} concentration increases a dominating symmetric γ peak builds up due to coupled pairs of Cr^{+3} ions which themselves are individually 6-fold coordinated. In contrast, Cr^{+2} and Cr^{+6} ions should not register any ESR signals, because their electron configuration is prone to Jahn-Teller distortion from their octahedral coordination.

The ESR spectra of glasses studied in this project were recorded on a ESR spectrometer Decca-X1[70], operating in the microwave band at ambient temper-
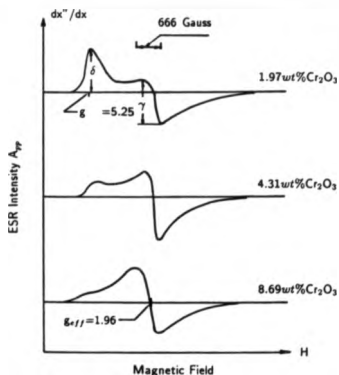
Figure 3.7: ESR spectra of Cr^{+3} in ZnO-Al$(PO_3)_3$ glass as a function of Cr_2O_3 content

ature. Approximately 20mg aliquots of samples, finely powdered, were analyzed in a matched 3mm fused quartz tube and to make quantitative comparisons, all analyses were normalized to a common set of ESR conditions (i.e. same gain, amplitude, and same sample size). Meanwhile, a series of glasses doped with varying concentrations of Cr_2O_3 were measured as standards so that further comparison could be made to determine the concentration of Cr^{+3} in unknown samples, see Fig.3.8. Since Cr diffusion into the glass studied is severe, the δ peak caused by trace Cr^{+3} in ESR spectra was neglected and the Cr doped glasses have a concentration range of 0.1-4wt%. It is worth pointing out that the ESR measurement for Cr^{+3} is limited to a concentration of 1.3wt% in this particular coating glass system since the saturation level of Cr^{+3} is then reached and consequently Cr^{+3} ions are not accommodated in the octahedral coordination but in an environment of $LiCr(SiO_3)_2$ precipitates in the glass. The change of environment of Cr^{+3} is shown in the ESR measurements by the curvature of the amplitude/concentration plot for concentration of Cr_2O_3 in excess of $\sim$2-2.5wt%

45
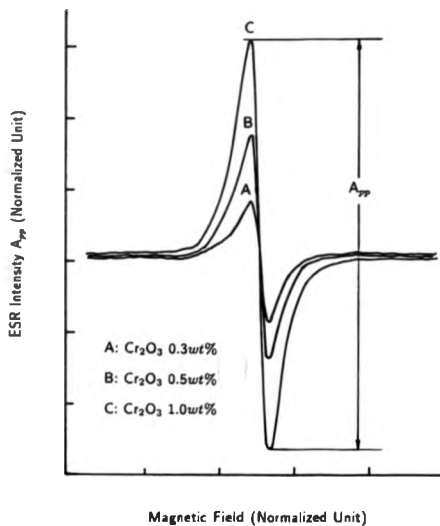
Figure 3.8: Typical ESR spectra for Cr_2O_3 doped Li_2O-SiO_2 glass as A_{pp} varies with the concentration of Cr_2O_3

corresponding to the Cr^{+3} concentration of 1.3wt%. Though the change affects the ESR measurement, it confirms the limitation of intake of Cr^{+3} in the glass system.(see more discussion in section 5.1.11.)

3.7   Chemical Analysis

Chemical analysis was used in this study to assist in determination of the Cr^{+2} concentration in the glass coating. Indirect chemical analysis, combined with ESR analysis, help to quantitatively measure the concentration of Cr^{+2}, Cr^{+3} and total Cr respectively. The chemical analysis procedure was adapted from the basic technique of Palecek & Peters[71], see Appendix 1. In this combined analysis, the Cr^{+2} concentration is derived by the difference of Cr^{+3} which is determined by ESR and total Cr concentration which is determined by this chemical colorimetric method.

3.8   Thermal Expansion Coefficient Measurement

The thermal expansion coefficients of substrate metal and coating glass or glass-ceramic are key factors in bonding two materials together because the close match of the thermal expansion coefficient minimizes the thermal stress at the interface of the coating assembly.(see section 2.3.)

The coefficient of thermal expansion was measured with a home-made fused silica dilatometer. Samples are usually cut into rods of 15mm length and reasonable cross section size to be accommodated in the apparatus. When the sample is heated or cooled in a furnace, the thermal expansion or the displacement is measured by a linear variable differential transducer (LVDT) whose electrical output varies with the displacement and can be recorded by a chart recorder. The apparatus was calibrated with a standard platinum rod to offset the error introduced by thermal expansion of the silica holder, and the specimen was heated from the room temperature at a rate of 2°C per minute up to the temperature required, usually 1000°C.

3.9 Measurement of Coating Adhesion

The measurement of coating adhesion is necessary to assess the bonding strength between the substrate metal and coating material. There are various ways of measuring the coating adhesion and most of them involve deformation or removal of the coating from the substrate metal by impact, bending or torsional twist, parallel shear and tensile loading. The adhesion tests for porcelain enamels or steel are given by A.S.T.M. C313[72] and P.E.I. Bulletin[73]. The use of fracture mechanics methods observing energy for crack propagation in the interface region was developed by Suga[74] and Berndt[75] et.al for plasma sprayed coatings. A relatively easy and quick evaluation of the bonding strength is achieved by a tensile pull method, see A.S.T.M. C633[76] and King[21].

The procedure of the tensile pull method, see appendix 2, requires an adhesive to bond a metal stud to the coating and the metal stud is connected with a self-aligned bar which exerts a tensile load to the stud. If the strength of the adhesive is stronger than the adhesion between the metal and coating, the coating can be pulled from the substrate metal. Judged from the energy applied to pull off the coating and also the area from where the coating is removed, the energy per unit area can be evaluated to measure the adhesion strength of the coating. Fig.3.9 schematically illustrates the device used in the tensile pull test. But, limitations remain in the test. They are a) a strong adhesive is needed to carry out the tensile stress, otherwise, the stud comes off before the coating is pulled away from the substrates. b) in spite of the self-aligned characteristics of the device, absolute line-up is too difficult to achieve so that certain shear forces act on the coating. This affects the accuracy of the strength measurement. c) being a brittle material, the glass-ceramic coating tends to fracture under the tensile load. The fracture is initiated by flaws which are randomly located, hence, the breaking point at which the coating fails from the metal substrate is rather inconsistent. As a result, a large number of measurements are needed for a single value. Nevertheless, the tensile pull test gives a very simple guidance to estimate the possible bonding strength between the coating and substrate. The

48
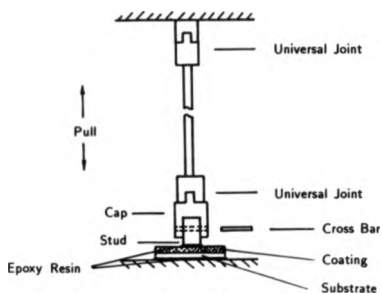
Figure 3.9: Tensile strength test for coating on substrate

results obtained in the Nimonic/glass-ceramic system in this project are shown in section 5.11.

Chapter 4

EXPERIMENTAL
PREPARATIVE TECHNIQUES

4.1 Material Preparation

To coat glass-ceramic onto metal successfully, both glass-ceramic and metal must
be chosen and prepared properly to achieve certain bonding requirements. In
addition, to obtain fundamental information on interaction and interdiffusion,
both glass-ceramic and metal should be well-characterized materials to avoid
any unnecessary complications caused by the uncertainty of these materials.

4.1.1 Glass compositions and their preparation

The glass composition used to provide experimental coatings on Nimonic alloy is
from the lithia-silica system (Li_2O-SiO_2) given in Table.4.1(glass A). The Li_2O-
SiO_2 glass system and its glass-ceramics have been well documented (see McMil-
lan[7]). In this system, SiO_2, as known widely, acts as glass former while Li_2O is

	SiO_2	Li_2O	K_2O	ZnO	P_2O_5
$wt\%$	78.1	13.0	2.5	4.5	1.9

Table 4.1: Glass-ceramic coating composition for Nimonic alloy

a major modifier. Other modifiers include K_2O and ZnO. Both the K_2O and ZnO favour the development of quartz as the silica crystal phase on conversion to the glass-ceramic. This is preferred to other silica phases such as cristobalite as the latter experiences a huge change of thermal expansion coefficient during heating or cooling of the glass-ceramic [77]. P_2O_5 is added as a nucleation agent to help the glass to form numerous nuclei, based on which, heterogeneous nucleation and crystallisation of the major phase develop. The major crystal phases desired in this glass-ceramic are quartz(SiO_2) and lithium disilicate(Li_2O2SiO_2). Both phases having high coefficients of thermal expansion of 132×10^{-7} and $116\times10^{-7}/°C$ respectively in the temperature range of 20-1000°C, the glass-ceramic can have an average coefficient around $130\times10^{-7}/°C$ to match reasonably closely to that of Nimonic alloy of $150\times10^{-7}/°C$. The lithium-silicate glass-ceramic system is the most preferred coating material from the whole range of glass-ceramic systems because of the close match of the expansion coefficients.

The glass-ceramic system used to coat titanium metal is a similar lithium-alumino-silicate (Li_2O-Al_2O_3-SiO_2) shown in the Table 4.2(glass B). This glass gives lithium metasilicate (Li_2OSiO_2) and β-spodumene/ quartz (s.s.) ($Li_2OAl_2O_1$ $4SiO_2/SiO_2$) as final crystal phases on conversion to the glass-ceramic. The composition is designed such as to give a thermal expansion coefficient close to that of the titanium metal of $91\times10^{-7}/°C$. Other alternative glass compositions, listed also in Table 4.2, were chosen to study the interactions between the coatings and titanium substrate. Due to severe interactions, described in the following chapter 5, the broad range of glass or glass-ceramic compositions are necessary in order to explore the possible mechanisms of the interactions and search for better coating compositions.

The chemicals used to make the glass are "Analar grade" reagents consisting of the oxides P_2O_5, ZnO, Al_2O_3 together with the carbonates Li_2CO_3, K_2CO_3, Na_2CO_3 and $CaCO_3$. The mass of carbonate added was that calculated to give the required quantity of oxides on decomposition. SiO_2 was introduced as Limoges quartz with impurity levels of K_2O 40, Na_2O 60, Li_2O 20, Al_2O_3 160, and Fe_2O_3 10 ppm. The required amount of chemicals were homogenized

51

	SiO_2	Al_2O_3	Li_2O	Na_2O	K_2O	CaO	MgO	P_2O_5
wt%	68.2	13.0	11.1		5.0			2.7
	Experimental composition							
mol%	60		20				20	
	60			20			20	
	60				20		20	
	65	5	30					
	65	5		30				
	65	5			30			
	60	10				30		
	60	10					30	

Table 4.2: Experimental coating compositions for titanium metal

by tumbling for 12 hr and then melted in a 90Pt/10Rh crucible in an electric furnace for 3hr. The temperature used was 1360°C for alkali containing batches and 1450°C for alkali free batches. The melt was quenched into deionized water and remelted for a further 3hr to ensure homogeneity. The final melt was cast into deionized water and dried in an oven. Part of the melt was cast as bulk glass in air and then annealed to eliminate thermal stress.

4.1.2 Conversion of the glasses into glass-ceramics

The conversion of the lithium silicate glasses into glass-ceramic is well reviewed in the literature [78] [79] [80]. The usual procedures of conversion of glasses to glass-ceramics include two stages A) nucleation B) crystallization. They are the controlled stages to increase the number of nuclei and to produce crystal growth. In general, the maximum nucleation does not occur at the same temperature as the maximum crystallization(Fig.4.1). Therefore, change of the temperature and time, i.e. heat treatment, will produce different microstructures of the glass-ceramics. By varying the heat treatment on a designed composition, a controlled glass-ceramic with desired properties can be produced.
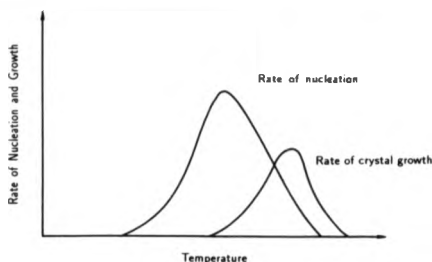
Figure 4.1: Rate of nucleation and growth versus temperature

The two basic glasses A and B used in this project for Nimonic alloy and titanium metal were analyzed by DTA. Fig.4.2 shows the differential thermal behaviour of both glass A and glass B. For glass A, the first exothermic peak at 620°C indicates the formation of crystalline lithium disilicate(Li_2O2SiO_2), and the second exothermic peak at 790°C is due to the appearance of α-quartz(SiO_2). The endothermic dip at 970°C shows the melting of the lithium disilicate phase. As recommended from the literature cited above, a heat treatment procedure was designed at 600°C for 3hrs and 800°C for 3hrs during which the temperatures correspond with those of specific crystal growth. XRD results in Fig.4.3(a) confirm the predicted crystal phases as lithium-disilicate (Li_2O2SiO_2) and α-quartz (SiO_2) after glass A was converted into the glass-ceramic. Glass B was also measured and heat treated at 600°C and 850°C for 3hrs respectively. The two major crystal phases are lithium metasilicate (Li_2OSiO_2) and some solid solution of β-spodumene/quartz ($Li_2O\ Al_2O_34SiO_2$), see also Fig.4.3(b). The thermal expansions of bulk glass A and glass-ceramic A were measured as 94.2 and 140.1×10^{-7}/°C respectively. Similar results for glass composition B are 78 and 97×10^{-7}/°C respectively. Fig.4.4 illustrates the closely matched thermal expansions of the coating materials on both Nimonic and titanium substrates (0-900°C).

It has to be pointed out that glass-ceramic produced from bulk glass may differ significantly from that of glass powder as the powder has a large surface
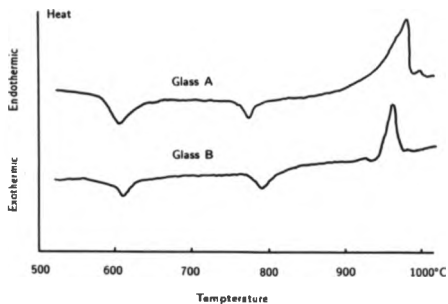
Figure 4.2: Differential thermal behaviour of glass A and glass B
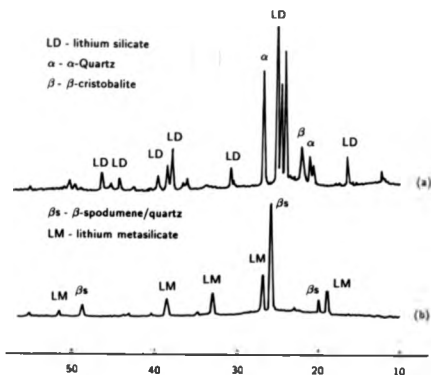
Figure 4.3: XRD (a&b) reveals the crystal phases formed after heat treatment of bulk glass A and glass B

54
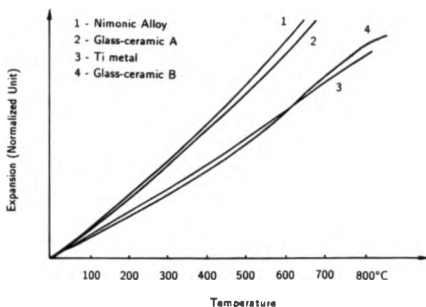
Figure 4.4: Closely matched thermal expansion between chosen metals and their coating glass-ceramics

energy to enhance the nucleation and crystallization process. Therefore, it is possible to omit the nucleation stage and bring the sintered enamel coating directly to crystal growth to convert the structure to a glass-ceramic[81]. In this study, as the coating was originally applied to the substrates as powder, the heat treatment was shortened to 30min at 600°C and 1hr at 800°C. In a simulated experiment, a powder slurry was made, which was then processed into a green rod. It was fired and heat treated under the same conditions as the coating shown in Fig.4.5 (a)&(b). The powdered samples were partially crystallized before the heat treatment was applied. XRD in Fig.4.6 (a)&(b) shows their structures after heat treatment. It can be seen that, in the powder route, glass-ceramic A for Nimonic alloy coating, α-quartz is diminished and tridymite and cristobalite dominate when compared with the structure of bulk glass-ceramic A in Fig.4.3. Powder route B shows little difference in its crystal type compared with its bulk glass-ceramic. Both powder route glass-ceramics A and B have thermal expansions of 136.6 and 100×10^{-7}/°C respectively showing fortunately
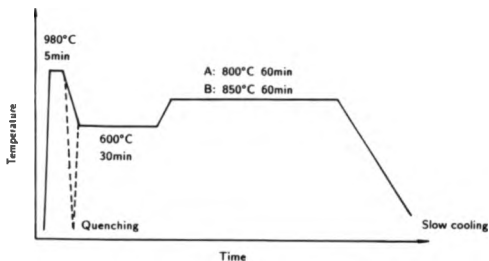
Figure 4.5: Firing and heat treatment for coating A and B
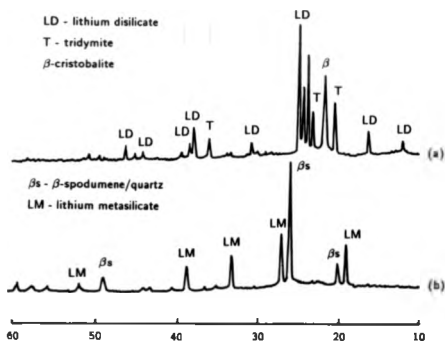
Figure 4.6: XRD (a&b) shows structure of powder routed glass-ceramic A and B

that there is only a little change from what was originally desired in terms of their thermal expansions.

4.1.3 Metal pretreatment and preoxidation

Both Nimonic alloy and titanium metal sheets were pretreated before the glass-ceramic coating was applied. The as-received sheets were vapour blasted, during which glass beads(0.2mm) were mixed with high pressure water at 40 p.s.i. pressure and blasted directly on the sheets in order to create a fresh, clean and also roughened surface. The vapour blast is necessary to enhance the adhesion between the metals and coatings as the surface roughness increases the mechanical interlock described in chapter 2. The vapour blasted sheets were cut into 10×10 mm square, degreased ultrasonically in acetone followed by washing in deionized water and drying.

Preoxidation is required for the metal sheets. The preoxidation was carried out in an open ended tube furnace in which all samples were rested on a refractory brick while temperature and time varied according to the chosen process. After being exposed to the air at a certain temperature, the oxidized samples were withdrawn from the furnace and stored in a sealed plastic bag when they had reached room temperature. Sections 5.1.8 and 5.2.7 give detailed results of the effects of preoxidation on the bonding and interactions.

4.2 Coating Procedure

4.2.1 Glass powder and ink formation

The glass melt, prepared as in section 4.1.1, was ball milled for initially 3-4 hr, then, methanol was added to the mill to give wet milling for a further 36hr. The resulting powder was dried and sieved to <200 mesh. The glass powder was made up into a paste or ink, suitable for coating application, in two different ways: a) an appropriate organic binder (Blythe 64/83)[82] was used to provide
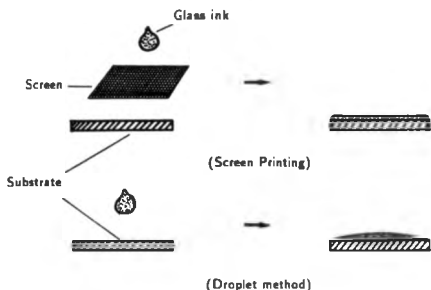
Figure 4.7: Schematically showing two methods of coating glass powder onto a substrate

a thick paste suitable for screen printing b) water was used to form a thin paste which can be used to form a "droplet" coating.

4.2.2 Screen printing techniques

The screen printing (printer supplied by Dek. Ins. Ltd)[83] technique was used to apply a thin layer of coating on metals in this project. In the screen printing process, the metal was positioned under a stainless steel mesh screen which carried an emulsion mask and the glass powder paste could be "printed" through the "mask" on to the metal. Under normal operating conditions, one screen printed layer does not form a sufficient thickness of coating. To obtain a thickness of 60-100μm three applications were needed. Another simpler technique of coating was also used to obtain a thickness of 100-150μm of glass powder layer. During this "droplet" method, a drop of slurry, mixture of glass powder and water, was directly applied onto the metal sheet and spread evenly. Due to the simplicity of this method, the procedure is easier but the control of the thickness can be more difficult. These two coating procedures are schematically illustrated in Fig.4.7(a)&(b). The printed layer of glass powder needs to be heated at a

58
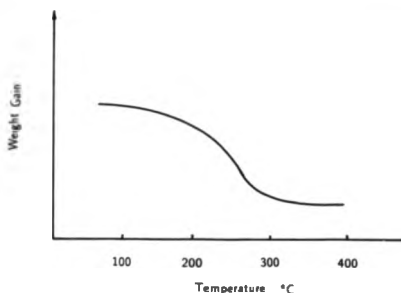
Figure 4.8: TGA shows the temperature at which organic binder burns off

reasonable temperature to burn off the binder. The results obtained from TGA analysis in Fig.4.8 show that the organic binder will decompose completely if the temperature is raised above 270°C. In this project, all screen-printed coatings, have been heated at 300°C for 15min to eliminate the binder residue before the coating is subjected to further treatment.

4.2.3 Firing condition and heat-treatment

The coated glass powder layer is fired at a suitable temperature for sufficient time to obtain a layer of homogeneous and nearly pore-free vitreous enamel before this layer could be converted into glass-ceramic. The firing was carried out in a gas tight tube furnace shown in Fig.4.9. To prevent excessive oxidation of the metal, an inert gas (commercial oxygen-free N_2 or Ar) was used during all the firing stages. A small sample bed was designed to hold the sample as close as possible to the thermocouple to get an accurate temperature reading as indicated. The furnace was heated to the required temperature and N_2 flow commenced so that after a certain period of time the temperature distribution along the tube was sufficiently stable to start the test. To maintain the glassy state of the coating layer, some samples taken from the tube were quenched
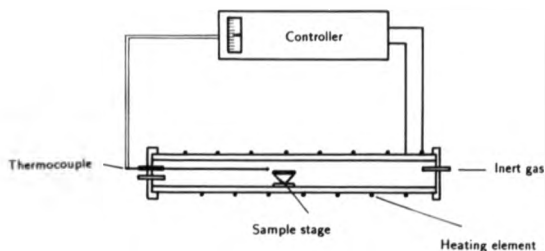
Figure 4.9: Tube furnace in which firing and heat treatment were carried out

onto a plate of metal. The heat-treatment was carried out in the same furnace under similar conditions but temperature and time was altered according to heat treatment requirements. The quenched samples were replaced in the furnace where the temperature was preset for nucleation and on completion of nucleation the temperature was raised for crystallization. The final samples were withdrawn from the furnace after the heat-treatment was finished. The firing and heat-treatment procedures were illustrated in Fig.4.5 and other detailed parameters are mentioned in the following section 5.1.3 and 5.1.4.

The following flow chart in Fig.4.10 summarizes the whole procedure through which the glass-ceramic coating is produced.
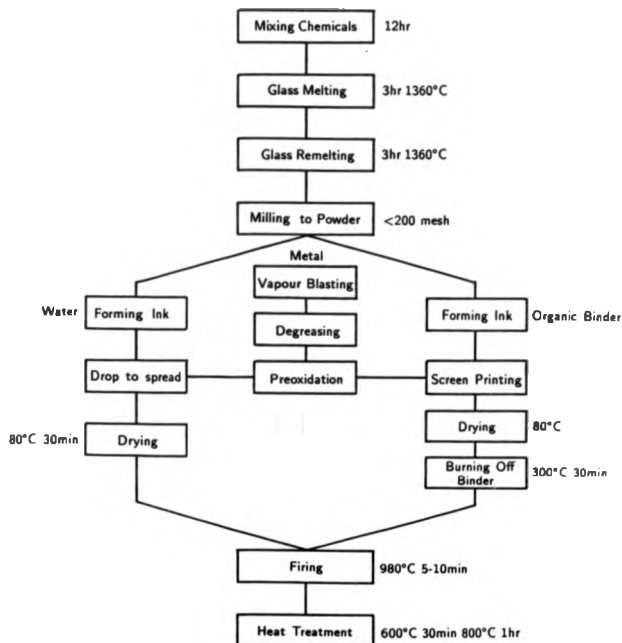
Figure 4.10: Procedures of glass-ceramic coating on metals

Chapter 5

RESULTS AND DISCUSSION

5.1 Coating on Nimonic Alloy Sheet

5.1.1 Introduction

Nimonic alloy 263 belongs to the Ni-Cr super alloy group which has been used widely in the aero industry. However, there is little work involving glass or ceramic coating on this particular type of alloy. Most of the relevant work concerning bonding between ceramics and substrate alloys concentrates on Ni-Cr dental alloys and other Cr-containing alloys such as Inconel. Reference[84], [18] and [85] give a few examples of similar studies in which various interactions caused by Cr were reported. Apart from other related works quoted in various parts of this thesis, main work involving glass or glass-ceramic coating on Inconel alloys has been reported during and on completion of this thesis work (see Loehman et.al. (1987), Moddeman et.al. (1989), and Metcalfe et.al. (1990)). In this project, the as-received Nimonic alloy sheets were pretreated. Both unoxidized and oxidized sheets were coated with glass powder either through screen printing or droplet techniques. The coated assemblies were subject to firing and heat-treatment to achieve a well-spread and strongly adherent layer of glass-ceramic. The glass-ceramic coated Nimonic alloy underwent microscopic examinations and compositional analysis of the interface to detect any possible

	%
C	0.04-0.08
Si	0.40max
Mg	0.60
S	0.007
Ag	0.005
Al	0.60
B	0.0005
Bi	0.0001
Co	19.0-21.0
Cr	19.0-21.0
Cu	0.20
Fe	0.7
Mo	5.6-6.1
Pb	0.0002
Ti	1.9-2.4
Ni	Balance

Table 5.1: Composition of Nimonic 263 alloy

interactions between the alloy and enamel and their influence on the subsequent microstructure development. Based on these examinations, some understanding of the mechanisms of adhesion between the alloy and glass-ceramic has been obtained. Various parameters which contribute to a successful adhesion have also been explored.

5.1.2 Morphology of uncoated alloy surface

Nimonic 263 alloy has the composition shown in the Table.5.1. SEM reveals the difference between as-received and pretreated alloy surfaces(Fig.5.1a&b). It is obvious that the pretreatment, i.e. vapour blasting, increases the roughness of the alloy surface. The roughness of the vapour blasted surface was recorded on a talysurf (Rank Taylor Hobson)[86] and a comparison was made with an unblasted surface (Fig.5.2). The uncoated alloy sheets were subject to a preoxidation treatment to grow a layer of oxide required in the subsequent coating procedure. An approximately 90mg sample of the roughened alloy was tested

63
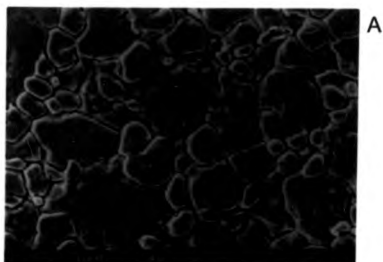
Figure 5.1: Surface of Nimonic alloy A) as received B) after vapour blasted

Surface Distance
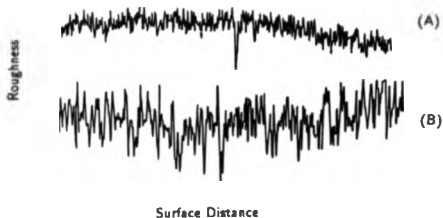
Figure 5.2: Surface roughness of A) as received alloy B) vapour blasted alloy

using TGA to observe oxide growth. It is found that the weight gain against time follows a parabolic law(Fig.5.3). Hauffer[87] described in detail the oxidation behaviour of various materials. Parabolic increase of weight, when the metal is exposed to the oxygen at constant temperature, refers to growth of the metal oxide according to:

$$Y = \alpha X^{1/2} \qquad (5.1)$$

Y – weight gain of oxide

α – coefficient factor

X – time

It is important to notice that in the case of parabolic behaviour the rapid growth of oxide usually occurs at the beginning of the oxidation. As time proceeds, the growth eventually slows down and levels off at a certain stage. From Fig.5.3 it seems that the Nimonic alloy is oxidized fairly rapidly during the first 3hrs. Thus, when a fully-grown layer of oxide is required, a long time is always preferred since long time tends to produce a well-grown oxide layer. The alloy which is briefly preoxidized can be problematic because further oxidation will take place in the process of firing, during which the growth of oxide can affect sintering
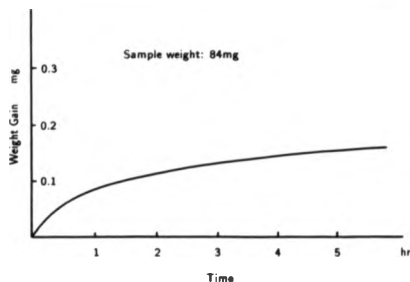
Figure 5.3: Oxidation behaviour of Nimonic alloy at 900°C in air

of glass powders (see the section 5.1.8.). The oxide growing on Nimonic alloy by preoxidation in air was confirmed as Cr_2O_3 by XRD in Fig.5.4. This agrees with the observation of most Ni-Cr super alloys whose oxidation is dominated by growth of a Cr_2O_3 rich adherent layer [87] [88]. EDX analysis also revealed a very small amount of TiO_2 in the Cr_2O_3 rich layer indicating Ti, one of the minor components of the substrate alloy, was oxidized during the preoxidation treatment. Due to the low concentration of Ti in the alloy, the formed TiO_2 is likely to exist as a solid solution in the dominating Cr_2O_3 layer, see also Fig.5.4. An interesting phenomenon of Cr diffusion in the alloy, during the process of oxidation, was found in this project. The Cr_2O_3 mainly and rapidly develops at the grain boundary area and only after a long period of time(1hr at 800°C) does the oxide eventually cover the whole surface. Clearly defined grain boundaries indicate the difference in composition between the boundaries and the rest of the surface area. EDX analysis in Fig.5.5 proves the enrichment of Cr_2O_3 at the grain boundaries. Moulin[89] et.al. observed volume and intergranular diffusion on oxidation of alloy of Ni-Cr between 800-1300°C. They claimed that a) the Cr diffusion is effectively intergranular and more rapid than Ni, therefore, as the first step, Cr_2O_3 develops mainly between the grains of the alloy, i.e. grain
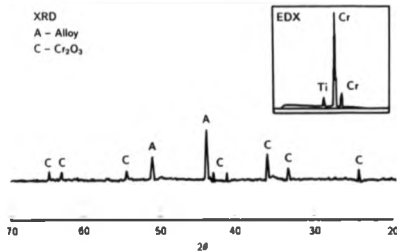
Figure 5.4: XRD and EDX analysis for preoxidised Nimonic alloy surface
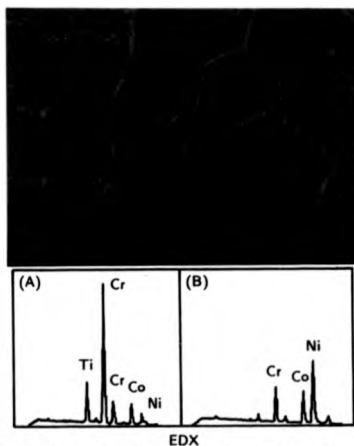
Figure 5.5: EDX spectra confirm selective oxidation *(A)* enrichment of Cr_2O_3 at the grain boudary *(B)* grain surface

boundary areas, and NiO develops in the centre of grains, b) Cr diffusion is not only intergranular but also through the volume. The diffusion rate is 2-3 times faster than Ni, thus, the Cr_2O_3 becomes the dominating oxide during the oxidation, and c) the diffusion of Cr follows a parabolic law, therefore, fast diffusion is expected at the beginning of the oxidation process. This relatively easy oxidation for certain elements in certain areas taking place in the same alloy is referred to as selective oxidation. The similar selective oxidation of Cr and fast diffusion can also be seen from the reports of Giggins[90] and Hauffer[87]. Due to the lack of experimental techniques such as autoradiography, precise data of the diffusion rate of Cr have not been obtained in our study. The observation of the Nimonic oxidation made here generally agrees with what was discovered in the literature. It is important to note the way in which Cr diffuses, i.e. fast and intergranular diffusion, in Nimonic alloy, as this behaviour will affect the interactions between the glass-ceramic coating and the alloy.(for more discussion see section 5.1.11.)

5.1.3 Coating quenched after firing

Coatings on oxidized and unoxidized Nimonic substrates were fired in a furnace and on completion of the firing they were quickly quenched to room temperature. In both cases, the standard firing condition is defined as 980°C for 5min. A N_2 atmosphere is needed to prevent further oxidation of the unpreoxidized alloy. The coating on preoxidized alloy is usually fired in an air atmosphere.

The coating on unoxidized Nimonic has a well fused layer of glass enamel. Its cross-section (Fig.5.6a) shows a well defined and intimate interface which bonds the coating and the substrate together. In the metal region, the roughness of the interface is mainly caused by the metal pretreatment, i.e. vapour blasting, which helps the mechanical interlock of the interfaces. A few pores, which are not shown here, exist due to incomplete sintering within the short firing time. The quenched coating remains basically vitreous, i.e. glassy, as XRD in the Fig.5.6(b) gives a very broad curve. It is noticeable that even within this short
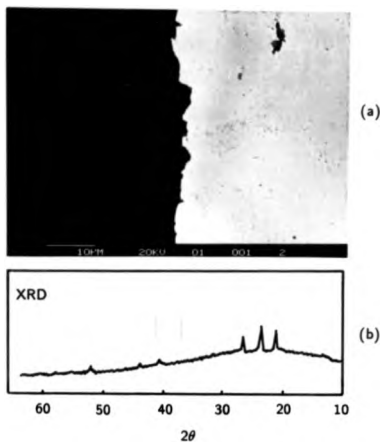
Figure 5.6: (a) Cross-section of coating fired at 980°C for 5min on unpreoxidized Nimonic alloy (b) XRD analysis showing mainly amorphous nature of coating
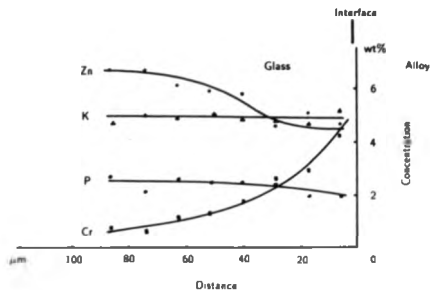
Figure 5.7: Diffusion profile of coating fired at 980°C for 5min on unpreoxidized Nimonic alloy

period of firing, some crystal features start to appear in the glass because of the high surface energy of the glass powders causing spontaneous crystallization shown as a few sharply defined peaks in the XRD pattern. It is also noticeable that an interfacial layer has appeared at the interface, though the layer is very thin (≈ 0.5 μm).

Microanalysis of the coating was carried out using the electron probe and it is found that some major components of the alloy, such as Ni and Co, are stable and no obvious diffusion is detected. However, the distribution of some elements across the interface(Fig.5.7) shows, within the firing time of only 5min, that Cr, another major component of the alloy, is detectable 60μm away from the interface. Meanwhile, the depletion of Cr within the alloy near the interface is also recorded. This means that Cr does diffuse into the glass coating from the unoxidized alloy very rapidly soon after the firing starts. Ti, a minor additive in the alloy, diffuses into the glass as well but not in a substantial amount as Ti concentration in the alloy is very low.(As required by EDX analytical techniques,

70

Figure 5.8: X-ray line scan of coating cross-section fired at 980°C for 5min on unpreoxidized Nimonic alloy

in all SEM pictures alloy substrates were placed at right hand side. The diffusion profiles of all elements were placed in a correspondent way.)

The glass former SiO_2 is stable and Si diffusion into the alloy is not evident. Li_2O, due to its low atomic number, is not detectable by EDX, hence, the distribution remains unknown. Diffusion of three other components K_2O, P_2O_5 and ZnO are shown in Fig.5.7. K_2O is not expected to interdiffuse and this is confirmed. P_2O_5 has a very low concentration so that the analytical errors may mask any variation. A local enrichment of P_2O_5 must occur as P_2O_5 acts as nucleation agent to form Li_3PO_4 nuclei at the early stage of firing or heat treatment. However, these nuclei will be only of nanometre dimensions. It is very surprising to notice that ZnO is depleted from the coating near the interface and a high concentration of Zn is detected within the alloy at the interface. As the original ZnO concentration should give about 8 wt%. It is obvious that an obvious Zn depletion exists in the coating glass. This indicates that Cr and Zn ions are the major interdiffusion species.

A continuous X-ray line scan across the interface(Fig.5.8) confirms the above observations giving the distribution of the major components in the coating and

71
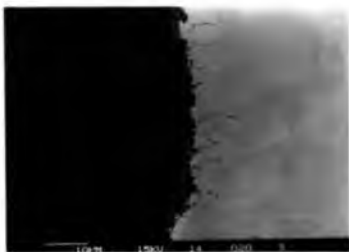
Figure 5.9: Cross-section of coating fired at 980°C for 5min on preoxidized Nimonic alloy

alloy. Apart from the relatively long range diffusion of Cr detected in the bulk coating, the interfacial layer along the coating side is found to be significantly Cr rich by showing a peak of Cr while Zn mainly alloys within the substrate Nimonic at the interface so that the peak occurs inside of the alloy. Although the probe analysis is not effective enough to decide the precise composition of the interfacial layer since the layer has submicron size, the line scan does indicate the way in which Cr and Zn enrich at the interface and this is very important in assisting the identification of the detailed reactions at the interface described in section 5.1.11.

The coating on preoxidized Nimonic also has a well fused layer of glass enamel. Its cross-section (Fig.5.9) differs only from that of unoxidized Nimonic by showing a well defined layer of preformed oxide(Cr_2O_3) between the coating glass and substrate alloy. In this case, the glass enamel bonds to the Cr_2O_3 while the Cr_2O_3 bridges to the substrate. In the metal region the grain boundaries of the alloy near the Cr_2O_3 layer are visible due to the selective oxidation and fast intergranular Cr diffusion during the preoxidation discussed in section 5.1.2. In the glass area the features are similar to those described in the coating
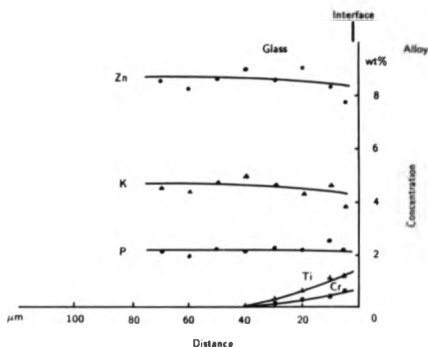
Figure 5.10: Diffusion profile of coating fired at 980°C for 5min on preoxidized
Nimonic alloy

of unoxidized Nimonic, i.e. a few pores caused by incomplete sintering plus some
crystallized phases growing during the firing of the coating. Microanalysis of the
coating reveals the distribution of some elements across the interface(Fig.5.10).
It is clear that Cr forms a well defined Cr_2O_3 layer between the coating and
substrate at the cost of the depletion of Cr concentration in the alloy near the
interface. Cr from the oxide diffuses only a little into the glass in contrast to the
fast Cr diffusion from the unoxidized substrate. A certain amount of Ti near the
interfacial area indicates a short range diffusion of Ti. As both Cr and Ti ions
originate from the preformed $Cr_2O_3(TiO_2)$ layer, it is likely that the existence of
Cr and Ti ions are via dissolution of these oxides. Due to this barrier of Cr_2O_3
between the glass and alloy, the interdiffusion of all elements including Ni, Co,
Mo, Si, K, Zn and P is hardly detectable. The observed phenomenon of Zn
alloying with the alloy as the counterdiffusion against Cr does not occur in the
coating on the preoxidized substrate. X-ray line scan in Fig.5.11 confirmed this
by showing a steep drop of Cr at the interface of glass/Cr_2O_3 and there is no

73
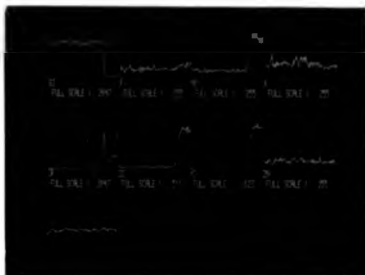
Figure 5.11: X-ray line scan of coating cross-section fired at 980°C for 5min on preoxidized Nimonic alloy

Zn rich peak inside the alloy.

5.1.4 Coating after heat-treatment

The quenched coatings described above are basically vitreous enamel coatings in terms of their microstructures. The coatings with both the oxidized and unoxidized substrates were heat-treated so that the vitreous state is converted to a mostly crystalline glass-ceramic structure. Nucleation at 600°C for 30min and crystallization at 800°C for 1hr are defined as the standard conditions in the heat-treatment process.

Fig.5.12 is a backscattered SEM picture showing a typical structure of the glass-ceramic coating on the unoxidized Nimonic alloy. The thin reacted layer during short firing has disappeared giving a region near the interface which is much more inhomogeneous than the bulk area, and a number of bright spots are scattered along the interface. The interfacial area has its own distinct features compared with the bulk in showing 1) lack of densely packed crystal phases and existence of more glass phase. 2) small elongated Li_2O2SiO_2 crystals predominate. Apart from that, in the residual glass areas further away from the

74
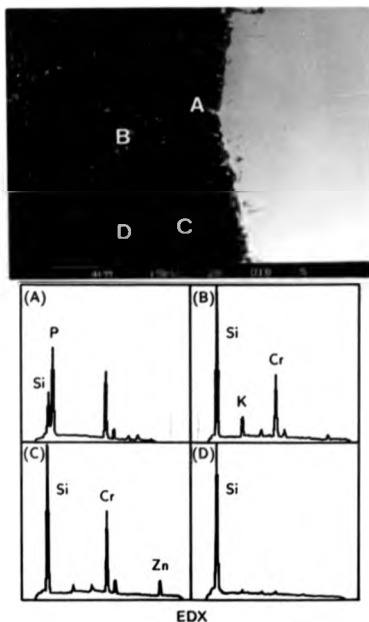
Figure 5.12: SEM and EDX spectra from the heat treated coating on unpreoxidized Nimonic alloy A) large bright spots along interface B) smaller spots cluster near interface C) residual glass near interface D) normal crystal phase in coating
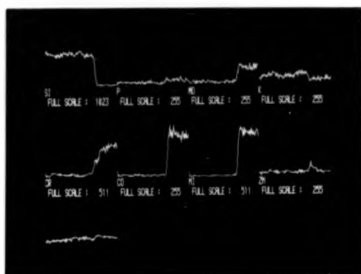
Figure 5.13: X-ray line scan of interfacial cross-section of heat treated coating on unpreoxidized Nimonic alloy

interface, very small bright particles are also found. EDX spectra in Fig.5.12 show that bright spots(A) along the interface are Cr-P rich phases and clusters of very small bright particles(B) away from the interface are Cr and Zn rich. The residual glass area(C) near the interface has high Cr and K concentration. In fact, K, Zn, and Cr are mainly found in the glass phases and Li and Si move into the major crystal phases(D). The localization of mainly Cr, Zn and K as well as two types of bright particles indicate reactions between diffused Cr and P_2O_5 or possibly ZnO in the glass. Elemental profiles using microprobe analysis proved difficult because the elements in the coating were no longer distributed homogeneously after the heat treatment. Hence, the inhomogeneity gave a series of irregular signals. Better X-ray line scans in Fig.5.13 gave the distribution of the major elements. Cr diffusion and Zn migration are similar to that in the fired only coating and they have not extended substantially during the heat treatment. It is possible that because the heat treatment temperature is lower than that of firing, therefore, further long range diffusion has not occurred but local migration of various ions has taken place. The reaction of this kind will be discussed in section 5.1.11.

76

XRD

T – tridymite
β – β-cristobalite
L – lithium disilicate

Figure 5.14: XRD of heat treated coating on unpreoxidized Nimonic alloy

Although there are some obvious interactions in the coating, the two main crystals are a) SiO_2 (tridymite), a triangular and light coloured phase, b) Li_2O2SiO_2(lithium disilicate), a needle-like, dark phase. These two phases are confirmed by XRD (Fig.5.14). The XRD also shows a well defined diffraction pattern which indicates nearly complete crystallization after heat treatment. Fig.5.14 differs sharply from the fired only coating(Fig.5.6) and a pattern very similar to that of a well heat treated bulk glass is obtained(Fig.4.5).

Fig.5.15 is a backscattered SEM picture showing a typical structure of the glass-ceramic coating on preoxidized Nimonic alloy. A very fine and homogeneously developed microstructure is formed throughout the coating. The preoxidized Cr_2O_3 layer is well maintained throughout the heat treatment and the reaction zone near the interface is not visible. EDX probe spectra revealed that K and Zn mainly migrate into the residual glass phases. Even in the residual glass area very near to the interface Cr diffusion is not seen whereas a very small amount of Ti exists. X-ray line scans in Fig 5.16 confirmed that Cr diffusion into the glass during heat treatment is negligible – also indicated by the lack of bright spots. In addition, the Zn enrichment of the alloy is not detected. In a word, during the heat treatment the interfacial microstructure established in

77

EDX

Figure 5.15: SEM and EDX spectra of heat treated coating on preoxidized Nimonic alloy (A) glass residual phase near interface (B) residual glass away from interface (C) crystal in coating bulk
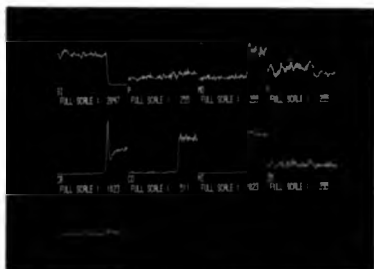
Figure 5.16: X-ray line scan of interfacial cross-section of heat treated coating on preoxidized Nimonic alloy

the firing stage is well maintained and the coating bulk develops into a fine and homogeneous glass-ceramic structure without substantial interdiffusion between the glass and substrate.

It can be summarized that 1) during the heat treatment stage, if the substrate Nimonic is not preoxidized, then interfacial reactions will proceed. These reactions consume the interlayer formed during the previous firing and a Cr-P compound precipitates along the interface and interdiffusion of Cr, Zn, P and Ti take place. 2) The preoxidized Nimonic has a stable layer of Cr_2O_3, which is well preserved during both firing and heat treatment. Little interdiffusion is observed across the interface of preformed Cr_2O_3. 3) The existence of interaction and interdiffusion between the glass and substrate affects the microstructure to a great extent during the glass-ceramic process. Comparatively, the microstructure of the coating on the preoxidized Nimonic is preferred.

5.1.5 Microstructure development in the coating

To observe normal microstructure development in the coating free from interference with the substrate, the series 1(P) was produced (coating on the preoxidized

79

Nimonic) since the preoxidized substrate reacts with the coating less severely. The firing and the heat treatment stages were then investigated by varying the parameters which contribute to coating development.

Fig.5.17(a-d) show a typical microstructure change in the coating versus the firing time. Although the firing temperature was set at 980°C, it is estimated that the actual temperature for those coatings fired for a few minutes is usually lower than the chosen one simply because the firing time is too short to reach and stabilize the set temperature before the coating assemblies are withdrawn. The actual removal temperature for the sample a and b is about 960 and 973°C for a firing time of 30sec and 1min respectively.

Fig.5.17(a) shows the coating after a short firing time of 30sec and 1min. The coating exists as particles which join together by some necking at the points of contact. The necking can be greatly enhanced by extending the firing for only a short time. Due to surface energy, crystallization originates at particle surfaces resulting in clusters of tiny crystals along these neck areas. XRD indicates the crystals to be β-cristobalite(SiO_2) and lithium disilicate(Li_2O2SiO_2). Thus, at the very early stage of firing, surface nucleation and growth of the subsequent crystals take place.

Fig.5.17(b) shows the coating after 3min of firing. The necking and crystallization have developed extensively. The only area remaining uncrystallized is the central part of the large particles. XRD indicates that the types of both crystal phases remain unchanged as β-cristobalite and lithium disilicate. On the other hand, a coarsening process has taken place because the numerous tiny crystals have been taken into solution to produce larger grains, i.e. the average grain size increases and the number of grains decreases. With increased firing time there is increased temperature so that some crystals may be redissolving. Consequently, it gave lower XRD peaks reflecting the lower crystal density.

Fig.5.17(c) shows a well fused coating after 5min firing. The necking disappears and a fused continuous coating is achieved. This indicates that a time of 5min is essential for a well fused microstructure and intimate contact with
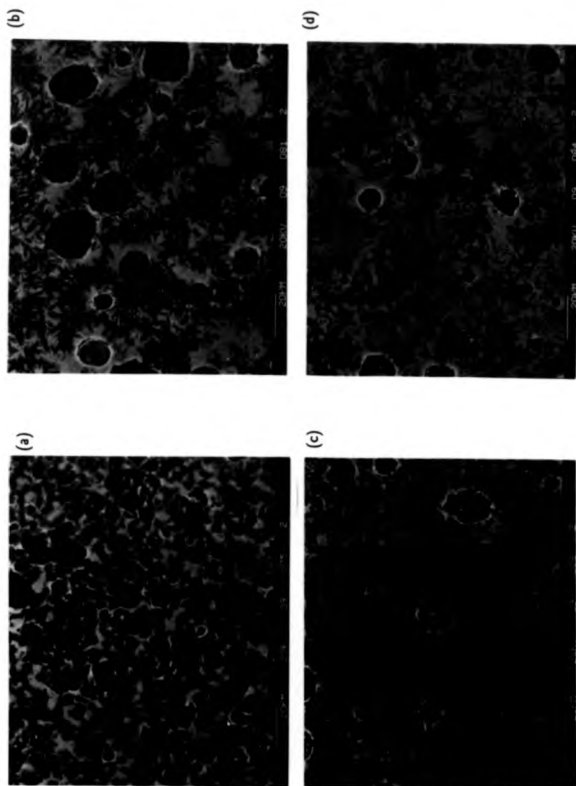
Figure 5.17: Structural development versus firing time at 980°C (a) 30sec-1min
(b) 3min (c) 5min (d) 20min

the substrate. Some pores are obvious, due to the entrapment of gas. XRD shows that there is some change of crystal types. Tridymite(SiO_2) and lithium metasilicate (Li_2OSiO_2) start to appear.

Fig.5.17(d) is a coating of 20min firing, which is sufficient to reduce porosity and complete fusion. The coarsening process continues, leading to a few large crystal phases determined by XRD as a mixture of mainly tridymite, lithium disilicate and a little lithium metasilicate. The rest of the material consists of the majority glass phase.

Fig.5.18, which summarizes XRD analysis of the coating glass as firing time proceeds, illustrates the change in the phase composition.

The following series (Fig.5.19-21) are illustrations of microstructure development after various heat treatments of the fired-only coating assemblies. The fired-only samples were subjected to either 600°C(nucleation), or 800°C(crystallization) or both temperatures. In the nucleated-only coating of Fig.5.19(a), finely dispersed tiny crystallites have been produced. XRD confirms that these phases are Li_2OSiO_2, Li_2O2SiO_2 and SiO_2(cristobalite and tridymite) but their growth is not sufficient. During the nucleation stage of 600°C it is believed that the numerous nuclei of Li_3PO_4, which are partially formed at the 980°C firing, and other nuclei such as Li_2SiO_3 grow and form nuclei for the major crystal phases SiO_2 and Li_2O2SiO_2 which grow epitaxially at the nucleation stage. Although this has been confirmed in Li_2O-SiO_2 glass-ceramics[80], XRD in our project did not pick up any diffraction signals to demonstrate the presence of the Li_3PO_4 as the nuclei are too small.

In the crystallized-only coating of Fig.5.20(a), a comparatively coarse structure is seen. Growth of both SiO_2 and Li_2O2SiO_2 takes place during the crystallization stage at 800°C. XRD shows high intensity of both crystal phases. However, lack of a nucleation stage has resulted in lack of nuclei numbers. This hinders the development of a fine and homogeneously dispersed glass-ceramic structure. Consequently, there is a certain amount of residual glass phase.

Fig.5.21(a) shows the development of the preferred coating microstructure
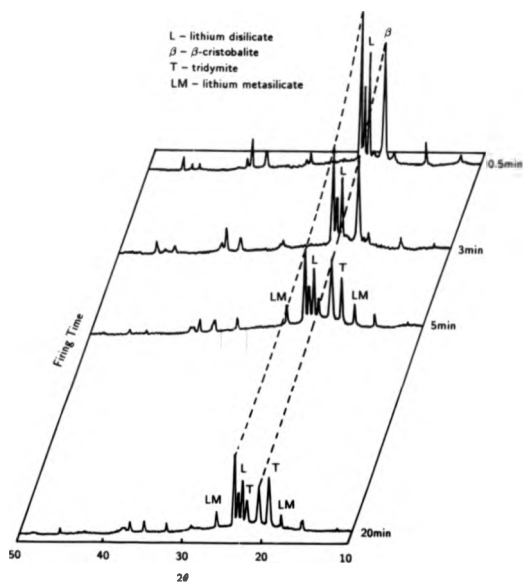
Figure 5.18: XRD of coating at increased firing times. β-cristobalite and lithium disilicate decrease whereas tridymite and lithium metasilicate increase

83
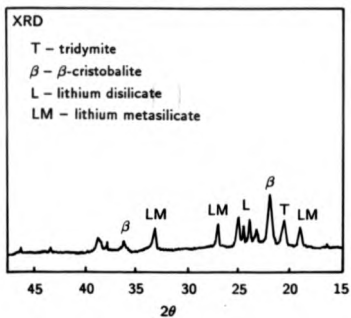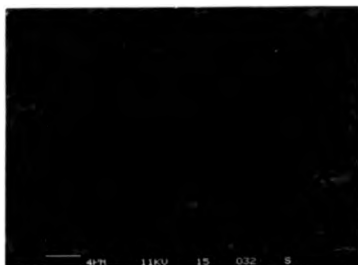
Figure 5.19: Structure of nucleated-only coating

84
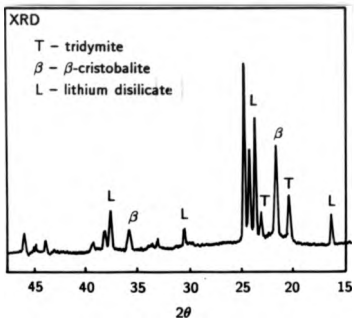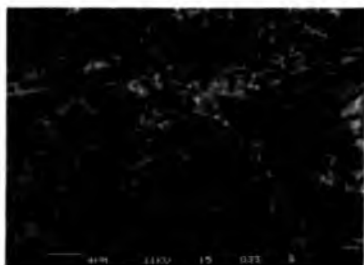
Figure 5.20: Structure of crystallization-only coating
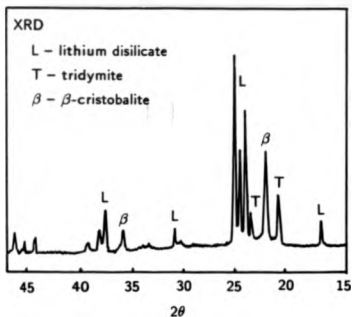
Figure 5.21: Structure after nucleation and crystallization
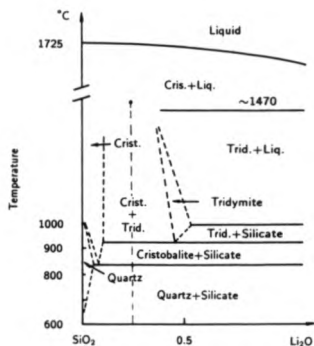
Figure 5.22: System of Li_2O-SiO_2 (Tested glass: $- - - -$)

after both nucleation and crystallization at 600°C and 800°C. The whole coating consists of well formed crystal phases and residual glass phase is reduced. This means a high density of crystals in the coating. XRD shows that the crystal phases remain unchanged.

It should be noted that the existence of SiO_2(cristobalite) is not desirable as its thermal expansion undergoes a huge change due to a structural relaxation in the range of 200-300°C. This may create stress in the coating causing possible microcracks. Therefore, the preferred SiO_2 crystals phases are either quartz or tridymite. Fig.5.22 gives a binary phase diagram[91] indicating that the coating firing temperature is very sensitive in determining the crystal type created. As there is a hold of 980°C during the firing, the production of cristobalite may be inevitable under the driving force of the surface energy possessed by the glass powder. At this firing temperature, cristobalite can be quickly produced even

if the firing time is very short (see Fig.5.18). However, if the firing and heat treatment can avoid the temperature range between 840-930°C and the firing time is optimized, it may help to create and maintain either tridymite or quartz crystals and minimize cristobalite. Other factors such as chemical composition and control of the fluctuation of firing temperature are also important. With careful consideration it is possible to produce acceptable amounts of cristobalite to avoid thermal stress in the coating and the microstructure of the coating in terms of crystal type, size and proportion can be tailored to requirements.

As seen above, the microstructure development of the coating is a complicated process. It involves a first stage when glass particles start to sinter together to fuse on the substrate metal. During this stage the high surface energy of the glass powder initiates surface crystallization to produce tiny Li_2O2SiO_2, mainly clustered along the necking area where the particles are brought onto contact. As firing proceeds, fusion extends and necking disappears. A few pores are trapped in the coating, meanwhile, crystal phases are coarsening at the expense of other small crystals. When the firing is finished, the coating consists mainly of fused glass and a few large crystal phases such as lithium disilicate and tridymite. The second stage is the nucleation during which the fired-only coating is treated at low temperature to grow numerous tiny nuclei. Though the nuclei are too small to be detected by XRD, they provide sites on which the desired major phases can grow epitaxially. The final stage usually is crystallization when a sufficient time is given to allow the crystals to grow to a desired size and density. In this project, the chosen firing and subsequent heat treatment generate two major phases in the coating. They are tridymite(SiO_2), although some cristobalite is possible, and lithium disilicate(Li_2O2SiO_2). These observations are in good agreement with similar glass-ceramic systems reported elsewhere [77].

5.1.6 Variation of firing temperature

Firing temperature is an important parameter which controls the sintering process of glass powder. In general, the higher the firing temperature, the quicker

the powder sinters together. However, high temperatures can have adverse effects. In a glass-ceramic coating, an appropriate firing temperature has to be considered combined with glass viscosity, particle size, coating workability and chemical reaction etc. In industry, to maintain precision of coating thickness and low energy consumption, a reasonable low temperature, is often emphasized.

In this project, the firing temperature has been varied to examine the microstructural change of the coating and its effect on bonding between the coating and substrate. Fig.5.23(a-d) show various kinds of coating structures when the firing temperature is varied from 800°C to 1100°C for a time of 5min. It is clear that when the firing temperature is too low (Fig.5.23(a)) the glass powder does not fuse, or wet the substrate metal. The intimate contact between glass and metal cannot be established within a limited time. In addition, a low firing temperature does not produce sufficient liquid phase to promote sintering. This solid-solid based sintering process is overall a slow process. As a result, particles are still loosely stacked giving a porous structure. Also, due to the high surface energy of finely ground glass powder, 800°C is high enough to initiate the crystallization, which further hinders the sintering process.

Fig.5.23(b) shows a coating fired at 950°C, which is slightly lower than the glass dilatometric softening point of 970°C. Substantial fusion and wetting has been achieved but the structure is not fluid enough to flow on the metal. Therefore, there are a large number of cracks caused by the shrinkage of glass particles during sintering, which obviously weakens the coating strength. The insufficient liquid phase can also lead to poor adhesion between the coating and substrate. On the other hand, the whole structure is extensively crystallized. This type of uncontrolled crystal growth due to the high surface energy of powders is often defined as "premature glass-ceramic process" which creates difficulties in control of crystal type and size at a later stage.

When the coating is fired at 980°C, which is very close to the glass liquidus temperature (also higher than the dilatometric softening point), the powder fuses well and flows on the metal (Fig.5.23(c)). This is the desired coating
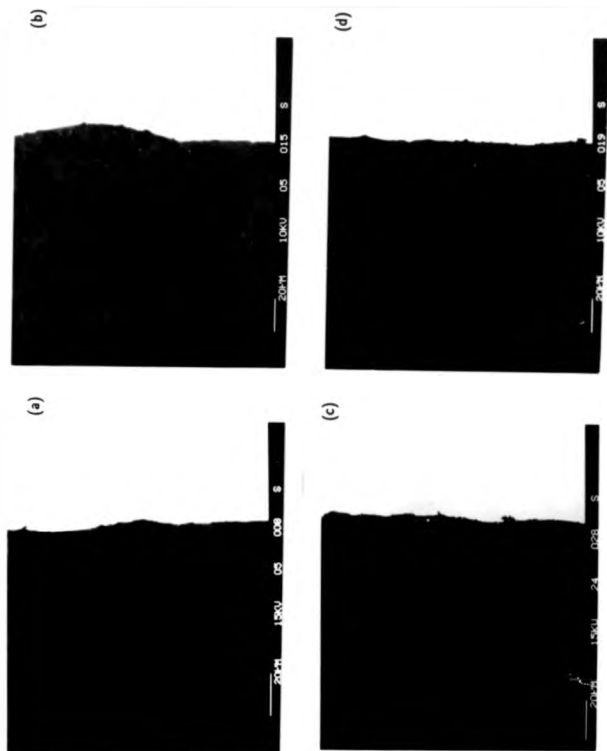
Figure 5.23: Coating structural development versus firing temperature for 5min
a) 800°C b) 950°C c) 980°C d) 1100°C

condition, under which the semi-molten glass creates an intimate contact or interface between the glass and metal. At the same time, glass melting accelerates the sintering. The migration of substances through a liquid phase is much faster than solid state sintering. Within 5min, loosely stacked glass powders are fused together to form a dense layer of coating on the metal. A few pores are still left behind due to the entrapment of gas. The viscosity of glass at 980°C is simply not low enough to mobilize the gas quickly and total escape of the gas may need either longer time or higher temperature. As discussed in section 5.1.5, some crystallization still takes place spontaneously, but the coating is predominantly vitreous.

If the coating is fired at a high temperature of 1100°C (Fig.5.23(d)), a completely fused and well wetted coating should be produced. The viscosity is obviously decreased as the temperature rises, thus, most pores drift to the coating surface and escape to the furnace atmosphere. This results in a dense coating structure. On the other hand, low viscosity may cause difficulty in maintaining the precise dimensions of the coating. In addition, high temperature does accelerate some harmful interactions between glass and metal. In this project, excessive reactions are observed at the interface when the assembly is fired at 1100°C or above.

XRD in Fig.5.24 summarizes the structural change when firing temperature increases. The decrease of lithium disilicate phase is certainly associated with the melting of the coating, hence, the wettability. Unless the temperature is high enough to suppress the fast growth of lithium disilicate phase, the glass coating will not spread well on the substrate. Meanwhile, low firing temperature produces quartz whereas high temperature gives a mixture of tridymite and β-cristobalite as high SiO_2 phases.

5.1.7 Variation of firing time

Firing time is another important parameter which controls the sintering process of glass powder. Adequate time is needed to sinter the powder completely to
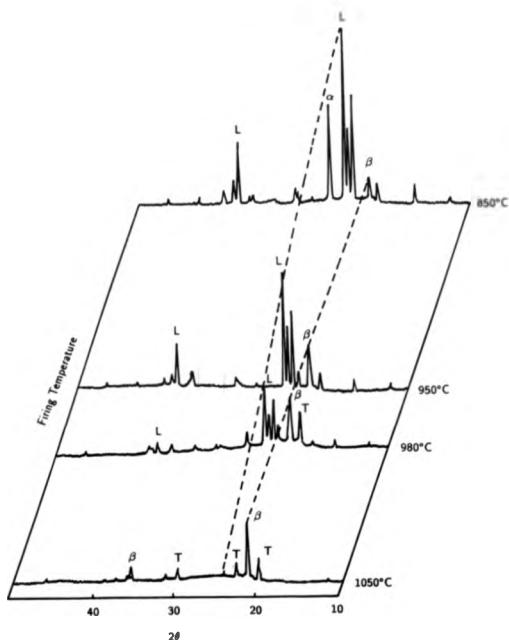
Figure 5.24: Crystal phase change versus firing temperature

minimize porosity and produce homogeneity. In industry excessively long firing is not cost-effective. The most commonly used firing time for ordinary enameling ranges from 5min to 15min[1]. In this project, much attention was guided to the effects of firing time on the subsequent interactions between the coating and metal. Nimonic alloy, one of the Cr-rich superalloys, is an active substrate which is likely to react with the coating to cause chemical interactions at the interface. These interfacial reactions are of major interest.

A range of coatings defined as Series 1, on unoxidized Nimonic, were tested at a standard firing temperature of 980°C in N_2 by varying the firing time from 5, 10, 20, 40 to 60min. The interfacial reactions and microstructure development were carefully studied. It is found that the coating on unoxidized Nimonic has progressive interactions in the interfacial area as well as in the bulk as the firing proceeds. The interactions are characterized mainly by:

1) Formation of a layer at the interface;

2) Disappearance of the above interfacial layer after a long time of firing;

3) Reaction between diffused Cr and glass component P_2O_5;

4) Occurrence of crystal phases on the surface of the coating.

The formation of the interfacial layer takes place at an early stage of the firing. The coating fired only for 5min(Fig.5.25) produces a layer of about $0.5\mu m$ at the glass/alloy interface. The layer is too thin to be analyzed by EDX probe technique to decide the exact composition. As described briefly in section 5.1.3 there was a substantial diffusion and counter-diffusion of Cr from the alloy and Zn from the glass. While other major components are stable, showing sharp drops at the interface by X-ray line scan, Cr and Zn peak at the interface, shown also in Fig.5.25. In spite of the submicron size and consequent interference from the background, the EDX spectrum does show that the Cr concentration in the layer is much higher than in the nearby glass. It would therefore seem that chromium ion has diffused from the metal to the interfacial layer. Silica is also present, most likely due to background interference. Therefore, for short firing time Cr diffuses away from the metal to form a Cr rich interfacial layer and at the
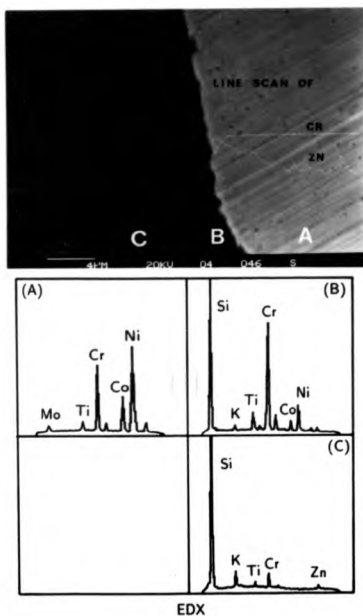
Figure 5.25: SEM and EDX spectra of Series1-1(5min) A) in alloy B) interfacial layer C) in coating

EDX
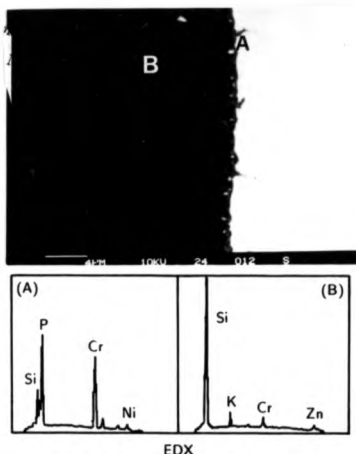
Figure 5.26: SEM and EDX spectra of Series1-2(10min) A) bright spot B) in coating

pear along the interface(Fig.5.26). The EDX spectrum revealed a high concentration of both P and Cr in these particles and a background Si signal was generated from the glass matrix. Despite the difficulty of analyzing these particles, EDX quantitative calculation gave a ratio of Cr to P as approximately 2/1. The formation of these particles means that further redox reaction has taken place.

Fig.5.27(a) shows a total disappearance of the interfacial layer if the coating is fired more than 20min. The molten glass starts to attack the alloy at the interface as firing proceeds. The interface shows grain boundary etching of the alloy and glass penetration, see also Fig.5.27(c&b), in which the coating was fractured and separated at the interface to expose both sides of coating glass and substrate alloy. The P-Cr particles extend into the glass coating to 10μm in Fig.5.27(a) indicating the progress of the reaction with time. At the coating surface some bright particles

Figure 5.27: a) SEM of Series1-3(20min) and its interfaces separated by fracturing b) glass-anchor formed due to penetration into alloy grain boundary and P-Cr reacted product c) alloy grain boundary and re-entrant cavity

96

is fired more than 20min. The molten glass starts to attack the alloy at the interface as firing proceeds. The interface shows grain boundary etching of the alloy and glass penetration, see also Fig.5.27(c&b), in which the coating was fractured and separated at the interface to expose both sides of coating glass and substrate alloy. The P-Cr particles extend into the glass coating to $10\mu m$ in Fig.5.27(a) indicating the progress of the reaction with time. At the coating surface some bright particles start to emerge and light coloured crystal phase exists, which will be more clearly shown in the following Fig.5.30. TEM picture together with an EDX spectrum in Fig.5.28 shows an area approximately 200nm away from the interface in the alloy with depleted Cr concentration and enrichment of Zn confirming the observed element distribution by SEM. TEM picture in Fig.5.29 and electron diffraction pattern, on the other hand, show that the P-Cr particles near the interface are hexagonal $Cr_{12}P_7$ crystals.

Fig.5.30 shows a coating of 40min firing at whose surface not only the bright crystal phase exists but also a second light coloured crystal phase which grows rapidly into the glass. EDX spectra(a&b) (windowless technique) proves that the tiny bright phase is a chromium oxide with some Zn enrichment whereas the major second phase is chromium containing silicate. XRD analysis in Fig.5.30 shows that the major phase at the coating surface is $LiCr(SiO_3)_2$ which colours the coating green and causes wrinkling.

Fig.5.31 shows a coating of 60min in which $LiCr(SiO_3)_2$ eventually grows into the coating bulk. This can change the coating structure substantially, hence, prolonged firing is very undesirable.

Fig.5.32 produced elemental profiles from cross-sectioned coatings for various firing times, in which some stable elements such as Si, Ni, Co and Mo are not included.

Though the elemental distribution neither reveals the detailed change at the interface, nor shows the mechanism of the surface crystallization due to the analytical difficulty, the general view of the distribution reflects the following points:
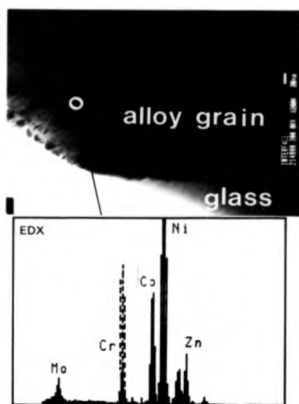
Figure 5.28: EDX analysis 100nm away from the interface in alloy via TEM shows depleted Cr and increased Zn concentration
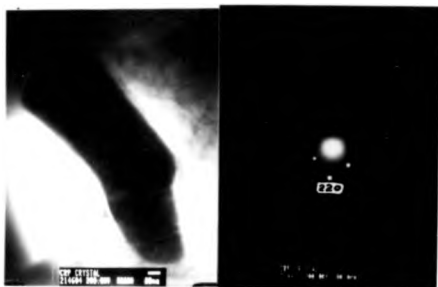
Comparison between d spacing via ED and XRD		
d_{ED}	d_{XRD}	hkl
3.24	3.048	101
2.580	2.592	300
2.264	2.245	220
2.180	2.199	211
2.054	2.041	301
1.951	1.944	400
1.763	1.784	230
1.689	1.697	140
1.660	1.656	002
1.322	1.314	312
1.282	1.287	151
1.185	1.185	142

d_{ED} − caculated d spacing via ED

d_{XRD} − d spacing via XRD from J.C.P.D.S

Figure 5.29: TEM and electron diffraction analysis of $Cr_{12}P_7$ crystal structure
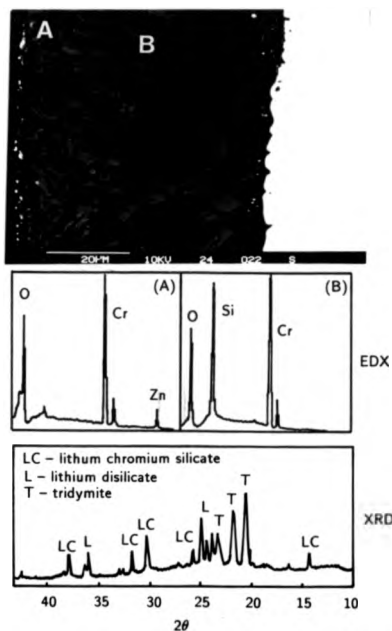
Figure 5.30: SEM, EDX and XRD of coating Series1-4(40min)
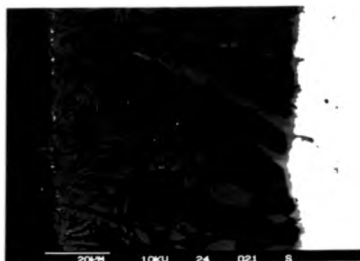
Figure 5.31: SEM of coating Series1-5(60min)

a) Cr and Ti, two of the most active elements in the alloy, continuously diffuse into the glass as firing proceeds. The diffusion produces mainly Cr oxide at the interface, $Cr_{12}P_7$ metallic phase near the interface together with $LiCr(SiO_3)_2$ phase at the coating surface. The following continuous diffusion of Cr into the glass gives the growth of $LiCr(SiO_3)_2$ phase into the glass from the coating surface. It is noticed that the concentration of Cr in the glass near the $LiCr(SiO_3)_2$ phase boundary has reached a saturation level of 2.5wt%.

b) ZnO, introduced into the glass as a modifier, is rapidly reduced to elemental Zn as a result of redox reaction. Subsequently, its fast migration into the alloy has taken place due to the chemical potential gradient. Zn concentration is very low after a prolonged firing indicating the continuity of certain reaction and diffusion when the firing proceeds.

c) K_2O, another glass modifier, is evenly distributed in the glass. There is no interaction observed involving K. If the crystal phases develop at the coating surface, which exclude K, then K tends to migrate inwards to the coating bulk resulting in a high concentration of K in the glass phase.

d) P_2O_5, the nucleating agent in the glass, reacts selectively with the diffused Cr to form $Cr_{12}P_7$, therefore, the concentration of P in the glass is locally reduced

101
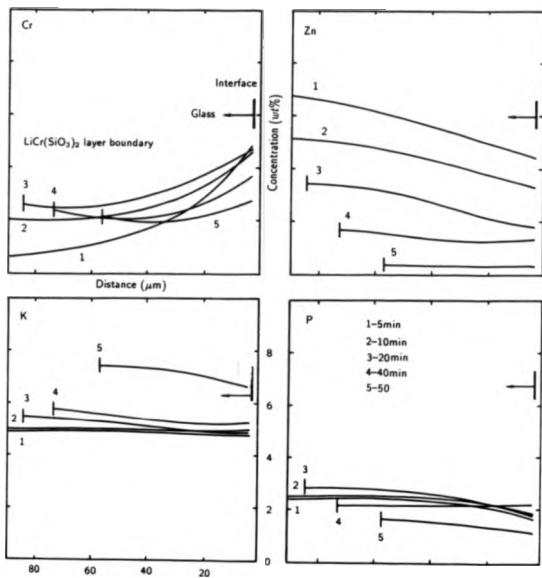
Figure 5.32: Diffusion profile with firing time of coating Series1 at 980°C

especially near the interface.

5.1.8 Variation of metal pretreatment

In section 5.1.5, it is briefly mentioned that the coating on the preoxidized Nimonic is less reactive with the substrate. The necessity of preoxidizing the alloy in achieving a successful bond has been reviewed in the literature, see section 2.3. How to oxidize the alloy and the nature of the oxidation have also been discussed in section 4.1.3.

It is clear that a relatively high temperature and long time are needed in order to stabilize the growth of Cr_2O_3 during the preoxidation. 4hr at 900°C in air is defined as standard preoxidation treatment, which creates a layer of Cr_2O_3 oxide of 34 μm thickness. A range of coatings defined as Series 1(P) with standard pretreatment of the alloy were prepared at the standard firing temperature of 980°C in air but firing time was varied from a few minutes to hours. Coatings on the alloy with different pretreatment were also investigated.

Under the standard preoxidation condition, short firing shows a well defined interface between the coating and substrate and there is little Cr diffusion into the coating. This has been described in section 5.1.3. With extended firing, a layer of crystal grows gradually from Cr_2O_3. This process is slow and needs firing times longer than 30min to provide any noticeable growth(Fig.5.33). An excessively fired coating of 1.5hr shows growth of the crystal extending to 4μm(Fig.5.34). EDX spectrum A (windowless) shows the crystal as Si-Cr-O compound with possible Li. Meanwhile, spectrum B, 5μm away from the grown phase, still shows a negligible concentration of Cr indicating that the diffusion of Cr is very short ranged. XRD analysis of an extended firing coating, which was HF etched to expose the layer, confirms that the layer is $LiCr(SiO_3)_2$. Sturgeon[26] proposed that the width of the $LiCr(SiO_3)_2$ layer is controlled by diffusion for increasing firing time in his study of lithium silicate glass-ceramic coating on a Cr_2O_3 compacted disc(Fig.5.35). Similar growth has been confirmed in this study. It is worth pointing out that the growth curve in quoted Fig.5.35
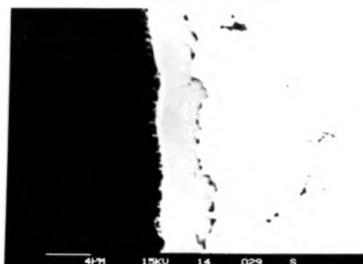
Figure 5.33: SEM of Series1(P)-4(40min)

should not be linear as the diffusion growth obeys parabolic law. Therefore, a parabolic curve is more precise.

It can be seen that various firing periods produce a very similar elemental distribution in the coating. X-ray line scan(Fig.5.36) reveals little interdiffusion of other major elements such as Ni, Cr, Si and Zn in a coating of long firing of 1hr, compared with the coating of short firing of 5min in Fig.5.16. It is found through quantitative EDX analysis that the concentration of diffused Cr near the interface 10μm away from the Cr_2O_3 layer remains constant at about 0.5 wt% irrespective of the firing time(Fig.5.37). It can be evaluated from the above that 1) Cr_2O_3 diffuses into the glass very slowly 2) solution rate of Cr_2O_3 into the glass seems faster than the diffusion. That explains why the adjacent area near the interface always remains constant in terms of Cr concentration. Fast solution and slow diffusion lead to saturation of Cr_2O_3 in this area. Consequently, the extended firing initiates the growth of $LiCr(SiO_3)_2$ on the Cr_2O_3 layer, which itself is a slow process. The saturation of Cr_2O_3 in lithium-silicate glass at the firing temperature has been confirmed by Sturgeon[26] in another test showing a concentration of 0.23 atm%, which was an equivalence to 0.4 wt%.

Interesting comparisons between Series 1, where Cr diffuses from the sub-

104
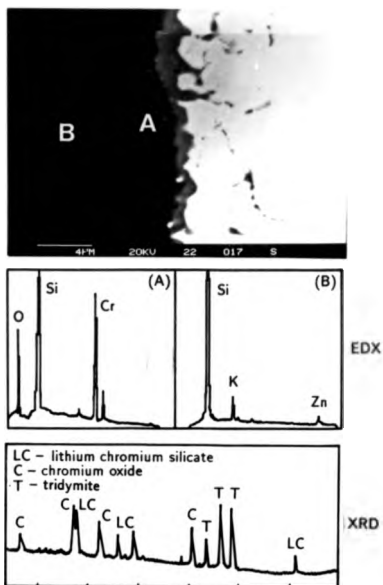
Figure 5.34: SEM, EDX and XRD of coating Series1(P)-E(5hr) at 980°C
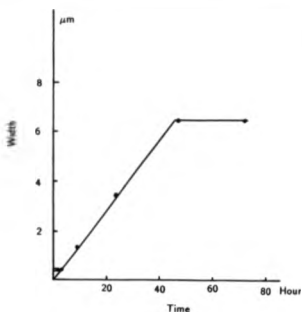
Figure 5.35: Width of lithium chromium silicate layer for increasing firing time [26]
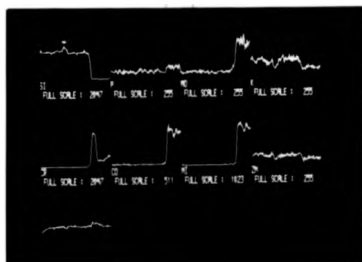
Figure 5.36: X-ray line scan of cross-section of Series1(P)-5(1hr)
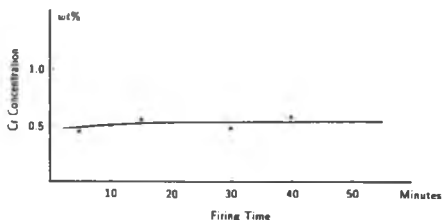
Figure 5.37: Concentration of diffused Cr^{+3} in coating Series1(P) $10\mu m$ away from interface

strate alloy into the glass continuously, and Series 1(P), where Cr_2O_3 was pre-formed to remain stable at the interface throughout the firing procedure, are made. This sharp contrast reveals the role of metal pretreatment in achieving a desired coating structure and controlling the subsequent interactions. Further detailed discussion will be in section 5.1.11.

The above observation was made when preoxidation of the alloy under stan-dard condition gives a layer of fully formed Cr_2O_3. In the case of shorter pre-oxidation, for instance, 1hr, a thinner layer of Cr_2O_3 is produced. These less preoxidized alloys or even unpreoxidized alloys were coated and fired under stan-dard conditions. The coating was found to wet the substrate poorly leaving a larger number of isolated pores in the coating. Fig.5.38 reveals some typical isolated pores viewing from the top of a coating assembly which is not cross-sectioned. EDX analysis at spot A in Fig.5.38 shows a Cr rich structure at the bottom of the pore as Cr_2O_3. The growth of Cr_2O_3 on the Nimonic coexisting with the fusion of the coating means that the oxidation persists even during the firing. Therefore, in those areas where glass particles fuse and quickly seal off air inlet from the atmosphere intimate contact between the coating and alloy
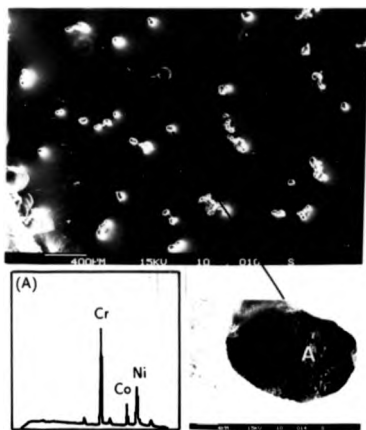
Figure 5.38: SEM and EDX spectrum of isolated pore in coating
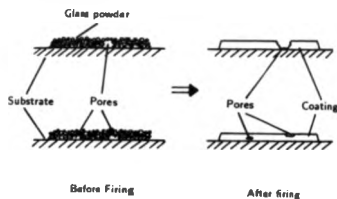
Figure 5.39: Formation of different pores in coating

can be established, while in those areas where poor packing of the glass powder leaves an open channel to air the completion of alloy oxidation persists and dominates the local structure development, i.e. the growth of Cr_2O_3. Since the unoxidized, less-preoxidized and fully oxidized alloy surfaces possess different reactivity, hence, wettability, the glass tends to spread on the metal unevenly. In particular, those areas where pores expose the substrate alloy to air, fast growth of Cr_2O_3 instead of glass fusion and wetting may prevent the glass spreading inwards. This phenomenon is also illustrated schematically in Fig.5.39.

It is possible to conclude that the preoxidation of the alloy has to be completed so that a stable continuous layer of Cr_2O_3 is created before the coating on this preoxidized alloy can be fired in air. Failing to achieve this, the further growth of Cr_2O_3 will persist during the firing. This kind of localized growth of Cr_2O_3 prevents the fused glass from wetting the alloy evenly, therefore producing porosity in the coating as clearly illustrated in Fig.5.40. Only if sufficient preoxidation is given to the alloy, can the subsequent coating be fired in air to obtain a well fused and spread enamel layer. This glassy layer is able to adhere to the substrate alloy without much interdiffusion or interaction with the alloy. Though it is likely that after an extended firing $LiCr(SiO_3)_2$ develops at the interface, it is overall a slow process. On the other hand, the growth of $LiCr(SiO_3)_2$ implies saturation of Cr_2O_3 at the interface. In theory, the saturation of metal oxide near the interface is usually desirable. Therefore, a well

109
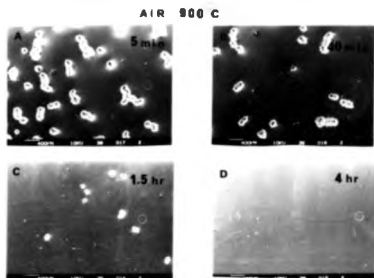
Figure 5.40: Time of preoxidation affects porosity in coating

developed bonding between the coating and preoxidized alloy can be produced.

5.1.9 Variation of firing atmosphere

Oxidizing, reducing or neutral atmospheres are used in coating technologies. They are vital, especially if redox reactions are involved between coating and substrates since different atmospheres alter the direction of the reactions. Variation of firing atmosphere was made with those coatings on the unoxidized Nimonic in this project, because the interactions are more severe than those of the coatings on preoxidized Nimonic.

The assembly was initially fired under oxygen free N_2 flow for 5min and then the N_2 atmosphere was suddenly switched off and air flow followed. Thus, after an initial stage of successful covering and wetting of coating by the substrate, the rest of the firing was carried out in air. The short N_2 fire at the beginning avoids the spontaneous growth of Cr_2O_3, hence, produces a well fused coating. Coatings fired in N_2 for the first 5min and then in air giving total time of 10, 20, 30, 40 and 60min are defined as Series 2-2, 3, 4, 5, and 6 correspondingly. Fig.5.41a, Series 2-2, shows the growth of a very distinctive crystal phase at the interface. Both EDX spectrum(A) and XRD confirm that it is $LiCr(SiO_3)_2$. There is
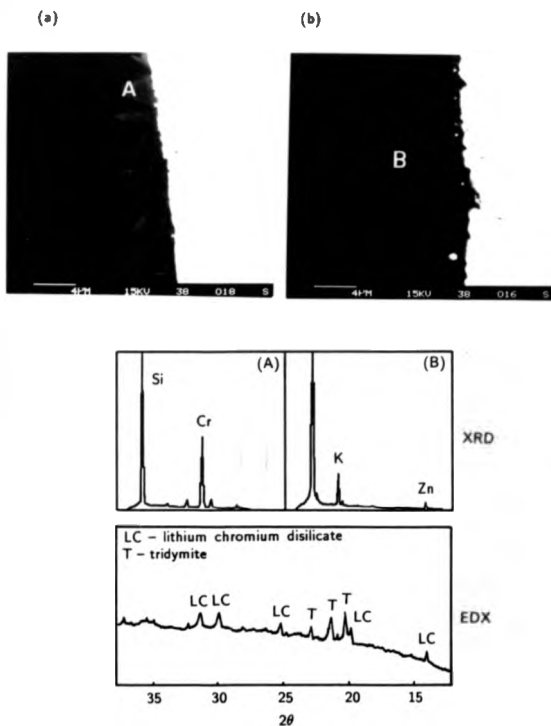
Figure 5.41: SEM and EDX spectra of Series2-2 and its comparison with Series1-2
a) 5min in N_2, then 5min in air at 980°C b) 10min in N_2 at 980°C

no detectable intermediate layer between the coating and the substrate alloy indicating that any Cr oxide had been converted to $LiCr(SiO_3)_2$. Glass coating $5\mu m$ away from the interface(spectrum B) shows no evidence of Cr diffusion indicating that the formation of these $LiCr(SiO_3)_2$ dendrites is limited to the interface. If the firing proceeded in N_2 for the same length of time of total 10min without being changed for air, the initial Cr oxide, possibly CrO, would gradually disappear and additional redox reactions could follow. Furthermore, the growth of $LiCr(SiO_3)_2$ would eventually take place at the coating surface rather than at the interface. This has been described in detail in the previous sections, and as a comparison the cross-section of Series 1-2 is again shown here in Fig.5.41b. EDX spectra obtained from a spot $5\mu m$ away from the interface in any of the Series 2 show little Cr diffusion similar to the spectrum B in Fig.5.41b. This implies that the diffusion of Cr^{+3} is not increased with firing time. The following Fig.5.42 (a&b) gives another illustration to verify this fact. In Fig.5.42(a) there is a $50\mu m$ Cr rich zone where very small bright phases cluster in the residual glass. Analytical difficulties prevent them being precisely identified, but they are Cr-Zn rich phases as described in section 5.1.4. In contrast, Fig.5.42(b) shows no sign of Cr diffusion apart from $LiCr(SiO_3)_2$ dendrites formed at the interface during the firing. Therefore, the occurrence of $LiCr(SiO_3)_2$ at the glass/unoxidized alloy interface can be determined by alternating the firing atmosphere. Low valent Cr oxide, such as CrO produced by redox reaction with ZnO, does not remain at the interface for long. Only Cr_2O_3 survives to give the growth of $LiCr(SiO_3)_2$ because of the easy saturation of Cr^{+3} in this glass system. Thus, changing the firing atmosphere controls the species of Cr created at the interface, and hence the subsequent reactions.

A neutral atmosphere throughout the firing process was provided by a continuous flow of oxygen free N_2. In addition, vacuum firing was also tried in a quartz tube where a vacuum of 10^{-4} torr was established before the firing was started. Under these two conditions the coating results proved to be very similar.
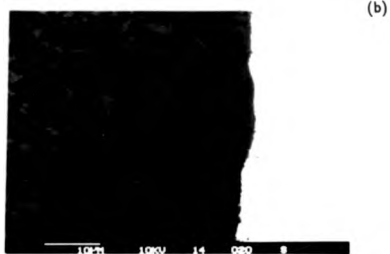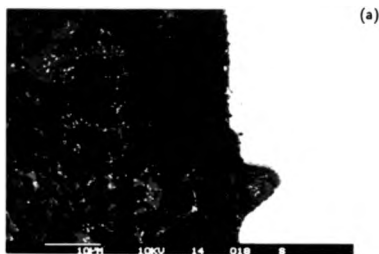
Figure 5.42: Cross-section of heat treated Series1-2 and Series2-2 a) Series1-2(H/T), reacted products in residual glass phases due to Cr diffusion b) Series2-2(H/T), no Cr diffusion apart from $LiCr(SiO_3)_2$ formed at interface

113

Figure 5.43: Coating wrinkled at the edge area

5.1.10 Variation of coating thickness

Surface wrinkling and colouration are the main problems in the coating of un-preoxidized Nimonic alloy. When the firing is extended, the problems increase. In Fig.5.43 shows a failed fired coating. Wrinkling and coloration may not be in proportion but they do often occur in the same area of the coating. Careful and wide comparisons were made and it was found that, under fixed pretreatment and firing conditions, the chance that a thin area will develop color and wrinkle are far greater than a thick area. In Fig.5.44, both the screen printing and droplet methods give rise to a thinner edge area of the coating. The cross-section of partially wrinkled and coloured coating was studied. The results(Fig.5.45) agree that, where the wrinkling and coloring develop, the $LiCr(SiO_3)_2$ phase exists on the surface. Thus, the most vulnerable parts subject to these problems are those coating edges or thin areas linked with the $LiCr(SiO_3)_2$.

It has been mentioned in the section 5.1.7 that Cr diffuses into the coating from the unoxidized substrate very rapidly. In terms of the diffusion at a set temperature and time the concentration of diffused elements in the coating is largely dependent on the thickness of the coated area. With development of Cr diffusion, eventually Cr reaches the coating surface and forms $LiCr(SiO_3)_2$

114
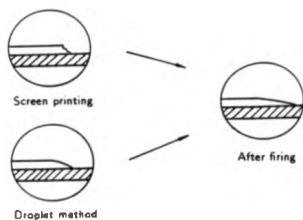
Figure 5.44: Formation of thinner edge area in coating
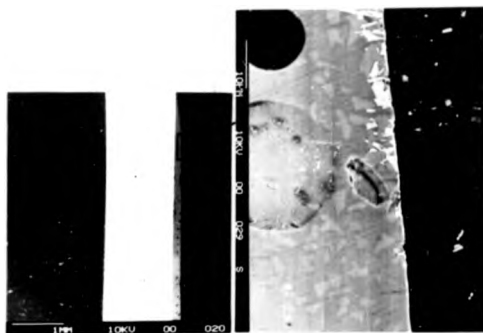
Figure 5.45: Formation of $LiCr(SiO_3)_2$ at coating edge or thin area

crystals. The colouration is mainly due to the presence of Cr^{+3}, which has been extensively reported in literature, in $LiCr(SiO_3)_2$ and wrinkling is caused by thermal differential contraction of the surface crystal phase and molten glassy bulk, see more details in section 5.1.11. Since the diffused Cr reaches the surface and forms $LiCr(SiO_3)_2$ faster in thinner areas than thick areas, this answers why the edges of the coating are more associated with problems. Therefore, thick coatings are necessary to reduce coloration and wrinkling.

As the coloration and wrinkling linked with the occurrence of Cr^{+3} usually starts at the coating surface instead of in the bulk, it implies that the Cr valence at the surface may differ from that in the bulk. The determination of Cr ion valence and the consequence of different species of Cr in the coating will be explored further in the following section 5.1.11.

5.1.11   Discussion

A. Formation of a layer at the interface

The formation of a layer at the interface clearly shows that some interaction is taking place between the glass coating and substrate alloy. In the case of glass/metal bonding, because of the incompatibilities of the two materials at the interface, especially when an unoxidized metal is used, a driving force towards thermodynamic equilibrium always exists. As a result, various redox reactions occur involving oxidation of the metal and reduction of a cation in the glass [92] [93] [94], see also in section 2.5.

The formation of a mono- or multi-molecular layer of oxide will eventually lead to the saturation of the interface with the oxide. Consequently, a chemical equilibrium or chemical bonding will be created as the metal oxide is compatible with both its metal and the glass. The general formula of the redox reaction can be summarized as:

$$M_I(metal) + M_{II}O(glass) = M_{II} + M_I O(interface) \qquad (5.2)$$

Such a layer need not be observable and may not survive to maintain the chemical equilibrium. It basically depends on how fast reaction(5.2) proceeds or how readily M_IO reaches a chemical activity of one. Other related factors are chemical composition of glass and oxygen partial pressure associated with the reaction. Frequently, the metal oxide at the interface may be dissolved rapidly or gradually by the glass as firing proceeds. This second stage reaction involving the dissolution of the metal oxide is generally represented by:

$$M_IO(interface) = M_IO(glass) \qquad (5.3)$$

In brief, thermodynamics determine which oxide is formed at the interface and solubility and diffusivity then determine the rate of dissolution of the oxide in the glass.

Judged from Table 2.3 of the Gibbs free energy, among the major components of Nimonic alloy Cr is the most thermodynamically active element and ZnO, K_2O and P_2O_5 in the glass could react with Cr to produce chromium oxide. The following Table 5.2 summarizes all possible reactions involving Cr, ZnO, K_2O and P_2O_5 to give either CrO or Cr_2O_3 at various negative free formation energy. Other major glass composition SiO_2 and Li_2O are also included. Data from reference[36] was used for all oxides except that the Δ G$^{\circ}$ for CrO was derived from reference[95].

In the system studied, the fast migration of Zn to the alloy and formation of a Cr rich layer at the interface indicates the following:

$$Cr(alloy) + ZnO(glass) = CrO(interface) + Zn \qquad (5.4)$$
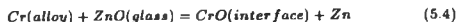
The thermodynamic equation for the reaction (5.3) can be expressed as

$$\Delta G = \Delta G^{\circ} + RT \ln \frac{a(CrO)_{interface} \times a(Zn)}{a(ZnO)_{glass} \times a(Cr)_{alloy}} \qquad (5.5)$$

The standard free energy at 1000°C, Δ G$^{\circ}$, was seen in Table 5.1 as -190.8kJ/mol. The reaction(5.4) thus is favourable under standard conditions. Because metallic

Reactions	ΔG° KJ/mol
$Li_2O + Cr = CrO + 2Li$	+29.5
$SiO_2 + 2Cr = 2CrO + Si$	-119.4
$ZnO + Cr = CrO + Zn$	-190.8
$P_2O_5 + 5Cr = 5CrO + 2P$	-1072.8
$K_2O + Cr = CrO + 2K$	-271.4
$Li_2O + 2/3Cr = 1/3Cr_2O_3 + 2Li_2O$	+158.5
$SiO_2 + 4/3Cr = 2/3Cr_2O_3 + Si$	+143.2
$ZnO + 2/3Cr = 1/3Cr_2O_3 + Zn$	-61.95
$P_2O_5 + 10/3Cr = 5/3Cr_2O_3 + 2P$	-428.8
$K_2O + 2/3Cr = 1/3Cr_2O_3 + 2K$	-142.6

Table 5.2: Free energy for reaction at 1000°C

Zn enters the substrate alloy when its oxide is reduced under the driving force of the free energy, the process may be considered irreversible. The fact that the metallic atoms produced are not free to revert to the ionic state makes the reaction proceeds very rapidly. However, it can be seen from the Eq.(5.5) that the reaction will become less favourable with local depletion of ZnO and build up of CrO and Zn.

Dissolution and diffusion of CrO take place spontaneously as Cr at 1wt% occurs about 70μm away from the interface after only 5min firing. Both solution and diffusion rates are much slower than the reaction rate at the beginning of the reaction. Thus, CrO concentration increases to form a layer of CrO at the interface. Due to analytical difficulties, it is not completely certain about the chemical formula of this Cr^{+2} rich layer. Thermodynamically, if ambient oxygen partial pressure $p(O_2)$ is greater than that of the dissociation $p(O_2)$ for bulk CrO, which is 4.6×10^{-12}Pa, then, it is possible for CrO to exist at the interface. Meanwhile, certain forms of Cr^{+2} containing silicates such as $Li_2Cr(SiO_3)_2$ or Li_2CrSiO_4 may be possible as alternatives to pure CrO. So long as the layer exists

and the solution and diffusion rate are slow, the interface should be saturated by the oxide. Consequently, the chemical bonding is realized by showing intimate contact between the glass coating and metal substrate. The fact that none of the quenched short-fired coatings peeled off or failed to spread plus the reasonable bonding strength achieved indicated the nature of the interface.

The interface in this particular system, however, does not remain as the firing goes on. As a second stage, the metal oxide formed at the interface is dissolved by the glass by:

$$CrO(interface) = CrO(glass) \tag{5.6}$$

Since the rate of reaction (5.4) decreases with increase of the reaction products, then eventually dissolution and diffusion (5.6) become dominant, and this leads to the disappearance of the formed CrO layer from the interface as well as increase in Cr^{+2} concentration in the coating.

As briefly mentioned above, apart from ZnO the reaction between Cr and glass components P_2O_5 and K_2O is also thermodynamically possible. The studied system did confirm the Cr/P_2O_5 reaction couple seen in the following sections but not K_2O. It is suggested that the larger ionic radius of K^{+1} (twice that of Zn^{+2} at 1.38) reduces its diffusivity, hence, a reaction similar to (5.3) is hampered in terms of dynamic conditions. The removal of K^{+1} is essential to progress the reaction of "$Cr + K_2O = CrO + 2K\uparrow$", and in the absence of a removal mechanism, K_2O remained stable.

B. Further redox reactions and the change of Cr valence

Disappearance of the CrO layer brings the substrate alloy directly into contact with the glass coating causing further redox reactions. All the reactions, as well as interdiffusion, are very complex processes in this multicomponent system. The key questions are the valence of Cr migrating into the coating, how fast Cr ions diffuse, and how they affect the coating structure.

Cr generally exists in a melt of glass in the most stable state of Cr^{+3} which colours the glass green[96]. However, other valences such as Cr^{+6}, Cr^{+4} and

Cr^{+2} could exist or co-exist depending principally on the base composition, melt temperature, oxygen fugacity, concentration, and other redox species[97]. Individual redox couples for the transition element Cr in the silicate melt system such as Cr^{+3}/Cr^{+2} and Cr^{+3}/Cr^{+6} have been widely investigated, see Schreiber [69] and Nath[98]. The situation becomes more complicated if a glass system contains two or more multivalent elements simultaneously, for instance, Cr and Ti, as the interaction between two redox couples inevitably changes equilibria, see also Schreiber[97]. In the case of glass coating, diffusion of Cr into the molten glass is always associated with some counter-diffusion of other elements from the glass and redox reactions take place at the interface readily.

In this coating, the diffused Cr is thought to exist mainly as divalent Cr^{+2}. Trivalent Cr^{+3} may co-exist but it is not observed as major species until the crystal phase $LiCr(SiO_3)_2$ precipitates at the surface of those prolonged fired coating. The evidence of this statement is as follows:

1) The lack of the typical green colour of Cr^{+3} in short fired coatings indicates the Cr rich layer is not Cr_2O_3. In addition, a visible blue colour, typical of Cr^{+2}, shows through the quenched transparent glassy coating. This means that the Cr rich layer is associated with Cr^{+2} ions.

2) Wet chemical analysis revealed the total diffused Cr in the coating of 5, 10, and 20min's firing as 0.22, 0.69 and 1.60 wt% respectively. However, ESR analysis calibrated by a series of standard Cr^{+3} doped glasses produced under the same firing conditions, showed that these three coatings have concentration of Cr^{+3} ions as 0.086, 0.304, and 1.047 wt% respectively, see Fig.5.46. The difference between total Cr and Cr^{+3} in the same coating clearly showed that the multi-valency of chromium ions does exist. The ratio of Cr^{+3}/Cr changes from 39.09, 44.06 to 65.44%, reflecting the fact that Cr^{+3} increases as firing proceeds with time. Although the ESR measurements tend to have errors up to +18.8% due to difficulties in quantitative control of the measurements, the data obtained is quite consistent, hence, reasonably convincing.

3) Deliberate additions of Cr_2O_3 were made to the base glass at both glass
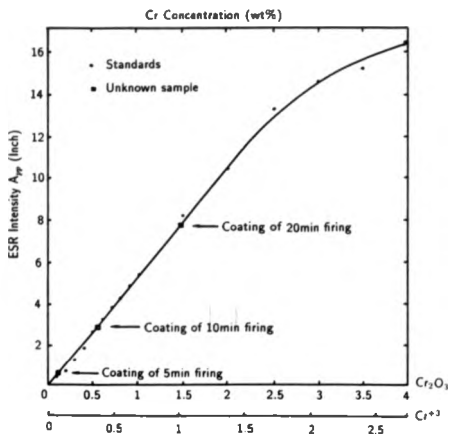
Figure 5.46: ESR intensity versus Cr^{+3} concentration in coating glass

melting temperature of 1360°C and coating firing temperature of 980°C. The former temperature is higher than that of the melting temperature for $LiCr(SiO_3)_2$ crystals(1260°C), therefore, the melt does not produce the precipitates and remains basically glassy after quenching. However, XRD shows distinctive peaks of Cr_2O_3 in the glass melt after the Cr_2O_3 concentration reached a certain level. This indicates that the glass is over-saturated with Cr_2O_3 and it cannot accommodate excessive Cr_2O_3 in its network, see Fig.5.47. The concentration of Cr_2O_3 which gives XRD peaks is about 3 wt%. At a lower firing temperature of 980°C, $LiCr(SiO_3)_2$ is expected to occur as evidenced in Fig.5.48, in which the concentration of Cr_2O_3 is about 2 wt%. The similar saturation is also recorded in ESR analysis by showing an obvious deviation in Fig.5.46. As doped Cr_2O_3 approached 2 wt%, the precipitation of $LiCr(SiO_3)_2$ crystals changes the originally 6-fold Cr^{+3} structural units and the registered ESR signals do not increase linearly as Cr^{+3} increases. All this evidence shows that, if Cr_2O_3 wt% is converted into Cr^{+3} wt%, the saturation level of trivalent Cr^{+3} in this coating is less than 1.3 wt% at 980°C and 2 wt% at 1360°C. Higher than the saturation level could lead to the occurrence of Cr^{+3} containing crystals in the glass, typically $LiCr(SiO_3)_2$. If we refer back to the EDX quantitative analysis in Fig.5.32, the actual concentration of chromium in the interfacial zone of 0-30μm in the coatings fired for 5, 10 and 20min is usually above the saturation level at 2-4 wt% without producing Cr^{+3} containing crystals, see section 5.1.6. This implies that a mixture of Cr valencies does exist at least in the interfacial areas.

4) Schreiber has pointed out in his discussion[99] that in a specific glass system oxygen fugacity could decide the individual redox equilibria. "At higher oxygen fugacities(e.g. air, $fO_2=10^{-0.7}$atm) higher redox states of Cr occur, while at lower oxygen fugacities Cr^{+2} becomes a viable species." Oxygen free N_2 and vacuum were used to fire the coating on unpreoxidized Nimonic alloy and redox reactions took place under low oxygen fugacities to produce Cr^{+2}. In addition, the low oxygen fugacities and short time of firing in the early stages may rule out the existence of high valent Cr species like Cr^{+6} because the redox equilibrium of $Cr^{+6}/$ Cr takes a long time (70 hrs) to achieve a ratio of 15.3% and needs
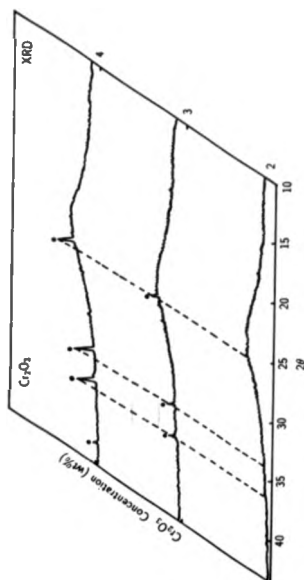
Figure 5.47: Saturation of Cr_2O_3 in coating glass melted at 1360°C
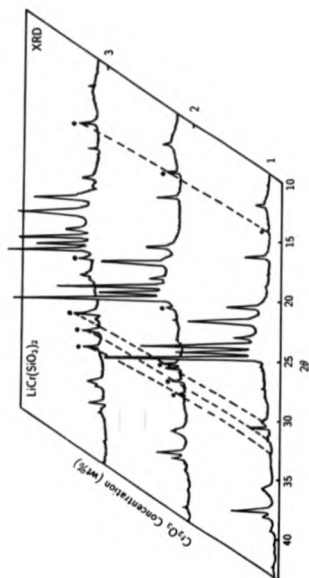
Figure 5.48: Saturation of Cr_2O_3 in coating glass fired at 980°C

124

oxidizing atmosphere, see reference[98].

5) The XPS (X-ray photoelectron spectroscopy) studies conducted by Brown [100] confirmed that chromium dissolved in glass from a Cr-containing alloy can exist as Cr^{+2} at the glass/metal interfacial area.

6) Sturgeon[26] in his work and also this study have proved that an intermediate layer of Cr_2O_3 at the coating interface is very stable and does not dissolve into the bulk coating readily. In fact, the slow diffusion rate of Cr_2O_3 results in the saturation of Cr_2O_3 at the interface followed by $LiCr(SiO_3)_2$ growth. In section 5.1.9, only by varying the firing atmosphere from low oxygen fugacities(N_2) to high oxygen fugacities(air), which helps convert the lower Cr valence to a higher one by redox reaction, does the intermediate Cr rich layer start to grow into $LiCr(SiO_3)_2$ instead of diffusing into the glass. This evidence indicates that the Cr rich layer formed at the early stage in N_2 is unlikely to be trivalent Cr^{+3} because a layer of Cr_2O_3 would have remained and growth of $LiCr(SiO_3)_2$ would have followed on further firing. No matter how Cr^{+3} is created at the interface, either via preoxidation (Series 1(p)) or via reaction during firing (Series 2), the stability of Cr^{+3} results in a very localized microstructural development at the interface instead of giving long-range diffusion affecting the whole coating structure.

7) Volf[96] gave a detailed account of field strength **F**, bonding strength **B** and coordination number **Y** of specific cations in glass. **F** is defined as Z/a^2 and **B** as Z/a, where Z is the formal valence and a is the internuclear distance. The value of **F**, **B** together with **Y** can be used to assess the insolubility of an oxide and participation of an element in the glass network. Table.5.3 gives the calculated results for chromium ions in glass. So long as the F value exceeds 0.8 and **Y** exceeds 4, ions of this particular element will have poor solubility leading to precipitation of its oxide compounds in glass because of the incompatibility between the silicate networks and the environmental preferences of the ions. In addition, stronger bonding strength means it is more difficult for Cr ions to break away from its neibouring oxygen, making it less soluble and mobile in the

125

	Field strength F	Bonding strength B	Coordination Number Y
Cr^{+2}	0.46	0.96	6
Cr^{+3}	0.78	1.53	6
Cr^{+4}	2.13	3.57	6 (4)

Table 5.3: Characteristics of Cr ions

glass network. This explains the limited uptake of Cr^{+3} or Cr^{+6} in glass and also their low mobilities in glass structure. The lowest **F** and the **B** values for Cr^{+2} among other Cr valencies indicates that Cr^{+2} has a relatively higher solubility and diffusivity.

Experimental evidence and an understanding of the behaviour of Cr ions in the coating allows the following description of the coating process. Firstly, Cr in the alloy at the interface interacts with ZnO in the glass to form CrO layer or its silicate at the interface and the reduced atomic Zn alloys with the substrate. Secondly, the CrO dissolves and diffuses quickly into the coating. Thirdly, the glass coating is brought into contact directly with the alloy after the disappearance of CrO. Under the driving force of chemical equilibrium further redox reactions take place.

The further redox reactions consist of the formation of $Cr_{12}P_7$ particles at the reaction zone near the interface. P, introduced in the form of P_2O_5 nucleating agent in the glass, is thermodynamically liable to react with Cr. Watkins et al[85] in their study discovered the interactions between P and Cr and determined a similar crystal phase as Cr_2P or solid solution with other alloy elements. They proposed that Cr reacts with P as follows:

$$22Cr(alloy) + 6Li_3PO_4(solid) = 2Cr_2P(solid) + Li_2O(glass) + 5Cr_2O_3(glass) \tag{5.7}$$

or

$$9Cr(alloy) + 2Li_3PO_4(solid) = 2Cr_2P + Li_2O(glass) + 5CrO(glass) \tag{5.8}$$

126
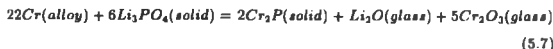
In both reactions, the Li_3PO_4 which should which provide the nucleation sites for the glass-ceramic process, is consumed. Loehman[61] in his latest interpretation gave $Cr_{12}P_7$ as the reaction products but the basic principles of these reactions remained the same. These two reactions have been observed in our study. In a more concise way, it is proposed that the following reactions take place:

$$59Cr(alloy) + 7P_2O_5(glass) = 2Cr_{12}P_7(precipitates) + 35CrO(glass) \quad (5.9)$$

or

$$142Cr(alloy) + 21P_2O_5(glass) = 6Cr_{12}P_7(precipitates) + 35Cr_2O_3(glass)$$
$$(5.10)$$
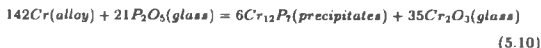
The precipitates of $Cr_{12}P_7$ are actually needle like crystals, see Fig.5.49a. Their growth is suggested to be based on a galvanic cell type of reaction shown in Fig.5.49b. "The reaction could proceed even though the dendrite may not be in physical contact with the substrate providing the intervening glass composition will allow the movement of electrons."[92] Reaction (5.9) and (5.10) in fact provide further sources of Cr^{+2} or Cr^{+3} species near the interface from which they diffuse into the bulk coating. As discussed briefly earlier, Cr^{+2} dissolves and diffuses into the glass melt more than Cr^{+3}, therefore, the overall diffusion of chromium is a continuous and fast process. These further redox reactions above agree with the assumptions that chromium diffused into the glass coating is likely to exist as Cr^{+2} and Cr^{+3}, whereas at the early stage divalent chromium dominates.

Redox reactions occur not only near the interfacial zone described above as the firing continues, but also, at the coating surface, $LiCr(SiO_3)_2$ crystal phase starts to grow indicating another redox reaction. The occurrence of the crystals at the surface suggests that Cr^{+2} is oxidized to produce excessive Cr^{+3} which then precipitates as chromium silicate. The Zn rich metallic phase detected at the coating surface confirms the following redox reaction:
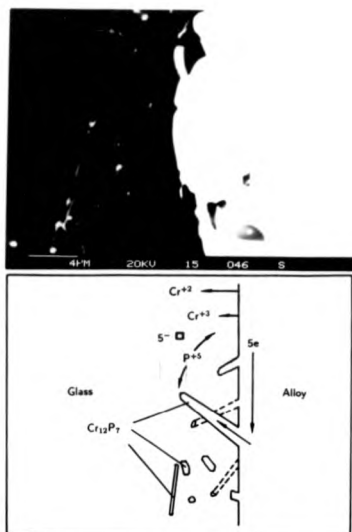
Figure 5.49: Galvanic cell type of reaction between Cr and P_2O_5

128

$$2CrO(glass) + ZnO(glass) = Cr_2O_3(glass) + Zn(precipitates) \qquad (5.11)$$

The reduced metal may be lost as a vapor or may precipitate at the surface, as seen in the X-ray mapping in Fig.5.50. Since a short migration path for the diffusion of Cr^{+2} exists via thinner areas of coating, these areas are obviously the most vulnerable to the reactions. Another interesting aspect of reaction (5.11) is to note the distribution of ZnO in the glass. As seen in section 5.7, after a short firing, most of ZnO near the interfacial area is depleted by contribution to the redox reaction at the interface producing CrO, whereas the exterior parts of the coating become relatively ZnO rich. Despite the high concentration of multi-valent Cr at the interfacial zone, it lacks the condition under which reaction (5.11) can proceed. Only if the diffusion of Cr^{+2} eventually reaches the coating surface, can the redox reaction takes place.

Another mechanism may be possible for the above reaction if a leakage of air is taking place in the furnace where the firing is carried:

$$4CrO(glass) + O_2(atmosphere) = 2Cr_2O_3(glass) \qquad (5.12)$$
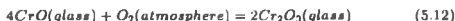
In both mechanisms (Eq.(5.11) & (5.12)), the formation of Cr^{+3} eventually leads to the precipitation of $LiCr(SiO_3)_2$ at the coating surface as the solubility of Cr^{+3} in the glass is very low. The precipitation of $LiCr(SiO_3)_2$ can be expressed as:

$$Cr_2O_3(glass) + Li_2O(glass) + 4SiO_2(glass) = 2LiCr(SiO_3)_2(precipitates) \qquad (5.13)$$
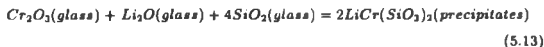
Thus, saturation of Cr^{+3} in certain areas of the coating due to a series of progressive redox reactions explains the surface crystallization in those prolonged-fired coatings and hence the wrinkling and colouration.

C. Dissolution and diffusion of Cr
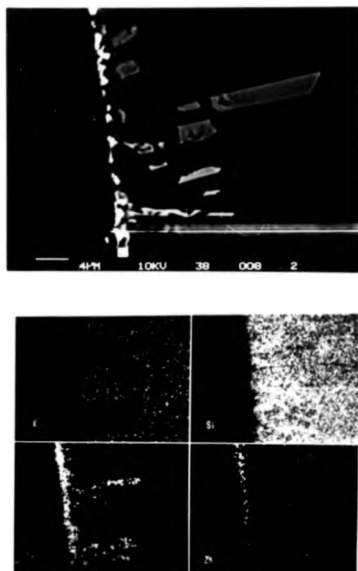
Figure 5.50: Coating surface and its X-ray mapping

130

To understand the extent to which chromium migrates into the coating within a given time it is useful to refer back to section 2.7 in which two approaches were given to asses the diffusion behaviour at interfaces, see Eq.(2.10) and (2.11).

The moving boundary approach in Eq.(2.10) could yield the diffusion coefficient $\bar{D}$ by plotting M^{+2} vs. t. However, this approach requires that the glass composition at the interface remain constant with time. In this study, the required condition cannot be met because interfacial reactions are involved. The rapid formation of CrO and its disappearance from the interface indicates that the composition at the interface is not constant throughout the firing. The progressive redox reactions that follow obviously complicate the diffusion of chromium from the alloy so that the whole diffusion of chromium is certainly not considered as a simple process of diffusion-controlled dissolution.

The Eq.(2.10) may provide a better approach as it deals with interactions and suits a system with a changing concentration at the interface. In this approach, the diffusion is controlled by the rate of transfer of material across the interface, i.e. interfacial reaction. Again, Eq.(2.10) can not be directly adopted in this particular study of the glass-ceramic coating on Nimonic alloy as different redox reactions occur successively or even simultaneously in the system. Instead of a single interaction taking place at the interface which dominates the diffusion, redox reactions include Cr/ZnO(Eq.5.4), Cr/P$_2$O$_5$(Eq.5.9 & 5.10) and CrO/ZnO(Eq.5.11). In addition, the diffusion kinetics given in Eq.(2.10) are restricted to the particular boundary conditions of the system, and more important, the system should be a closed one. In this study of the glass-ceramic coating, a finite length of the glass with respect to the diffusion path is used. Certain substances involved in the interactions may leave the system as a vapour, which has been confirmed by reaction (Eq.5.11). Thus, under these conditions reaction equilibrium may be difficult to attain, and therefore, the reactions would continue to a greater extent than a closed system. The awareness of this type of extended reaction in an open system was mentioned in reference[43].

131

To obtain some specific data on the diffusion in the glass/Nimonic alloy system, both the glass and alloy have to be simplified. It is advisable that a future study of diffusion of chromium be carried out in a chromium and Li_2O2SiO_2 glass system from which the work can be extended into more practical coating systems involving Cr-containing alloys and complex glasses. The reaction-controlled diffusion and diffusion-controlled dissolution are too interelated in the present coating system for Nimonic. This, plus certain analytical difficulties, prevents a detailed investigation giving quantitative values of the chromium diffusion. The most relevant work on a Cr/sodium disilicate glass was carried out in 1986 by Pask et al proving the complexity of this type of study, and other information on similar kinetic work is very limited. Nevertheless, it is important to understand the kinetics of chromium diffusion in lithium silicate glasses since this may relate to applied systems.

D. Effects of interactions on coating structure

The diffusion of Cr causes several interactions which significantly change the coating structure and properties. Firstly, the reactions between P_2O_5 and Cr described earlier proceed at the expense of Li_3PO_4 nucleation sites. As a result, the heat treated glass ceramic coating shows a very coarse structure throughout the reacted zone. As this reaction zone is more glassy than the bulk glass-ceramic, its direct effect is that the zone can be comparetively weak in mechanical strength. Furthermore, the reaction zone is likely to have its own thermal expansion differing from that of the both substrate alloy and bulk coating. Kunz[101] estimated a thermal expansion mismatch of 25% in a similar reaction zone created between substrate Inconel alloy and bonded lithium silicate glass-ceramic.

Secondly, the formation of $LiCr(SiO_3)_2$ at the coating surface disrupts the continuity of the microstructure from the bulk to the surface leading to the wrinkling of the coating. It is believed that with the diffusion of Cr, the thermal expansion of the coating glass decreases[102]. In our study, the thermal expansion of the coating glass and its glass-ceramic with increased Cr_2O_3 con-

132

centration has been tested as in Fig.5.51a. It is interesting to see that a small amount of Cr^{+3} decreases the thermal expansion compared to the parent glass or glass-ceramic whereas further increase of Cr^{+3} has less effect on the original thermal expansion. Since the distribution of Cr in the coating is continuous, higher near the interface and lower toward the coating surface, the thermal stress caused by differential thermal expansion in the coating is accordingly continuous and favourable in the sense that a suitable thermal expansion gradient is built. Here, it is assumed that the diffused Cr(either Cr^{+2} or Cr^{+3}) has a similar effect observed in this simulated test. However, the occurrence of surface $LiCr(SiO_3)_2$ whose thermal expansion coefficient is only $56 \times 10^{-7}/°C$ provides an abrupt change which inevitably causes stress between the surface layer and bulk coating underneath(Fig.5.51b). It is obvious that where excessive Cr^{+3} exists, or precisely, $LiCr(SiO_3)_2$ phase precipitates, then the wrinkling is inevitable if the coating is quenched from the semi-molten state.

Thirdly, the large amount of Cr diffused into the coating affects the glass-ceramic development itself in addition to the reaction forming $Cr_{12}P_7$ and $LiCr(SiO_3)_2$ mentioned above. Thakur[103] found that Cr^{+3} cannot act as an effective nucleating agent in $Li_2O\text{-}2SiO_2$ glass-ceramic. Other reports [104] [105] show that Cr^{+3} decreases the crystal growth rate as a result of the increase in glass viscosity as the concentration of Cr_2O_3 increases. Cr^{+2} has also been reported to reduce the crystal growth rate but not as much as Cr^{+3}[104]. It is not easy to assess the exact effects on the glass-ceramic development of those chromium ions diffused into the coating from the substrate because their valence is predominantly Cr^{+2} and redox reactions proceed continuously followed by changes of valence. Under normal conditions divalent Cr^{+2} is difficult to introduce and maintain in glass without redox reactions occurring, otherwise a strong reducing atmosphere is needed. This prevents a detailed simulation work as the concentration of Cr^{+2} or Cr^{+2}/Cr^{+3} ratio needs to be carefully controlled in a bulk glass.

E. Role of a preformed metal oxide layer

As stated earlier, the absence of metal oxide or an oxide saturated layer at
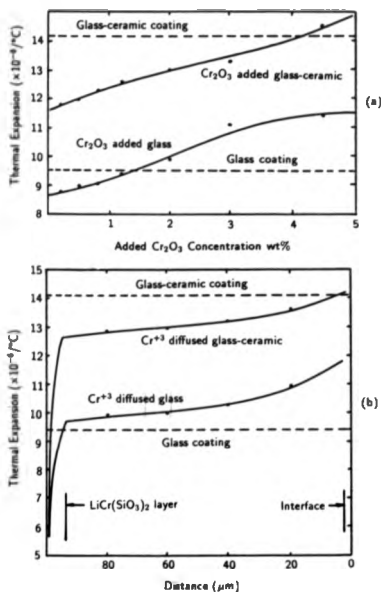
Figure 5.51: (a) Thermal expansion change versus Cr_2O_3 concentration in coating glass and glass-ceramic (b) Assumed thermal expansion change versus distance in glass and glass-ceramic coating

the interface, allows further redox reactions to occur. Particularly in this study, after a layer of CrO dissolves into the coating, severe interactions take place. However, if the preoxidized alloy with the glass coating was subject to a same firing treatment used in the unoxidized alloy, then, some different results are obtained, see section 5.1.8. A stable intermediate Cr_2O_3 layer of thickness of $3-4\mu m$ can be created by proper pretreatment. This layer of Cr_2O_3 plays an important role in the bonding between the glass and metal and in their subsequent heat treatment. In general, the layer prevents glass from reacting directly with metal and all the redox reactions discussed above are greatly hindered. Any reactions producing Cr_2O_3 near the interface become thermodynamically unfavourable simply because the glass is already in contact with Cr_2O_3.

Manfredo[106] claimed that the saturation level of Cr_2O_3 in a complex sodium silicate glass at 1500°C is 0.35 atomic%. William[108] has found the saturation level of Cr_2O_3 to be 0.1 atomic% in a sodium calcium silicate glass at 1500°C. Tomsia[84] gave saturation level of 2.6 wt% for Cr_2O_3 in sodium-silicate binary glass system. As briefly stated in section 5.1.11.B the strong ability of Cr_2O_3 to form its own cationic complexes in the glass structure decides the low solubility and stability of the oxide. Because of this, the saturation of Cr_2O_3 in the adjacent glass can always be maintained creating the desired bonding condition. On the other hand, it is still possible for the limited Cr_2O_3 to dissolve in the adjacent glass, to exceed saturation, and eventually to develop $LiCr(SiO_3)_2$ along the interface between the glass and oxide after firing for a few hours. Sturgeon[26] proved the usefulness of this layer and its contribution to bonding strength merely from the point of view of mechanical keying. One should, however, consider the stress at this type of interface as the growth of $LiCr(SiO_3)_2$ introduces a very low thermal expansion coefficient which may not be accommodated by the interface without causing stress. Therefore, overfiring on the preoxidized alloy still needs to be avoided. Tensile tests show that the unoxidized alloy and coating glass has a bonding strength range of $15-33MN/m^2$ whilst the oxidized alloy increases the range to $24-50MN/m^2$. The failure always occurs at the interface between the preformed Cr_2O_3 and substrate in those coatings

135

on the oxidized alloy. This means that the actual bonding strength between coating and Cr_2O_3 layer is much stronger than $50MN/m^2$ and the desired interfacial structure with saturation of preoxidized Cr_2O_3 layer has probably been achieved. On the other hand, the bonding strength of the coating on preoxidized Nimonic alloy is limited by the bonding strength of preformed Cr_2O_3 layer and substrate.

In brief, all redox reactions taking place between the glass coating and substrate alloy are detrimental to the subsequent glass-ceramic process in this particular glass/Nimonic system. The preoxidized layer halts these reactions, and as a result, the heat treated glass-ceramic coating forms the desired fine microstructures. Fig.5.52(a & b) gave a typical comparison between these two different coating structures.

5.2 Coating on Titanium Metal Sheet

5.2.1 Introduction

Titanium is used in aerospace and commercial applications because of its high strength-to-density ratio, good fracture characteristics and general corrosion resistance. However, various forms of deterioration can occur especially when titanium is used at elevated temperatures. Myers et al[107] reported a variety of corrosion attack on titanium and its alloys. The hightened capability of titanium to absorb oxygen or nitrogen to form a solid solution was studied earlier by Eremenka[108] and Morozidr[109]. It is found that above 550°C, titanium will absorb oxygen in air to form both an oxide scale and a brittle, sub-surface layer which can initiate surface cracks[110]. By alloying titanium with other elements, some titanium alloys with better oxidation resistance and other useful mechanical properties have been developed but their service temperatures are not higher than 590°C[111]. The oxidation behaviour of titanium based alloys for applications in turbines and other areas can be found in the same reference. It is obvious that use of attractive and cost-effective titanium metal and its al-

(a)

(b)
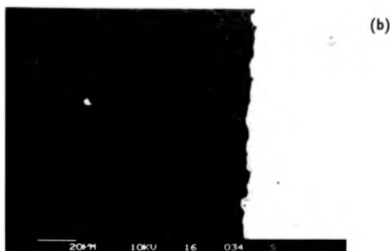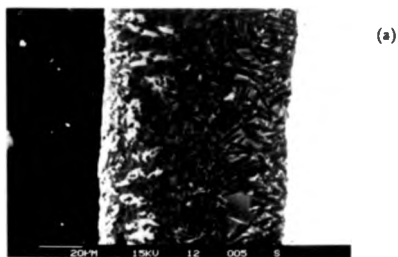
Figure 5.52: (a) Heat treated glass-ceramic coating on unpreoxidized Nimonic alloy (b) Heat treated glass-ceramic coating on preoxidized Nimonic alloy

loys is limited in existing applications due to the poor oxidation resistance. A protective layer on the metal may provide a solution to the problem. Ion plating has already been used to coat a very thin (1μm) layer of noble metal platinum onto the surface of titanium and improved oxidation or corrosion resistance has been obtained[112] [113].

Attempts have been made to use cheap silicate based enamel coatings to coat titanium and its alloys. Most of the work was conducted by Russian scientists, see Kornilova[114], Kheitets[115], Gorbatenko[116] and Sitnikova et al[117]. Some interactions between the enamel coating and the titanium substrate have been reported. Sitnikova[118] studied the influence of melt composition on the character of the interaction of titanium with various glass melts, in order to find oxides which could be used to develop coatings having the most effective protective action in aggressive media. Sitnikova [118] also studied the interactions between low-alkali silicates containing refractory oxides and titanium alloys. It is claimed that adhesion of the coating and physical as well as chemical properties of the substrate can be mainly determined by the interactions during the firing process. Kheitets[120] in his study discovered that additions of V_2O_5 and Nb_2O_5 may form an intermediate layer and improve adhesion of the enamel to titanium. Despite all the work concerning enameled titanium there is still very limited information involving Ti-molten glass systems in terms of interactions and thermodynamics, though some relevant work can be found in the studies by Passerone et al[121] and McColm et al[122]. In the glass-ceramic coating area, where a normal glass enamel undergoes heat treatment to convert it into a superior glass-ceramic, work has been developed mainly with metals such as copper, steel, tungsten and molybdenum. How various glass-ceramic compositions interact with the reactive metal titanium, and how these interactions affect not only the glass-ceramic compositions, structures and properties but also the titanium substrate structure and properties are areas where further and detailed work needs to be done.

In this study, the received titanium sheets were vapour blasted, cut and degreased. Both unoxidized and oxidized sheets were coated by various glass-

138

	ppm
Al	500
Cr	500
Mn	500
Ni	500
V	300
Fe	200
Cu	200
Si	200
Sn	200
N	80
O	2000
Ti	Balance

Table 5.4: Composition of used titanium substrate

ceramic coatings. The coating assemblies were fired in a Ar atmosphere to protect the titanium substrate from being oxidized, and further heat treatment was applied to change the vitreous glass enamels into crystallized glass-ceramics. Cross-sections of the coating assemblies were analyzed under SEM to observe possible diffusions and interactions. XRD and other experimental techniques were also used to explore these interactions and their consequent effects on the coating microstructural changes. An understanding of how the glass-ceramic system reacts with titanium and how to control these reactions is discussed and future work will be suggested.

5.2.2 Morphology of uncoated metal structure and its surface

Table 5.4 shows the composition of tested titanium metal (Goodfellow Metal Ltd)[123] with its purity at 96.6%. As customarily classified in the titanium industry, titanium metal or its alloys can be grouped as α, β or $\alpha+\beta$ type depending principally on whether their structures contain a hexagonal close-packed phase(α) or body-centered cubic phase(β) or a mixture of both. At 882°C, titanium undergoes an allotropic transformation from a low temperature (α) phase

Figure 5.53: Optical micrograph of the etched titanium sheet

to a (β) phase which remains stable up to the melting point. Because α-phase and β-phase have different properties, by adjusting the proportion of these two phases through different processing and heat-treatment, different products can be produced to suit various applications. In general, α-titanium shows greater toughness with improved fatigue performance whereas β-titanium gives better creep behaviour. Though the structure related properties can be easily manipulated by controlling these two phases, problems arise when a coating is to be used for the metal. First, the coating firing and heat treatment have to be chosen so as not to alter the titanium metal structure greatly. This sometime will impose difficulties in designing a proper thermal history for the coating. Second, the interaction at the interface between titanium and the coating may cause interdiffusion resulting in a change of the titanium composition, hence, properties. For instance, titanium can be embrittled by the diffusion of oxygen. Within specified limits, oxygen strengthens the α-phase. The individual or combined effects of oxygen with other elements enhance titanium metal in its hardness and tensile strength but reduce ductility greatly.

In order to study possible metallurgical changes of titanium during the coating procedure, Fig.5.53 shows an optical microscopic picture of titanium struc-

140
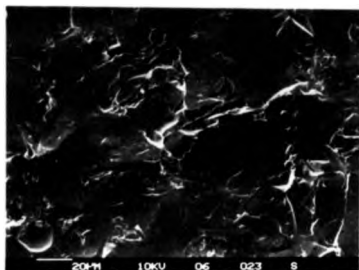
Figure 5.54: SEM micrograph of vapour blasted surface of titanium sheet

ture which is not yet subject to any coating treatment. The structure is typical of the phase mixture determined in the manufacturing process. The surface of vapour blasted titanium sheet is also revealed in Fig.5.54. via SEM.

5.2.3 Coating quenched after firing

Coatings on unoxidized titanium substrates were fired in a furnace where Ar flow was used to protect the titanium from being further oxidized during the firing. The firing temperature was 970°C and time was for 5min. No attempt was made to bring the firing temperature below the titanium α/β transition of 882°C in this exploratory study. The fired coatings were quenched in air by quickly withdrawing from the furnace. Therefore, these coatings remained vitreous. Meanwhile, the metallic structure of titanium was expected to change as confirmed in Fig.5.55 showing Widmanstatten plates of α after air-cooling from the β-phase field. This is very different from its original equi-axed grain structure in Fig.5.53. It is very surprising to find that the coating on the unoxidized titanium was very porous. Numerous tiny bubbles were trapped in the glass coating giving an appearance of foam. Fig.5.56 gives a SEM cross-section picture which shows clearly bubbles trapped in the glass coating. Relatively

141

Figure 5.55: Change of phase structure of titanium after being fired at 970°C for 5min in Ar (Optical microscope)
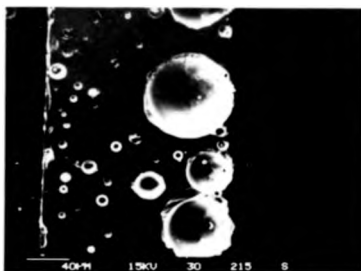
Figure 5.56: SEM shows bubbles in the coating fired in Ar at 970°C for only 5min

142
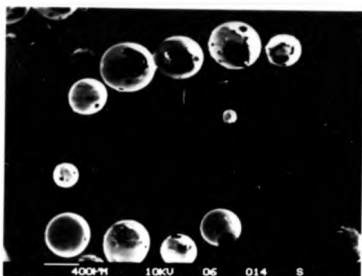
Figure 5.57: Bulk glass fired on titanium showing similar bubbling effect as with coating produced from powder

long fired coatings show the structural deterioration and the coating itself becomes very uneven and rough, though it adheres to titanium well. The porous or foamed structure of the coatings indicates a severe interaction taking place at the interface. It is assumed that the interaction involving release of gas is responsible for disrupting the coating structure as the coating flows at low viscosity during the firing. To eliminate possibility of trapped gaseous phase being caused by using glass powder as the original coating material, bulk glass with same chemical composition as that of the powder was thinned down to a slice of a thickness less than 0.5mm and then the slice was placed directly onto titanium followed by the firing. The bubble disrupted coating structure was confirmed again in Fig.5.57. The use of inert Ar atmosphere in the furnace eliminates the possibility of any reaction between titanium and the atmosphere in the furnace chamber, thus, any chemical or physical changes of the coating are results of direct contact of the coating and titanium. The coating assemblies were deliberately fired for a longer time of 40min and then etched in 60% HF solution for 30sec to partially remove the coating glass. Fig.5.57 shows the glass layer, an intermediate reaction layer and the substrate titanium grains. EDX analysis

143
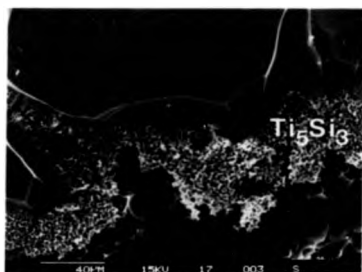
Figure 5.58: A reacted layer of Ti_5Si_3 formed between the glass coating and titanium

and XRD reveal that the reaction layer is a titanium silicide (Ti_5Si_3). So far as the reaction layer is concerned, there are two basic reactions between SiO_2 in glass and substrate titanium to produce Ti_5Si_3. One is proposed as:

$$8Ti(metal) + 3SiO_2(glass) = Ti_5Si_3(interface) + 3TiO_2(glass) \qquad (5.14)$$

The other is proposed as:

$$5Ti(metal) + 3SiO_2(glass) = Ti_5Si_3(interface) + 3O_2 \qquad (5.15)$$

Because the coating fired in Ar on the unoxidized titanium is so disrupted, it is likely that reaction 5.15 dominates in this particular case in which released gaseous oxygen forms bubbles in the glass that has a low viscosity at the firing temperature.

The coatings on preoxidized titanium ($700°C$ for 30min in air) fired under the same condition showed a very similar coating structure full of bubbles and pores. This indicated that the current preoxidation condition would not provide the

144
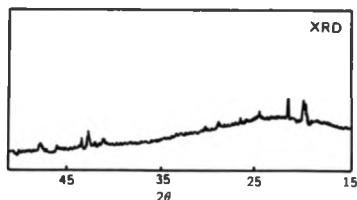
Figure 5.59: XRD indicating the basically vitreous state of the fired only coating with a few crystals due to spontaneous crystallization

coating with a sufficient transition layer to establish a desired interfacial structure, and the damaging bubbling effect caused by interaction was not stopped. The reasons will be discussed in the following sections.

XRD of the coatings on both unoxidized and oxidized titanium shows similar broad curves (Fig.5.59) indicating the vitreous state of the quenched coating although a few distinct peaks confirm the existence of some crystal phases. These crystal phases occurring at the early stage in the firing are SiO_2(quartz) and $Li_2O \cdot SiO_2$(metasilicate) due to spontaneous crystallization caused by the high surface energy possessed by finely ground glass powders.

5.2.4 Variation of firing temperature

Due to the high reactivity of titanium metal, a low firing temperature is preferred in order to avoid an acceleration of the reactions. Furthermore, to avoid uncontrolled α/β phase transformation of titanium metal itself the firing temperature needs also to be as low as possible. On the other hand, the temperature of firing should satisfy the requirements for sintering glass powder in the coating and wetting the substrate by the coating.

145
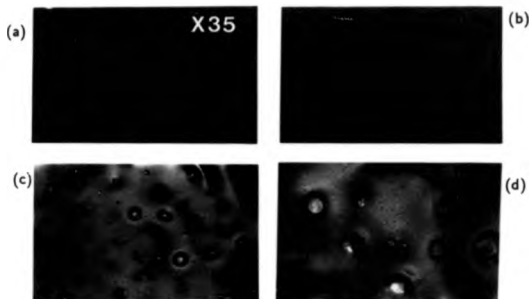
Figure 5.60: Bubbling effect increases with increase of firing temperature for a fixed time of 5min (a)900°C (b) 950°C (c)980°C (d)1000°C

The firing temperature has been varied from 900°C, 950°C, 980°C to 1000°C respectively for a time of 5min. The porous coating structure prevented preparation of a series of satisfactory SEM microscopy samples but it is still possible to judge from coating appearance that with increase of the firing temperature, the reaction producing Ti_5Si_3 and O_2 is getting more severe, see optical microscopy picture in Fig.5.60. XRD results and careful observation reveal that when the firing temperature is below 950°C, the coating tends to crystallize quite rapidly but it is not porous enough to show any foaming or bubbling. When the firing temperature is above 950°C, the coating is more vitreous with less crystal phase but it is so porous that the coating has a very foamed appearance with numerous tiny pores trapped. It is suggested that there are two factors associated with firing temperature to control the bubbling phenomena. First, the low temperature decreases the speed of reaction 5.14. and the glass is less fluid, resulting in a slow solid-solid based reaction, hence producing less gaseous phase. Secondly, the much higher viscosity at this relatively low temperature hampers the disruption to the coating structure by any gaseous phase. However, problems remain *1)* the premature glass-ceramic process at a lower firing temperature

146

may produce large amounts of uncontrolled crystal phases which may change the overall properties of the glass-ceramic coating in later heat-treatment. 2) a too low firing temperature produces inadequate amounts of molten glass to wet the substrate and sintering of the loosely packed glass particles is less effective. Therefore, pores may well exist due to insufficient sintering instead of those from the interactions.

Various temperatures were also used to fire the coating on preoxidized titanium. Unless titanium is excessively preoxidized there is little difference between results of coatings on unoxidized titanium and those on oxidized titanium.

5.2.5 Variation of the metal pretreatment

Titanium was preoxidized before being coated in order to create a layer of compatible titanium oxide as well as a barrier at the interface. Detectable titanium oxide can be obtained if received titanium sheets are exposed to air at above 700°C for 20min. XRD analysis revealed that the produced oxide is predominately TiO_2 and 700°C is just about the temperature at which the oxide grows rapidly. It was originally defined that 700°C for 30min should be the standard preoxidation condition for subsequent coatings. It is found, however, that the preformed TiO_2 layer can be easily dissolved by the coating glass to give a ternary SiO_2-Li_2O-TiO_2 glass system. Unless the preformed TiO_2 layer on the substrate is thick enough, dissolution may bring the titanium substrate into direct contact with the coating and subsequent interaction will follow. Therefore, the TiO_2 created between 500-800°C proved to be nondurable. This has been briefly mentioned in previous sections.

An alternative preoxidation was set at 900°C for 20min in this project in an attempt to produce TiO_2 of thickness of 8-10μm to act as a barrier. The thick preformed TiO_2 does prevent the damaging interaction between SiO_2 and Ti resulting in an excellent coating structure, but it does not produce a strong or adherent intermediate layer. Most of the coating assemblies failed during the cutting and polishing in preparation for electron microscopy samples. It would

147

be appropriate to say that it is not adequate to overcome the problem of reactivity by merely creating a transition layer of TiO_2 by the preoxidation. In addition, severely oxidized titanium can significantly alter the metallic structure and properties, at least at the metal surface. This can be very undesirable if the original characteristics of metal are to be maintained. Thus, the non-adherent oxide and the possible change of metal structure means that there is no advantage in the use of a preformed TiO_2 as an interfacial transition layer. Among a few successfully made cross-section samples, Fig.5.61a shows a crack between preformed TiO_2 and substrate Ti caused by weak bonding strength, whereas dissolution of TiO_2 by the glass has taken place as Ti silicates grow adjacent to the TiO_2 layer once the TiO_2 saturation level is reached. Furthermore, Ti ion is also detected in the glass coating bulk $20\mu m$ away from the interface indicating some diffusion of Ti ions. Fig.5.61b shows that, if the firing is prolonged, then the TiO_2 will eventually be converted into titanium silicates grown on the TiO_2 layer.

On a trial base, titanium sheets were nitrided before being coated. A N_2 flow was used to treat titanium sheets at 900°C, resulting in a golden layer of TiN. This intermetallic layer should be chemically compatible with the coating if the type of the bonding can be achieved like (-O-Si-N-Ti-), though mechanically the intermetallic structure can be very brittle. The coating fired at 980°C with N_2 flow showed very similar results to those obtained from the unoxidized titanium sheets fired in Ar. A similar foamed or porous structure of the coating is assumed to be created by the following reaction:

$$5TiN(interface) + 3SiO_2(glass) = Ti_5Si_3(interface) + 3O_2 + \frac{5}{2}N_2 \quad (5.16)$$
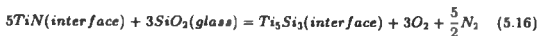
Or, the precreated TiN layer is too thin to stop the previously mentioned reaction(5.15) from proceeding.

148
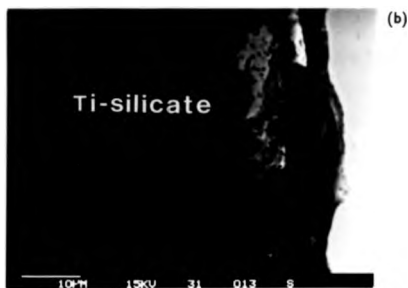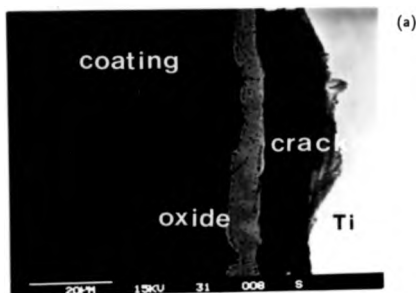
Figure 5.61: Heavily preoxidized titanium with glass coating (a) coating cracks at oxide/metal interface (b) preformed oxide dissolves and forms titanium silicate at the interface after 25min at 970°C.

149
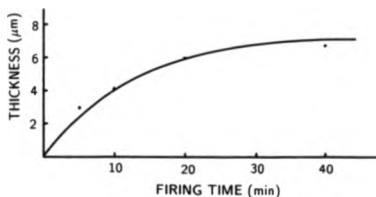
Figure 5.62: Thickness of Ti_5Si_3 layer versus firing time shows the diffusion controlled growth

5.2.6 Variation of firing time

It is predictable that long time firing may cause deterioration of the coating on unoxidized titanium as the reaction proceeds with time. It has been found that increase of the thickness of the reaction zone is slow but steady. At the standard firing temperature of 980°C in Ar the thickness of reaction zone was measured under SEM by varying the firing time(Fig.5.62), showing the steady advance of the reaction. EDX analysis reveals distributions of elements across the interface, and short range interdiffusion is detected mainly due to Si and Ti(Fig.5.63). The diffusion of O into titanium to form a solid solution is well known[124] but due to lack of analytical facilities, neither the rate of O diffusion into the substrate titanium nor the depth of diffusion was studied here.

Apart from generating bubbles in the molten glass coating, the O_2 produced by reaction 5.15 is also likely to form a variety of Ti oxides or solid solution with the Ti substrate. These oxides can either coexist with the reacted Ti_5Si_3 interfacial layer or diffuse into the glass. The step reaction to produce Ti oxides (possibly in various other forms) after the reaction 5.15 can be described as:
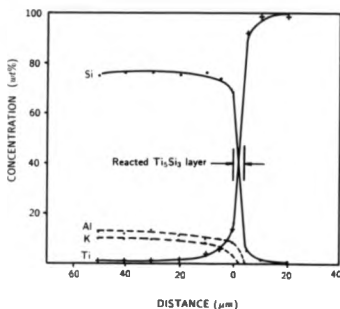
Figure 5.63: EDX quantitative analysis reveals short ranged diffusion of Ti ions and Si ions across the interface

$$Ti + O_2 = TiO_x \qquad (5.17)$$

The EDX of compositional distribution revealing a short ranged Ti concentration near the interface may indicate the existence of a small amount of Ti ions in the form of titanium oxides. But the level of Ti ions is low and therefore there is no detected titanium silicates which usually require a higher saturation concentration of Ti oxides in the area. This gives confirmation that the reaction 5.15 producing O_2 instead of TiO_2 dominates compared with the reaction 5.16, though the step reaction 5.17 can coexist but to a far lesser extent.

When firing is carried out under Ar, another interaction occurs between P_2O_5 and Ti substrate giving a reaction zone containing numerous tiny bright particles(Fig.5.64). These particles have a size of less than half μm making EDX quantitative analysis impossible but EDX spectrum in Fig.5.64 shows clearly the high concentration of P and Ti together with interference of the matrix giving Al, Si and K peaks. Literature records two P-Ti intermetallic compounds, i.e. TiP_2 and Ti_4P_3. It is suggested in this project that Ti_4P_3 is more likely as EDX registered a higher concentration of Ti. The following reactions are proposed to

151
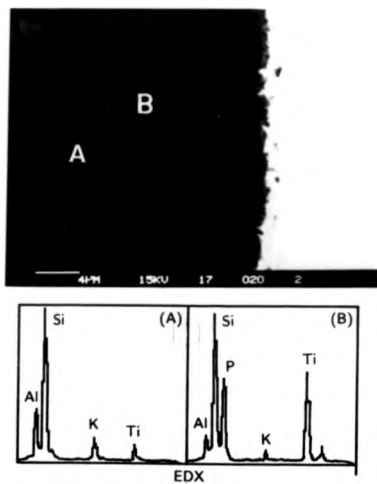
Figure 5.64: A reaction zone formed containing mainly P-Ti particles after long firing time

152

show that P_2O_5 may assist the disruption of the coating structure as the reactions can produce gaseous O_2 as well:

$$16Ti + 6P_2O_5 = 4Ti_4P_3 + 15O_2 \qquad (5.18)$$

$$9Ti + 3P_2O_5 = 2Ti_4P_3 + 7O_2 + TiO \qquad (5.19)$$

$$17Ti + 6P_2O_5 = 4Ti_4P_3 + 14O_2 + TiO_2 \qquad (5.20)$$
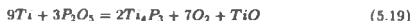
Due to analytical difficulties it is difficult to determine which reaction predominates. However, these reactions provide a similar mechanism to produce gaseous O_2. Referring back to the reaction 5.15, we found that SiO_2 and P_2O_5 react with substrate in parallel ways, both giving a gaseous phase and resulting in a very porous coating structure. The picture in Fig.5.65 (a, b&c) are coatings subject to HF solution etching to reveal porous structures. In Fig.5.65(a) the coating is of the original composition containing Al_2O_3, SiO_2, P_2O_5, K_2O, and Li_2O. Due to reactions 5.15 and 5.18 bubbles are formed in the coating having diameters up to $400\mu m$. In Fig.5.65(b&c) the coating has an adjusted composition containing only Al_2O_3, SiO_2 and Li_2O so that the possibility of reaction between P_2O_5 and titanium is ruled out. The bubbles are still produced with diameter up to $200\mu m$. Though smaller than those in Fig.5.65(a), they are still very significant, and are caused only by reaction 5.15. This comparison shows that reaction 5.15, involving Ti and SiO_2 to produce gaseous O_2, is a major reaction. Reactions 5.18 involving Ti and P_2O_5 can proceed simultaneously to exacerbate the problem.

There is little interfacial reaction in the coating applied on the preoxidized titanium with increase of firing time. Thus, a coating fired at the standard temperature for as much as 20min shows an even, glazed appearance indicating successful wetting and sintering. However, prolonged firing resulted in roughening of the edge area of the coating and possibly many extremely small pores. It is assumed that the preformed TiO_2 on the substrate can eventually dissolve

153
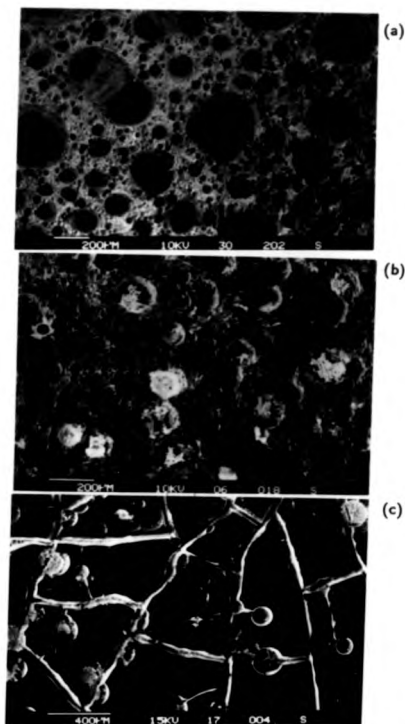
Figure 5.65: HF etched coating exposes bubbles caused by both interaction of SiO_2/Ti and P_2O_5/Ti type. (a) P-containg Li_2O-Al_2O_3-SiO_2 glass (b) P free Li_2O-Al_2O_3-SiO_2 glass (c) P free Li_2O-Al_2O_3-SiO_2 glass at deeper etching depth whereas crack caused by either TEC mismatch of the interfaces or H^+/Li^+ replacement during the etching process

154

into the molten glass under these firing conditions. It is possible to reach saturation and create Ti silicates while further dissolution will lead to direct contact between the glass melt and the Ti metal substrate causing interactions. This was demonstrated in Fig.5.61 (a&b).

5.2.7 Variation of the firing atmosphere

Due to the reactivity of titanium metal, choice of firing atmosphere is quite restricted. Reducing atmospheres, created normally by flowing H_2 or adding carbon powder in the furnace, are not possible because of reaction with Ti. N_2 reacts with titanium and of course oxygen can react very quickly with titanium at elevated temperature. In this project, Ar was used to achieve an inert atmosphere under which most of the firing occurred. Occasionally, air was used to create an oxidizing atmosphere.

By varying the atmosphere from Ar to air, an interesting comparison was made. The coating on the unoxidized titanium fired in Ar was very porous. However, the same coating fired in air gave a dense structure and evenly wetted appearance. Fig.5.66 (a&b) gives a comparison between 5mins' air fired and Ar fired coatings. The coating fired in air is so dense that even an HF solution etched coating exposes a very homogeneous structure giving only a very few isolated small pores(Fig.5.67). This is not comparable with the porous structure shown in Fig.5.65.

The dense structure produced in air implies that there is little gaseous phase produced. However, at the interface of the coating, a Ti_5Si_3 layer still forms as firing proceeds, and XRD analysis of the interfacial area after HF etching reveals that coatings fired either in air or Ar give rise of Ti_5Si_3 at the interface(Fig.5.68). Because different atmospheres give different redox potentials, which in turn affect progress of different interactions, it is possible that in the case of using air reaction 5.14 instead of reaction 5.15 takes place without generating any gaseous phase.

As the reaction 5.14 creates TiO_2 instead O_2, formation of either TiO_2 or

155
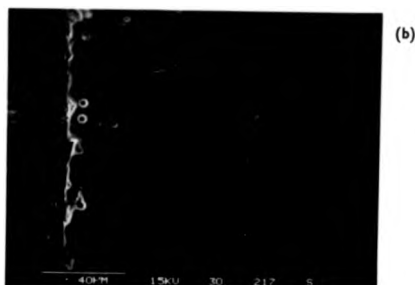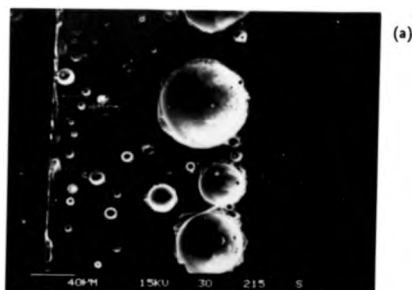
Figure 5.66: Same P-containing Li_2O-Al_2O_3-SiO_2 coating glass fired in different atomsphere gives different coating structure (b) in air (a) in Ar
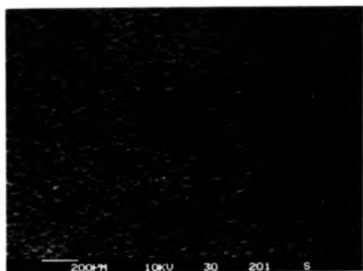
Figure 5.67: HF etched coating fired in air shows a very dense structure
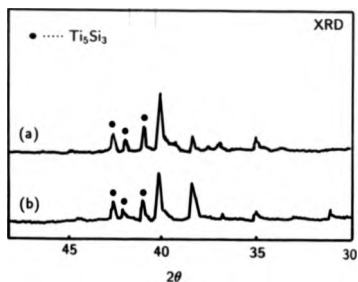
Figure 5.68: XRD reveals that coatings fired in both air (a) and Ar (b) give rise to Ti_5Si_3 at interface. (Top layer of coating was etched off before XRD)
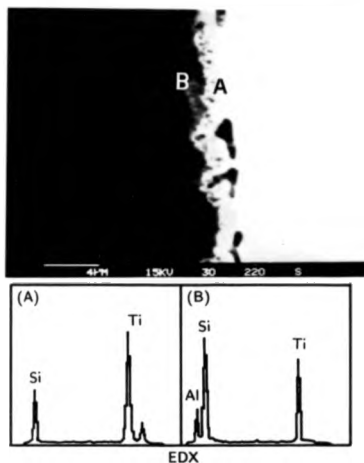
Figure 5.69: Air fired coating shows an additional layer (A) forms on Ti_5Si_3 (B) after 20min of firing

its silicates should be expected in the coating at least at the interface. Fig.5.69 confirms the formation of high Ti content phases attached to the Ti_5Si_3 layer in its EDX spectrum. This type of phase was not found in the coating fired in an Ar atmosphere. Furthermore, the interaction 5.18 involving Ti and P_2O_5 in Ar atmosphere does not occur here in the coating fired in air. This clearly illustrates that different atmospheres alter the direction of interactions.

Both air and Ar fired coatings with same firing time of 20min were HF etched to expose interfacial areas where the Ti_5Si_3 layer is expected (Fig.5.70 (a&b)). In the air fired coating there are some needle like bright phases embedded in between the glass coating and the Ti_5Si_3 interlayer. The EDX spectrum (windowless) proves them to be TiO_2 (or lower oxides). In the Ar fired coating only a pure Ti_5Si_3 layer is observed. This observation supports the proposed reactions

158
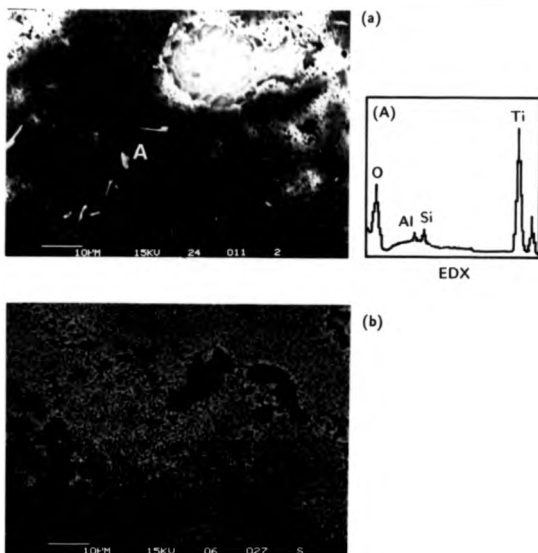
Figure 5.70: (a) Air fired coating shows some crystals attached to Ti_5Si_3 interfacial layer after HF etching (b) Ar fired coating shows a pure layer of Ti_5Si_3 after HF etching

5.14 and 5.15 according to the different experimental conditions.

Though the coating fired in air has a very satisfactory structure, it is difficult to prevent the uncoated area from being severely oxidized. It may be possible to fire in air provided that the substrate titanium piece can be covered completely with an homogeneous layer of glass powder and this layer must fuse easily at firing temperature to prevent air penetration as soon as the firing initiates.

5.2.8 Variation of the coating thickness

Since the interaction mainly take place at the interface between the coating and unoxidized titanium the thickness of the coating has little effect on the overall reaction. However, the interaction 5.15 involves the release of O_2. This gaseous phase is normally trapped in the molten glass to form the porous structure when the coating is fired. The thicker the coating is, the more difficult it becomes for the gaseous phase to escape. It is also understood that the edge areas of the coating are subject to more roughness and porosity simply because the edge areas are usually thinner than the central area.

It should be pointed out that the reaction, and therefore, the structural change, is also decided by the characteristics of the glass system itself, especially by its viscosity. If the coating glass is very viscous, or if the sintering process is operated at low temperature which does not provide enough liquid phase, then, the reaction may be insufficient to disrupt the structure. The pores produced are either trapped only in the interfacial area or they escape through the non-sintered region.

5.2.9 Variation of glass composition

Thermodynamically, titanium is an active element and will react with various oxides used in the glass-ceramic system. Judged from the free energies of formation listed in Table 2.1[36], most of the oxides, including SiO_2, can react with titanium due to their less negative free energies ΔG° than that of titanium oxide. The reactivity of titanium produces problems in designing a glass

Amounts of TiO_2 (wt%) in Glasses of the
Composition $0.8Na_2OMe_mO_n3.2SiO_2$

Me_mO_n	Amount of TiO_2	Me_mO_n	Amount of TiO_2
BeO	0.032	CoO	1.20
MgO	0.10	NiO	0.20
CaO	0.03	FeO	0.49
SrO	0.067	PbO	0.52
BaO	0.03	B_2O_3	0.045
MnO	0.034	Cr_2O_3	0.20
ZnO	0.041	Fe_2O_3	1.56
CdO	0.24	CeO_2	0.03
CuO	1.12	SnO_2	0.47

Table 5.5: Reaction produced TiO_2 in $M_m N_n$-Na_2O-$2SiO_2$ glass systems

coating composition. An ideal bonding interface between titanium and its coating requires some but not extensive interaction. Sitnikova et al[118] [119] did some exploratory work to provide general guidance as to the usage of individual oxides. Table 5.5[118] shows the amount of TiO_2(wt%) as a result of the reaction between titanium and various ternary M_mO_n-Na_2O-SiO_2 glasses. The "*" marked oxides are comparatively less reactive with titanium. These data indicate the following group of oxides as M_mO_n: Li_2O, BeO, CaO, BaO, SrO, MgO, ZnO, MnO, B_2O_3 and CeO_2 have less effect on the corrosion of titanium by silicate melts. However, this cannot be used as the base to design the best coating compositions, since a glass-ceramic coating system suitable for coating has to be considered in terms of its wettability, viscosity, thermal expansion, chemical stability and mechanical properties, and thermodynamic calculation can be complicated if a multi-component system is involved. It is overall a very complex task to choose a proper glass-ceramic coating for titanium.

In this project, the main purpose was not to design the best glass-ceramic coating composition, but to study the general interactions and seek for possible solutions. The model coating system is based on Li_2O-Al_2O_3-SiO_2 and other glass-ceramic systems were also examined as in Table 4.2. All coatings were

161

fired in Ar atmosphere.

The alkali metal oxide silicate system shows some very interesting results. The Li_2O-Al_2O_3-SiO_2 glass wets the substrate titanium well, but as expected, the coating structure is very porous due to reaction(5.14). In this system, the data of free energies ΔG°(Table 2.1) indicates SiO_2 as the oxide most vulnerable among others to reaction with Ti. The O_2 released from the reaction disrupts the molten glass leading to the porosity. This was already demonstrated in previous sections in detail. In contrast, the Na_2O-Al_2O_3-SiO_2 glass not only wets the titanium well but is also dense and even. In this particular system, Na_2O instead of SiO_2 is the most vulnerable oxide according to ΔG°. Thus, the substrate titanium reacts with Na_2O in the following way:

$$Ti(metal) + 2NaO_2(glass) = TiO_2(glass) + 4Na \uparrow \qquad (5.21)$$

The TiO_2 formed contributes to the adhesion and enhances wettability, whereas the atomic Na escapes via vaporization. A Na contaminated area was found on the sample support on which the coating assembly was placed during the firing. Fig.5.71 shows Na_2O-Al_2O_3-SiO_2 glass coated titanium with desired coating structure but a very complicated interface structure. EDX in Fig.5.71(A) compared with that of Ti_5Si_3 in (B) gives a different intensity of Ti and Si concentration indicating the formation of Ti rich phase adjacent to the inner Ti_5Si_3 layer. The very familiar Ti_5Si_3 layer, on the other hand, illustrates that the reaction 5.19 is not the only reaction in the system and reaction 5.14 or reaction 5.15 which give Ti_5Si_3 persists. It is not clear why the vapourized Na did not form bubbles in the coating structure. It could be that very low viscosity of the glass helps the escape of gaseous Na from the molten glass at the initial stage of the firing. In any case, the existence of a TiO_2 rich layer and escape of Na confirm the reaction(5.19) and shows that under different thermodynamic conditions, titanium can react with different oxides in glass. The K_2O-Al_2O_3-SiO_2 glass failed to bond to titanium because of the thermal expansion mismatch, so a comparison was not made.
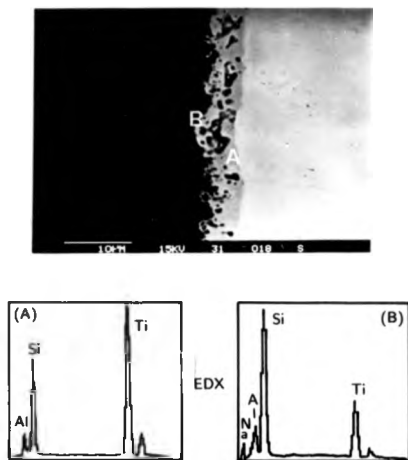
Figure 5.71: SEM of cross-section of Ti/Na$_2$O-Al$_2$O$_3$-SiO$_2$ system (B) Ti rich area (A) Ti$_5$Si$_3$ layer

The weight gain or loss was also monitored by weighing the assemblies, before and after firing, on a balance(Oertling)[124]. It was discovered that on firing at 980°C for 1hr the uncoated titanium sheet of an average weight of 0.5g would gain 0.62% weight verifying the existence of slight oxidation due to a leakage of air in the furnace, especially in a lengthy firing process. One side coated titanium sheet is expected to have almost half of the weight gain since only one side is exposed to the atmosphere, provided the coated side does not have severe reactions with the substrate. The weight gain of one side coated titanium with $Li_2O-Al_2O_3-SiO_2$ was 0.22% close to that of the expected value of 0.31%. Obviously, the release of O_2 caused by the reaction 5.14 does not result in significant weight loss off-setting the weight gain caused by the oxidation on the uncoated side. This implies that most of the released oxygen has been entrapped in the porous structure without escaping to the atmosphere. However, in the case of the $Na_2O-Al_2O_3-SiO_2$ coating, the one side coated titanium experienced the weight loss of 0.24%, confirming that the evaporation of Na exceeds the weight gain caused by the oxidation. These weight tests illustrate the feasibility of the reactions between titanium and various alkali oxides in the glass depending on the thermodynamic conditions, and the reaction mechanism can be very different.

Other coating systems including $Na_2O-CaO-SiO_2$, $B_2O_3-Al_2O_3-SiO_2$ and $Li_2O-MgO-SiO_2$, were also tested and the results are similar, i.e. certain oxides always react with Ti in the way of reaction 5.19 if thermodynamically they are more favourable than SiO_2 to react with Ti. The reacted TiO_2 is likely to form titanium silicates adjacent to the interface, whereas reaction to give Ti_5Si_3 layer always coexists because of the major SiO_2 content in the coatings, see Fig.5.72 (a),(b) and (c) and their respective EDX spectra. Between the reaction 5.14 and 5.15, which both produce Ti_5Si_3, it is more likely that reaction 5.14, which does not give gaseous O_2, dominates in all these systems as there are no visible bubbles in the coating structure. The reason to say so is that whenever the reaction 5.19 type is involved, the produced TiO_2 at the interfacial area may change the O/Si ratio, and hence, the redox potential, which can decide the way

164
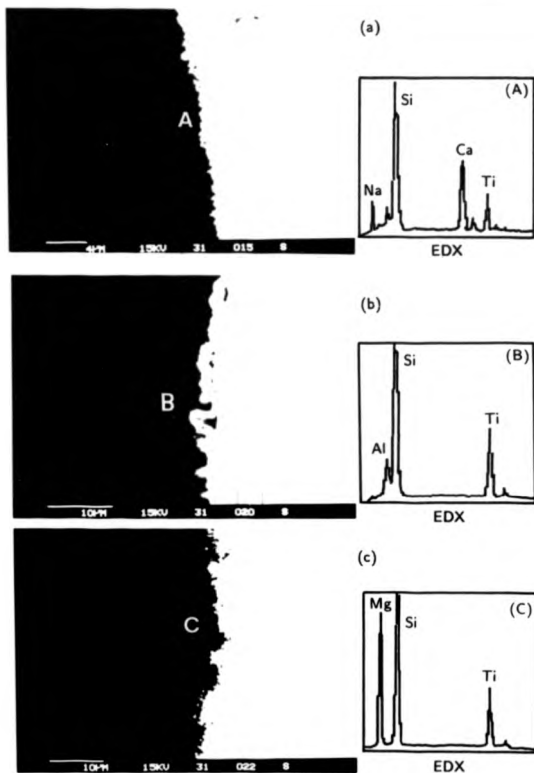
Figure 5.72: (a) Ti/Na$_2$O-CaO-SiO$_2$ system (b) Ti/B$_2$O$_3$-Al$_2$O$_3$-SiO$_2$ system (c) Ti/Li$_2$O-MgO-SiO$_2$ system

165

Figure 5.73: Formation of Ti_5Si_3 layer and less disrupted coating structure due to highly viscous CaO-Al_2O_3-SiO_2 on titanium

SiO_2 and titanium react in favour of reaction 5.14 rather than reaction 5.15.

Alkaline earth metal oxide silicate systems based on CaO-Al_2O_3-SiO_2 or MgO-Al_2O_3-SiO_2 were also tried. Because these glass systems are much more viscous, the firing temperature has to be increased to the range of 1000-1100°C, or even higher, to make the glass flow to wet the substrate. The high firing temperature is certainly not favourable as the reactivity of titanium is enhanced. To avoid an excessive high firing temperature, B_2O_3 was added into the basic composition at 6 wt%. The thermodynamic data of the alkaline earth metal oxide systems also indicate the possibility of reaction between Ti and SiO_2. Therefore, the formation of certain titanium silicides is expected(Fig.5.73) and bubbles originated from the interface find it difficult to escape to the coating surface. The disruption of coating structure is not as severe as it is in those alkaline metal oxide systems simply because the alkline earth metal oxide systems are too viscous.

It is known that the enrichment with titanium oxide at the interfacial area helps the establishment of an ideal bonding structure. The introduction of TiO_2 into the CaO-Al_2O_3-SiO_2 system also coincides with the function that TiO_2 can

Figure 5.74: Dense coating structure achieved by introducing TiO_2 oxide into $CaO-Al_2O_3-SiO_2$ system

act as a nucleating agent for crystallization. 10 wt% of TiO_2 was added into the basic $CaO-Al_2O_3-SiO_2$ system and relatively good result was obtained. In Fig.5.74, compared with Fig.5.73, a dense coating structure has developed in spite of a persistent formation of Ti_5Si_3 at the interface. The dense structure indicates that the introduction of TiO_2 obviously changes the O/Si ratio and the altered oxygen potential favours the reaction 5.14 instead of 5.15.

The high viscosity of these systems may create problems of wettability and sintering unless some modifiers are added or the firing temperature is sufficiently raised. Other problems associated with these systems are high melting point and poor crystallization characteristics[126]. All these factors could contribute to difficulties of glass manufacture at the beginning and control of crystal structure in the subsequent glass ceramic process. On the other hand, the high refractoriness and chemical stability of these non-alkali metal oxide systems are very useful as glass-ceramic coatings frequently require these characteristics.

In the traditional enameling industry, certain components called adhesion oxides are always used in base compositions in order to increase the adhesion between the enamel coating and metal substrates. The adhesion oxides, defined

167
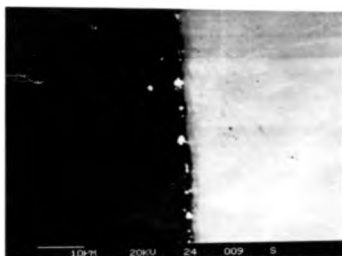
Figure 5.75: CoO containing $Li_2O-Al_2O_3-SiO_2$ system gives a dense coating structure

as those which have less negative formation energy ΔG° than most of other oxides in the glass compositions, can easily be reduced to metals whereas the substrate metals can be oxidized. The formation of substrate metal oxides helps to develop an oxide saturated zone and thus to achieve better adhesion, see reference[93]. In this project, a typical adhesion oxide CoO was used in the basic $Li_2O-Al_2O_3-SiO_2$ system. As described in this section, coating with basic $Li_2O-Al_2O_3-SiO_2$ glass produces severe bubbling due to the interactions and low viscosity of the glass. By adding CoO to the basic glass but treating the coating in the same way, significant improvement has been achieved. The CoO containing glass coating shows(Fig.5.75) a very dense and even appearance. The metallic spots(i.e. Co) near the interface as well as within the bulk coating verify the redox reaction taking place in the following way:

$$Ti(metal) + 2CoO(glass) = 2Co(precipitates) + TiO_2(glass) \qquad (5.22)$$

The reaction(5.22) produces metallic Co, which forms dendrites near the interface, and TiO_2. Both are very useful in satisfying the requirements for an ideal interfacial structure and increase the adhesion. Fig.5.76 is a quantitative EDX analysis of compositional distribution of Ti and Co ions which illustrates the

168
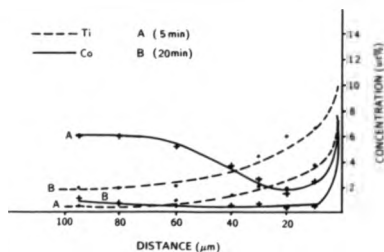
Figure 5.76: EDX analysis reveals the change of elemental distribution of Ti and Co across the interface with firing time

change of their concentration with firing time as redox reaction 5.20 develops. The SiO_2 and Ti reaction still proceeds and produces an interfacial layer, see also Fig.5.76. However, it is obvious that this reaction is less severe than it was in the non-CoO coating as the reaction layer is thin. The coatings were subjected to impact forces and it was found that CoO containing coatings always break cohesively instead of adhesively. This means that the interfacial bonding is even stronger than the coating glass-ceramic material itself.

5.2.10 Discussion

A. Formation of titanium silicide at the interface and its effects on the coating

The free energy ΔG° data in Table 5.3 clearly shows the possibility of SiO_2 reaction with titanium. In those glass systems in which most of the oxides have more negative formation energy than SiO_2, e.g. CaO-Al_2O_3-SiO_2, CaO-MgO-SiO_2 and Li_2O-Al_2O_3-SiO_2 etc, SiO_2 itself always becomes the most vulnerable oxide to reaction with titanium especially at elevated temperature. However the reaction between SiO_2 and titanium can vary depending on experimental

169

conditions. The following reactions are found to occur widely in the glass systems examined in this project.

$$8Ti(metal) + 3SiO_2(glass) = Ti_5Si_3(interface) + 3TiO_2(glass)......(5.14)$$

$$5Ti(metal) + 3SiO_2(glass) = Ti_5Si_3(interface) + 3O_2 \uparrow ......(5.15)$$

The titanium silicide formed at the interface is always very hard and brittle therefore the properties of the surface will differ from the titanium substrate. Due to lack of available data, the thermal expansion coefficient of Ti_5Si_3 is not known nor how much difference exists between the reacted layer, coating or substrate titanium. Cracks shown in Fig.5.65c may have demonstrated that the interface involving the glass-ceramic coating, Ti_5Si_3 layer and titanium substrate can be highly stressed.

Factors deciding the nature of the interaction in the coating systems mainly are glass composition and firing atmosphere, which determine the redox reaction potentials. If the reaction develops in the way of 5.14, the glass coating can sinter without giving excessive porosity. However, if reaction 5.15 dominates, then the coating is usually very porous as O_2 is evolved. The porosity, of course, will also depend on viscosity, firing temperature and firing time of the glass. When the basic $Li_2O-Al_2O_3-SiO_2$ system is used, the glass flows very easily at the firing temperature and the molten glass traps the gaseous phase to give a foamed coating structure. This effect prevents the normal coating from forming. Therefore, to coat titanium successfully with a glass-ceramic system, the reaction 5.15 has to be avoided.

B. Role of various oxides and adhesion oxides

In the case of the interaction between titanium and other oxides in glass, thermodynamics plays a decisive role in determining the types of reactions. The reduced metal oxides are precipitated in the glass in either metallic form, as indicated in reaction(5.22), or escape as vapour, as shown in reaction(5.21). It is known that the formation of the metal oxide of the substrate titanium, TiO_2, near the interface is very useful as the interfacial equilibrium, maintained by the metal oxide, increases the adhesion. The diffusion of TiO_2 to the glass coating

170
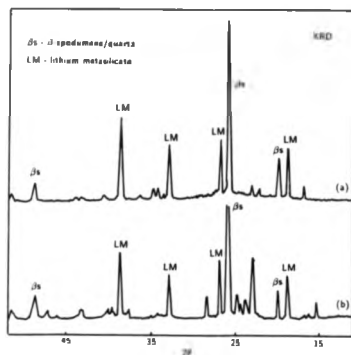
Figure 5.77: XRD of heat treated glass-ceramic coatings (a) non-CoO containing (b) CoO containing

and gradual distribution of the oxide may also help to build an ideal structural gradient. Adding TiO_2 into the glass system is certainly useful as shown in the previous sections whereas to create a TiO_2 rich zone by in situ redox reaction such as the reaction 5.22 is even more important. An even distribution of TiO_2 throughout the coating in Fig.5.76 proves that this can be achieved by using so-called adhesion oxides. The formation of metallic deposits as well as metallic dendrites, as part of the reaction products, is also advantageous as the dendrites increase mechanical keying between the coating and substrate[93].

During the subsequent conversion of glass into glass-ceramic coating, the redox reactions will certainly affect both the interfacial and bulk coating structures depending on how these redox reactions develop. This complicated subject needs to be studied in further detail. Fig.5.77 gives XRD spectra of coatings with and without CoO after heat treatment showing that the basic crystal phases have remained unchanged.

C. Role of adhesion oxides

171

In the porcelain enameling industry, the adhesion oxides play "a role in attaining and maintaining equilibrium compositions at the interface." "Their most important function is to participate in the formation of alloys whose compositions under proper conditions can readily adjust themselves to maintaining chemical equilibrium with the changing compositions of the adjoining glasses." In addition, "the adherence oxides lead to the formation of dendrites and a corresponding roughening of the substrate interface; this roughening contributes to mechanical adherence and becomes especially important with the loss of phase equilibrium, and thus chemical bonding, at the interface." — Borom & Pask[93].

In this project, CoO has been used as an adherence oxide to promote the adhesion between LiO_2-Al_2O_3-SiO_2 glass-ceramic coating and the titanium substrate. Generally speaking, an adherence oxide should be reduced to metal and this metal should form a continuous solid solution with the metal substrate. In the particular case of a glass-ceramic coating, the effect of adherence oxides and their reactions on further development of glass-ceramic structures also has to be considered. The use of CoO may not be the best choice as in this study the use of adherence oxides has not been optimized. However, the use of CoO illustrates the principle of how the adherence oxide works and proves the necessity of adding the oxides in the glass-ceramic coating for titanium. The use of the adherence oxides achieves not only the functions described by Borom and Pask, but more important, it is found that the adherence oxides help to hinder the direct interactions between titanium and SiO_2. The interactions between titanium and the adherence oxides always take place in preference to reaction between titanium and SiO_2, hence, the damaging reaction involving SiO_2 is less advanced. Additionally, the reactions between titanium and the adherence oxides do not produce gaseous oxygen which give rise to foaming of the coating structure, instead, TiO_2 and Co-Ti dendrites are produced, and both reaction products enhance the bonding between the coating and titanium.

D. Problem of using P_2O_5 as nucleating agent in the coating

As indicated by thermodynamics, P_2O_5 and the titanium substrate can easily

react according to reaction 5.18 (Fig.5.2.12). Although the accurate identification of submicron P-Ti particles in this project is very difficult, there is no doubt that the reaction between P_2O_5 and Ti can generate a gaseous phase to make the molten glass porous. The reaction is mainly observed in an Ar atmosphere but not in air showing that the reaction is dependent on oxygen potential. The existence of reaction 5.18 not only affects the coating structure due to the gaseous phase but also the consumption of P_2O_5 can decrease the nucleation and crystallization in the reaction zone and thus fail to produce the desired coating structure. Either another nucleating agent must be used or reaction 5.18 avoided, to coat titanium successfully.

E. Problem of titanium reactivity and possible solution

"The main problem with conventional oxidation resistance coatings on titanium is the high reactivity of the coating material with the alloy substrate. This leads to interface reactions which cause severe degradation of surface related properties such as low and high cycle fatigue"— Eylon et al[111]. In the glass-ceramic coating of titanium, the formation of titanium silicides illustrates this difficulty. Glass-ceramic coatings can be used to provide a barrier for oxidation resistance or corrosion resistance but in applications where stress will be experienced, it is essential to avoid or suppress the discussed reactions especially the one involving release of gas and at the same time to maintain the strong adhesion between the coating and substrate via chemical bonding.

One possible solution is to reduce the firing temperature at which the coating and titanium seal, as high temperature enhances the reactivity of titanium greatly. In fact, all interactions proceed rapidly in the firing range of 9501100°C when molten glass severely attacks titanium. It would be less reactive if the firing could be carried out at a lower temperature. On the other hand, the glass-ceramic coating should remain refractory enough to meet the demands of high temperature applications. In order to sinter or fire the refractory glass-ceramic coatings poperly and make them bond to titanium at relatively low temperature, ordinary enameling coating techniques have to be changed or modified. One of

the practical ways of achieving this is to use sol-gel technology to coat titanium. The main advantages of using sol-gel technology to provide oxidation protection are a) much lower sintering temperature required for glass or glass-ceramics b) much more homogeneous and controllable thickness of coating obtainable (see Jones[126]). Application of sol-gel coatings as diffusion and oxidation barriers for metal matrix and ceramic-matrix composites have been reported by Nelson et.al.[127].

The other solution to reduce the reactivity of titanium is to use certain kinds of adherence oxides in the glass composition such as CoO tested in this project, to divert the harmful direct interaction between SiO_2 and the titanium substrate into other reactions which are helpful to strengthen the adhesion without affecting the properties of the glass-ceramic coating significantly. Important initial results have been obtained in this project, yet further work needs to be carried out in order to optimize adherence oxides.

The third solution, possible but least popular, is to develop a certain kind of barrier between titanium and the glass-ceramic coating to prevent the direct contact between titanium and glass. The likely candidates for the barrier can be some thermodynamically stable metals, intermetallics and oxides. The introduction of a barrier inevitably complicates the interfacial structures in a sense that thermodynamics, chemical and physical properties and coating technologies would have to be carefully considered for the necessary overall compromise. This is to be a very difficult task, hence, the barrier solution has yet to be addressed.

Chapter 6

Conclusions and Future Work

Bonding of glass ceramic coatings to high-temperature alloys is a complex process. In the case of reactive metal substrates, severe reactions occur and the interactions and interdiffusions tend to change the microstructures and properties of glass-ceramic coatings from those intended.

The investigation of a coating system consisting of lithium silicate glass-ceramic on a Nimonic alloy has revealed that Cr in the substrate is the most active element from a thermodynamic point of view. Redox reactions were observed at the glass and alloy interface and they greatly affected the bonding and the subsequent glass ceramic process in the following way:

1) The coated glass readily reacts with the substrate alloy to form a chromium oxide (CrO) layer at the interface which tends to dissolve rapidly into the glass.

2) The Cr reacts with P_2O_5, which is added to the glass as a nucleating agent, to form $Cr_{12}P_7$ compounds near the interface. This decreases the available nucleation sites and coarsens the glass-ceramic structure in the reacted zone.

3) $LiCr(SiO_3)_2$ results from the reaction between diffused Cr and glass. Its formation occurs not only at the interface but mainly on the surface of the coating. It is proposed that the reaction proceeds by oxidation of Cr from the substrate alloy and reduction of ZnO in the glass as a continuous redox reaction.

4) Preoxidation of the alloy forms a well-adherent Cr_2O_3 layer on the alloy surface. This Cr_2O_3 layer tends to behave very differently from the reaction

175

formed CrO. There is an optimum thickness at which the Cr_2O_3 hinders the undesired reactions since it acts as a stable barrier. With careful choice of pretreatment, firing and heat-treatment a preferred coating structure can be achieved.

5) Comparison with other glass/metal systems indicates that high valence oxides are generally stable and can form a protective intermediate layer, but low valence oxides are subject to dissolution and diffuse more easily in the glass/metal systems.

In the investigation of the lithium aluminium silicate glass-ceramic/titanium metal coating system, the reactivity of titanium metal creates problems in achieving a satisfactory bond. The interactions between the coating and substrate can be summarized as:

a) Direct contact between various silicates and titanium at elevated firing temperature forms the silicide of Ti_5Si_3 at the interface. The reaction is based on two major machanisms. One produces titanium oxide and the other produces gaseous O_2 phase in addition titanium silicides. The oxygen produced by the reaction disrupts the coating or form various bubbles at the interface. This reaction, therefore, should be avoided.

b) The non-adhering pre-oxidized TiO_2 cannot act as a transitional layer due to its mechanical weakness though the interfacial structure is chemically desirable.

c) Certain adherence oxides are needed as these oxides react with titanium prior to SiO_2 so that a TiO_2 rich interfacial area can be produced. The reduced adherence oxides should produce metal to form dendrites with the substrate at the interface to promote the mechanical adhesion. This type of interfacial structure is important because it retards the direct reaction between titanium and SiO_2.

d) P_2O_5, added as a nucleating agent, reacts with titanium substrate very severely especially in Ar atmosphere. It has a similar bubbling effect as the reaction between SiO_2 and Ti. P_2O_5 may not be a desirable nucleating agent in the case of glass-ceramic coating on titanium.

This project has provided some essential understanding of how the chosen glass-ceramic systems interact chemically with Nimonic alloy and titanium metal. Based on the understanding from this project, proposals can be made as to future work aimed at improved design and applications.

In the Nimonic/glass-ceramic coating system, first, the refractoriness of the glass-ceramic itself needs to be increased by modifying the glass compositions to meet the demands of practical use. At the moment softening temperature of the chosen glass-ceramic system is about 870°C while a working temperature of about 700-800°C is required. Second, though a preoxidized Cr_2O_3 layer proves to be chemically desirable the thermal mismatch with the substrate and coating needs to be studied in full detail to avoid any build-up of excess stress at the interface. Third, the coating assembly requires endurance testing at normal service temperature to determine any further physical and chemical changes affecting the coating properties. Fourth, the screen printing technique used in this project provides an easy route to applying the coating to the substrate alloy, but screen printing may not be the best route to coat complex profiles such as blades. Other technologies of applying coatings, for instance, sol-gel or electrostatic spraying, etc. have to be adopted to provide thinner and more precise coatings.

In the titanium/glass-ceramic coating system, the glass-ceramic compositions need to be optimized by considering their thermodynamics and other chemical or physical properties. Second, as discussed before, the reactivity of titanium can only be overcome by decreasing the sintering temperature at which the glass-ceramic coatings and titanium seal, therefore, a route of low firing coating below 800°C, possibly via sol-gel technology, has to be explored. Third, the use of adherence oxides has proved to be very effective to retard the deleterious reactions between SiO_2 and titanium. The effectiveness of such oxides needs to be studied fully as well as the consequent effects on the microstructure of the glass-ceramic coating. Fourth, when the optimized coating composition and adherence oxides are decided, the reactivity of titanium has to be determined in relation to the temperature at which the coating is normally used in order to

177

assess the durability of the glass-ceramic coatings.

REFERENCES

[1] K.A.Maskall & D.White, (1986), "Vitreous Enameling", Pergamon Press, London.

[2] G.Fisher, (1986),, Ceramic Bulletin, 65, (2).

[3] A.I.Andrews, (1961), "Porcelain Enamels", Twin City Printing Co.

[4] V.V.Vargen, (1967), "Technology of Enamels", Pergamon Press, London

[5] J.Havac, (1983), "The Technology of Glasses and Ceramics", Elsevier Press, Amsterdam.

[6] S.D.Stookey & R.D.Maurer, (1962), "Progress in Ceramic Science", Pergamon Press, London.

[7] P.W.McMillan, (1979), "Glass-ceramics", Academic Press, London.

[8] U.S. Patent, (1965), 984,446.

[9] Material Engineering, (1980), 92, (6).

[10] K.T.Scott, (1984), British Ceramic Proceedings, 34, (8).

[11] British Patent, (1977), 1,467,459.

[12] A.J.Sturgeon, D.Holland, G.Partridge & C.A.Elyard, (1986), Glass Technology, 27, (3), pp102-07.

[13] U.S. Patent, (1982), 4,358,541.

[14] R.C.A. Review, (1981), Special issue on porcelain enameled steel boards for electrical applications, 42, (2).

[15] Edited by M.H.Lewis, (1988), "Glass and Glass-ceramics", Chapman& Hall Press, London.

[16] E.A.Logan et.al, Proceeding of "1988 IEEE European IEMT Electronic Manufacturing Technology Symposium", Paris, France.

[17] L.L.Hench & J.Wilson, (1984), Science, 226, pp630-636.

[18] A.P.Tomsia & J.A.Pask, (1986), J.Am.Ceram.Soc., 69, (10), C-239-C-240.

[19] Kazutomo Hoshino & Hidefuse Takahara, (1989), Japanese J. of Applied Physis, 28, (7), pp1214-16.

[20] J.C.Richmond, D.C.Moore, H.B. Kirkpatrick & W.H. Harrison. (1953), J. Am. Ceram. Soc., 36, (12), pp410-16.

[21] B.W.King, H.P.Tripp & W.H.Duckworth, (1959), J.Am.Ceram.Soc., 42, (11), PP504-25.

[22] J.A.Pask, (1971), Proc.Porcelain Enamel Inst.Tech.Forum, 33, pp1-16.

[23] G.R.Baran, (1979), J. of Dental Research, 58, (11), pp2095-2104.

[24] M.Ruhle, K.Burger & W.Mader, (1986), J. Microsc. Spectrosc. Electron., 11. pp163-77.

[25] S.Morozumi, M.Kikuchi & T.Nishino, (1981), J. Mater. Sci., 16 pp2137-44.

[26] A.Sturgeon, Ph.D. Thesis, (1987), Warwick University, U.K.

[27] F.Hong & D.Holland, (1989), Surface and Coating Technology, 39/40, pp19-27

[28] J.A.Pask, (1987), Ceramic Bulletin, 66, (11), pp1587-92.

[29] D.H.Buckley, (1981), "Surface Effects in Adhesion, Friction, Wear and Lubrication", Elsevier Press.

[30] ASM, (1963), Nonmetallic Coating Processes, pp509-31.

[31] J.J.Brennan & J.A.Pask. (1973), J. Am. Ceram. Soc., 56, (2), pp58-62.

[32] A.G.Evans & M. Ruhle, (1985) Mat. Res. Soc. Proc., 40, pp153-66, Material Research Society, New York.

[33] A.Atkinson, (1976), J. Mat. Sci., 11, pp994.

[34] P.R.Sharps, A.P.Tomsia & J.A.Pask, (1981), Acta. Metall., 29, (7), pp855-65.

[35] C.E.Hoge, J.J.Brennan & J.A.Pask, (1973), J. Am. Ceram. Soc., 56, (2), pp51.

[36] L.B.Pankratz, (1982), U. S. Bureau of Mines Bulletin, P672.

[37] P.Mayer, J.A.Topping & M.K.Murthy, (1974), J. Cana. Ceram. Soc., 43, pp43-46.

[38] F.M.Sun & D.Holland, (1990), J. Euro. Ceram. Soc., 24, pp1-7.

[39] K.A.Onsager, (1945), N. Y. Acad. Sci., 46, p241.

[40] Y.Oishi, A.R.Cooper & W.D.Kingery, (1965), J. Am. Ceram. Soc., 42, (2), pp88-95.

[41] A.W.Hofmann, (1980), "Physics of Magnetic Processes", Princeton University Press, U.S.

[42] R.Terai & R.Haymi, (1975), J. of Non-cry. Sol., 18, pp217-64.

[43] M.P.Borom & J.A.Pask, (1967). Physics and Chemistry of Glasses, 8, (5), pp194-202.

[44] M.P.Borom & J.A.Pask, (1968), J. Ame. Ceram. Soc., 51, (9), pp490-8.

[45] D.K.Bowen & C.R.Hall, (1975), "Microscopy of Materials", MacMillan Press, London.

[46] F.Maurice, L.Meng & R.Tixies, (1978), "Microanalysis and Scanning Electron Microscopy", Les E'ditions de Physique, Orsay, France.

[47] R.T.Greer, (1976), Scanning Electron Microscopy, pp669-74.

[48] D.E.Newbury, (1977), Scanning Electron Microscopy, pp553-67.

[49] M.Yakowitz, (1974), Scanning Electron Microscopy, pp1029-42.

[50] Cambridge Instruments, Rustat Rd., Cambridge, U.K.

[51] Link Systems, Halifax Rd., High Wycombe, Bucks.

[52] N.C.Barbi, A.O.Sanborg, J.C.Russ & C.E.Soderquist, (1974), Scanning Electron Microscopy, pp151-57.

[53] J.M.Cohen, (1989), Microscopy and Analysis, (May), pp17-21.

[54] Reed, EDAX Edition, 3, (5), p10.

[55] G.Thomas & M.J.Goringe, (1979), "Transmission Electronic Microscopy of

Materials", John Wiley & Sons Ltd, New York.

[56] M.H.Loretto, (1984), "Electron Beam Analysis of Materials", Chapman and Hall, London.

[57] P.J.Goodhew, (1975), "Electron Microscopy and Analysis", Wykeham Publications Ltd, London.

[58] Ed. by A.M.Glauert, (1973), "Electron Diffraction and Optical Diffraction Techniques", North-Holland Publishing Company, Amsterdam.

[59] M.I.Manning & W.M.Rowland, (1980), Br. Corros. J., 15, (4), pp184-9.

[60] M.I.Newcomb & W.M.Stobbs, (1982), "Electron Microscopy and Analysis 1981", The Institute of Physics, pp137-46.

[61] R.E.Loehman, (1989), Ceramic Bulletin, 68, (4), pp891-6.

[62] JEOL Ltd, Tokyo, Japan.

[63] I.M.Reaney & G.W.Lorimer, (1988), Mater. Sci. and Tech., 4, May, pp391-7.

[64] M.I.Pope & M.D.Judd, (1977), "Differential Thermal Analysis", Heyden Press, London.

[65] Philips Electronic Instruments, Philips Gloeilampentabriew, N.V., Eindhoven, Nertherland.

[66] Stanton and Redcroft, TG-750, Copper Mill Lane, London.

[67] J.Wong & C.A.Angell, (1976), "Glass Structure by Spectroscopy", Marcel Dekker Inc. New York.

[68] H.D.Schreiber, T.Thanyasiri, J.J.Lach & R.A.Legere. (1978), Phys. and Chem. of Glasses, 19, (6), pp126-39.

[69] H.D.Schreiber & L.A.Haskin, (1976), Proc. Lunar. Sci. Cof. 7th, U.S.

[70] Decca ESR Spectrometer-X1, Decca Radar Limited, London

[71] Compiled by M.Palecek & A.Peters, (1984), Glass Technology, 25, (2), pp55-61.

[72] ASTM C313, Adherence of Porcelain Enamel and Ceramic Coating to Sheet metal.

[73] PEL T-29, Adherence of Porcelain Enamel Copper Coats Direct to Steel.

[74] T.Suga & G.Elssner, (1985), Mat. Res. Soc. Symp. Proc., 40, pp203-8.

[75] C.C.Nerndt & R.McPherson, (1980), Astralian Dent. J., 25, pp34-8.

[76] ASTM C636.

[77] G.Partridge, (1979), Glass Technology, 20, (6), pp246-51.

[78] P.F.James, (1974), Phys. and Chem. of Glas., 15, (4), pp95-105.

[79] W.F.Hammetter & R.E.Loehman, (1987), J. Am. Ceram. Soc., 70, (8), pp577-82.

[80] T.J.Headley & R.E.Loehman, (1984), J. Am. Ceram. Soc. 67, (90), pp620-5.

[81] D.M.Mattox, (1972), J. of Mat. Sci., 7, pp184-8.

[82] Blythe Colours Ltd., Cresswell, Stoke-on-Trent, Staffs. U.K.

[83] DEK Printing Machines Limited, Weymouth, U.K.

[84] A.P.Tomsia, F.P.Zhang & J.A.Pask, (1985), J. Am. Ceram. Soc.,68, 1, pp20-25.

[85] R.D.Watkins & R.E.Loehman, (1986), Adv. Ceram. Mat., 1, (1), pp77-80.

[86] Rank Taylor Hobson Ltd, Great Glen, U.K.

[87] K.Hauffer, (1965), "Oxidation of Metals", Plenum Press, New York.

[88] M.M.Ryabkina & I.L.Rogelberg, (1977), Protection of Metals, 13, (1), pp82-5.

[89] P.Moulin, A.M.Huntz, G.Beranger & P.Lacombe, (1977), Metallurgica, 11. pp533-7.

[90] C.S.Giggins & F.S.Petti, (1969), Trans. TMS-AIME, 245, pp2509-14.

[91] S.B.Holmquist, (1961), J. Am. Ceram. Soc., 44, (2), pp85.

[92] J.A.Pask, (1971), Proc. Porcelain Enamel Inst. Tech. Forum., 33, pp1-16.

[93] M.P.Borom & J.A Pask, (1966), J. Am. Ceram. Soc., 49, (1), pp1-6.

183

[94] J.A.Pask & R.M.Fulrath, (1962), J. Am. Ceram. Soc., 45, (12), pp592-6.

[95] R.T.Grimley, R.P.Burns & M.G.Inghram, (1961), J. Chem. Phys., 34, (2), pp664-7.

[96] M.B.Volf, (1984), "Chemical Approach to Glass", Elsevier Press, Amsterdam.

[97] H.D.Schreiber, (1980), J. of Non-cryst. Sol., 42, pp175-84.

[98] P.Nath & R.W.Douglas, (1965), Phys. and Chem. of Glas., 6, (6), pp197-202.

[99] H.D.Schreiber, (1978), Contribution to Mineral and Petrology, 66, pp341-2.

[100] R.K.Brown, (1987), J. Am. Ceram. Soc., 70, C129-C131.

[101] S.C.Kunz & R.E.Loehman, (1987), Adv. Ceram. Mat., 2, (1), pp69-73.

[102] J.W.Mclean & I.R.Sced, (1973), British Ceram. Soc. Trans., (Jul.), 72, pp235-8.

[103] R.L.Thakur, (1971), "Advances in Nucleation and Crystallisation in Glasses", Am. Cer.Soc., No.5, p166.

[104] J.Williamson, (1970), Mineralogical Magazine, 37, (291), pp759-70.

[105] K.J.D.Mackenzie & I.W.M. Brown, (1975), Phys. Chem. Glas., 16, (1), pp17.

[106] L.J.Manfredo & R.N.McNally, (1984), Com. Am. Ceram. Soc. 67, C155-C158

[107] J.R.Myers, H.B.Bomberger & F.H.Froes, (1984), J. of Met., (Oct.), pp50-8.

[108] V.I.Eremenko, (1960), "Titanium and Its Alloy", Izd. AN UKrSSR.

[109] L.S.Morozidr (1960), "Titanium and Its Alloy", Sudpromgiz, Leningrad.

[110] I.J.Polmear, (1981), "Light Alloy — Metallurgy of the Light Metals", Edward Arnold, London.

[111] D.Eylon, S.Fujishiro, P.J.Postans & F.H.Froes, (1984), J. of Met., (Nov),, pp55-62.

[112] S.Fujishiro & D.Eylon, (1978), Thin Solid Films, 54, pp309-315.

[113] S.Fujshiro & D.Eylon, (1980), Met.Trans.A., 11A, pp1259-63.

[114] Z.I.Kornilova & D.V.Ignatov, (1970), Protection of Metals, 6, pp665-667.

[115] V.S.Kheifets, (1969), Protection of Metals, 5, pp255-7.

[116] V.E.Gorbatenko, Yu.K.Krichevskii & A.Ya.Sitnikova, (1974), Soviet Materials Science, 10, pp143-7.

[117] A.Ya.Sitnikova et.al, (1972), Akademiya Nauk SSSR, Institute Khinii Silikatov Im I.V., Grebenshchikova, pp189-99.

[118] A.Ya.Sitnikova, A.A.Appen, I.S.Anitov, V.N.Fedorov, A.M.Kalinia & M.M. Piryntko, (1974), J. of App. Chem. of USSR, 47, pp1922-6.

[119] A.Ya.Sitnikova, I.S.Anitov & I.A.Sudonoikin, (1971), J. of App. Chem. of USSR, 44, pp1475-9.

[120] V.S.Kheifets, (1972), J. of App. Chem. of USSR., 45, pp210-2.

[121] A.Passerone, G.Valbusa & E.Biagini, (1977), J. of Mater. Sci., 12, pp2465-74.

[122] I.J.McColm & C.Dimbylow, (1974), J. of Mater. Sci., 9, pp1321-4.

[123] Goodfellow Metals Ltd., Science Park, Cambridge, U.K.

[124] Oertling Ltd., Orpington, Kent, U.K.

[125] J.A.Topping, (1977), Ceram. Bulletin, 56, (6), pp574-7.

[126] R.W.Jones, (1988), Metals and Materials, (December), pp748-751.

[127] R.L.Nelson, J.D.F.Ramsay, J.L.Woodhead, J.A.Cairns & J.A.A.Crossley, (1981), Thin Solid Films, 81, pp329-37.

APPENDIX 1

A COLORIMETRIC DETERMINATION OF CHROMIUM OXIDE Cr_2O_3 IN GLASS

1.PRINCIPLE

After decomposition of the unknow Cr-containing glass sample in a hot HF and H_2SO_4 mixture, the residue is then dissolved in hot diluted sulphric acid and boiled. The solution is cooled and 1.5-Diphenylcarbazide solution (0.2% w/v) is added. The mixture is finally diluted to a certain volume in a volumetric flask. Aliquot portions are taken, on which the absorbance of the chromium-diphenylcarbazide complex is measured at 546nm wavelength on a spectrometer. A calibration graph is prepared by measuring a series of solutions of known Cr^{+3} concentration on a spectrometer. Thus, the Cr^{+3} concentration of unknown samples can be compared.

Because other valency of Cr ions, such as Cr^{+2} or Cr^{+6}, are not stable in the presence of sulphric acid or hydrofluoric acid, the conversion to the most stable Cr^{+3} ions takes place at the initial stage of the analysis. Thus, regardless of their different original valency, Cr^{+3} concentration determined in this analysis is the total concentration of Cr ions in the glass.

2.PRODEDURE

A. Weigh to the nearest 0.0001g 10mg of the unknown sample in a platinum crucible

B. Add 5ml HF and a few drops of concentrated H_2SO_4 into the crucible and gently boil in a ventilated cabinet until dry

C. Prepare 1.5-Diphenylcarbazide solution(0.2% w/v) by dissolving 0.1g of the solid reagent in 10ml of glacial acetic acid and dilute to 50ml (prepare the solution immediately before use)

1

D. Take the crucible with the residue into a beaker and dissolve the residue in 40ml of sulphric acid (1+17) and warm up until a clear solution is obtained. Add 1ml of silver nitrate, 0.5g ammonium persulphate and boil for 15min, cool and transfer to a 100ml volumetric flask. Pipette 2ml of read-made Diphenylcarbazide solution into the volumetric flask and then dilute to the mark and mix thoroughly.

C. Take an aliquot portions from the volumetric flask using a suitable cell and measure the absorbance on a spectrometer at 546nm wavelength.

3.CALIBRATION GRAPH

Within an expected range, transfer aliquots of the chromium standard solution into separate beakers, mixed with 40ml of sulphric acid (1+17) followed by boiling for a minute. Cool, add 1ml of silver nitrate solution and 0.5g ammonium persulphate. Boil gently for 15min, cool, and transfer to 100ml volumetric flask. Add 2ml of diphenylcarbazide solution, dilute to the mark, and mix.

Measure the absorbance and plot the measurements against the concentration of Cr_2O_3.

APPENDIX 2

TENSILE PULL TEST FOR COATING ADHESION

1.PRINCIPLES

A strong adhesive is used to bond both the coating and substrate to a test device on which a tensile load is applied. If the strength of adhesive exceeds either the bonding strength of the coating or the coating itself, the failure should occur at the coating/substrate interface or within the coating body. If the area where the fracture occur is known, the tensile strength can be taken as an estimation to access the coating adhesion.

2. PROCEDURE

A. Use Araldite 2007 heat cured resin supplied by Ciba-Geigy Company. All pieces used including the coating assembly, aluminium stud (8mm diameter as contact surface) and sample stage need to be chemically pretreated to achieve required cleanness and roughness. Soak all the pieces in a mixture of $Na_2Cr_2O_7$ (3.75g), H_2SO_4 (7.5ml) and H_2O (50ml) at 60-65°C for 30min, and rinse in deionised water followed by drying in air.

B. Apply a thin layer of adhesive at required interfaces, carefully align up the stud, coating assembly and stage and cure the adhesive in oven at 80°C for overnight.

C. Assemble the whole piece into the device shown in Fig.3.9 and mount the jig on an Instron mechanical test apparatus. Tensile load was applied at rate of 0.25mm per min until failure occur. Record the tensile strength at the breaking point.

3.RESULT

A. Each reading was taken from three reasonable measurements and presented as their average. The following are typical samples of glass-ceramic coating on Nimonic alloy:

Series1-4(Non-preoxidation)	Series1-4(Preoxidation)
(MN/m^2)	(MN/m^2)
29.0	58.6
37.5	51.2
21.7	42.7
Average: 29.4	50.5

B. There are different failures observed in the tensile test. They are adhesive failure, cohesive failure, mixed failure and epoxy failure. The adhesive failure gives fracture along the coating/alloy interface and the fractured interface shows very neat and clean alloy on the alloy side. The cohesive failure occurs within the coating bulk, which usually does not expose the coating/alloy interface in the fracture area. The mixed failure is the failure between the adhesive and cohesive, in which only part of the interface is fractured. Epoxy failure sometimes occur between the coating and the Arodite resin leaving the coating virtually unaffected. In the case of coating on Nimonic system, unpreoxidized samples tend to have more cohesive failure at lower strength value than the preoxidized samples.

PUBLICATIONS AND PRESENTATIONS

1. PUBLICATIONS

F.Hong & D.Holland, **"Study of Interactions between Glass-ceramic Coating and Metals"**, *J. of Non-crystal Solids, 112, (1989), pp357-367.*

F.Hong & D.Holland, **"Bonding Glass-ceramic Coatings to High-temperature Alloys"**, *Surface and Coating Technology, 39/40, (1989), pp19-27.*

F.Hong, D.Holland, A.Sturgeon & F.M.Sun. **"Glass-ceramic Coatings on High Temperature Metals"**, *Proceeding of 1989 European Conference on Advanced Materials and Process, April, 1989.*

D.Holland & F.Hong, **"Applications of Glass-ceramic Coatings for Titanium"**, *Proceeding of 1990 European Conference on Titanium and Aluminium, March, 1990.*

D.Holland, F.Hong, E.Logan & S.Sutherland, **"Glass Ceramic Coating for Extended Performance"**, *Proceeding of 1990 IOP Spring Meeting (New Materials and Their Applications), April, 1990.*

D.Holland, F.Hong, E.Logan & A.Sturgeon, **"The Effect of Reactions At Glass-ceramic/Metal Interfaces"**, *Proceeding of Institute of Ceramic/Society of Glass Technology, October, 1990.*

PRESENTATIONS

(P) **1988 IOP Autumn Meeting,** University of Warwick, U.K.

(O)* **1988 Material 88,** University of Birmingham, U.K.

(O)**1988 Shanghai International Glass Symposium,** Shanghai, China.

(O) **1989 International Conference of Metallurgical Coatings,** San Diego, U.S.

(O) **1989 European Conference on Advanced Material and Process,** Aachen, Germany.

(O)* **1990 European Conference on Titanium and Aluminium,** Paris, France.

(O) **1990 IOP Spring Meeting,** University of Warwick, U.K.

(O) **1990 Interceramex (Surface and Interfaces),** NEC Birmingham, U.K.

  * Part of the oral presentation by Dr.E.Logan and Dr.D.Holland